

PPPL-3234 - Preprint: February 1997, UC-420, 421, 425, 426

Results from Deuterium-Tritium Tokamak Confinement Experiments

R.J. Hawryluk

Princeton Plasma Physics Laboratory
Princeton, New Jersey 08543

Abstract

Recent scientific and technical progress in magnetic fusion experiments has resulted in the achievement of plasma parameters (density and temperature) which enabled the production of significant bursts of fusion power from deuterium-tritium fuels and the first studies of the physics of burning plasmas. The key scientific issues in the reacting plasma core are plasma confinement, magnetohydrodynamic (MHD) stability, and the confinement and loss of energetic fusion products from the reacting fuel ions. Progress in the development of regimes of operation which have both good confinement and are MHD stable have enabled a broad study of burning plasma physics issues. A review of the technical and scientific results from the deuterium-tritium experiments on the Joint European Torus (JET) and the Tokamak Fusion Test Reactor (TFTR) is given with particular emphasis on alpha-particle physics issues.

CONTENTS

- I. Introduction
- II. JET and TFTR Devices
 - A. Auxiliary heating
 - B. Diagnostics
 - 1. Neutron measurement
 - 2. Escaping alpha measurement
 - 3. Confined alpha measurement
- III. Regimes of Operation
 - A. L mode
 - B. Enhanced confinement regime
 - 1. H mode
 - 2. Supershot
 - 3. High ℓ_i
 - 4. Reverse shear
- IV. Fusion Power Production
- V. Confinement in D-T
 - A. Isotope effects on energy confinement
 - B. Particle transport
- VI. Heating of D-T Discharge
 - 1. Neutral beam heating
 - 2. ICRF heating
- VII. Alpha Particle
 - A. Single particle effects
 - 1. First orbit loss scaling
 - 2. Stochastic ripple diffusion
 - 3. Passing-trapped particle boundary effects due to ICRF
 - B. Confined particles
 - 1. Sawteeth instabilities
 - 2. Stochastic ripple diffusion
 - C. He Ash
 - D. Interaction with MHD
 - 1. Disruptions
 - 2. Low m-n modes
 - 3. KBM
- VIII. Collective Effects
 - A. Toroidal Alfvén Eigenmodes
 - B. Ion Cyclotron Instabilities
- IX. Alpha Heating Experiments
- X. Future Directions
 - A. Alpha heating
 - B. Alpha channeling
 - C. Isotope effects in diverted H-mode plasmas

- 1. Divertor operation
- D. Ignition devices

XI. Conclusions

Acknowledgments

Appendix: Tritium and Activation Considerations

- A. Tritium systems
 - 1. Tritium retention
- B. D-T Neutronics
 - 1. Shielding
 - 2. Machine activation

References

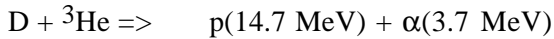
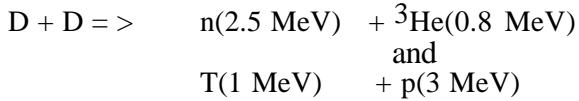
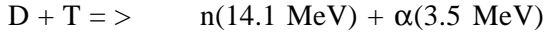
I. INTRODUCTION

Over the past three decades, extraordinary progress has been realized in magnetic fusion science. Recent developments in the understanding of plasma transport, plasma stability and impurity control have enabled the achievement of record plasma parameters including temperature, pressure and confinement time, and have created the conditions under which significant fusion reaction rates and, consequently fusion power, have been demonstrated. The magnetic configuration which has been most successful in achieving high performance parameters necessary for significant fusion reactions to occur has been the tokamak. A tokamak (Artsimovich, 1972; Furth, 1975) is a toroidal magnetic confinement device which confines the plasma by a helical magnetic field through a combination of an external toroidal magnetic field and the self-field produced by a toroidal plasma current. In tokamak experiments on the Joint European Torus, JET, (JET Team, 1992), JT-60U (Kikuchi *et al.*, 1995; Ushigusa *et al.*, 1996), DIII-D (DIII-D Team, 1995) and the Tokamak Fusion Test Reactor, TFTR, (Hawryluk *et al.*, 1995; McGuire *et al.*, 1996) many of the plasma parameters expected in an operating fusion reactor have been generated. The extension in operating parameters has been accompanied by a deeper understanding of the underlying physics which is responsible for the confinement and stability of the discharge. Experiments to date have been primarily conducted using either hydrogen or deuterium plasmas though tokamak reactor concepts principally plan on utilizing mixed deuterium (D) and tritium (T) plasmas due to the higher cross-sections and higher yield per D-T reaction.

Until the operation of the present generation of large tokamaks, the plasma parameters which determine the reaction rate and the concentration of fusion products were not adequate to warrant using tritium fuel, which is a radioactive isotope of hydrogen, and the consequent increase in machine activation from the increased plasma reactivity. However, present experiments on TFTR have now produced conditions in which the fusion power density and the resulting population of energetic alpha particles are comparable to a reactor. Thus, the study of deuterium-tritium plasmas has enabled the study of critical physics issues associated not only with deuterium-tritium fuel, but also with

alpha-particle physics. The production and confinement of the energetic alpha particles and their subsequent thermalization will be the central scientific issues for a burning plasma.

The fusion reactions of principal practical interest for fusion power production are:



The transfer of energy from the energetic charged particles produced by fusion to the background plasma can, in principle, be used to heat the plasma. Eventually in a reactor, the transfer of energy from the high energy fusion products to the background plasma will be used to sustain the temperature of a reactor. The energetic neutrons leave the plasma and are absorbed or scattered by structures outside. In a reactor, the neutrons would be absorbed in a blanket containing ${}^6\text{Li}$ surrounding the plasma and the tritium would be regenerated by the reaction:



thereby releasing a further 4.8 MeV.

The fusion power density due to D-T reactions in the plasma is given by:

$$P_{\text{fus}} = n_t n_d \langle \sigma v \rangle 17.6 \text{ MeV}$$

where n_t and n_d are the tritium and deuterium densities and $\langle \sigma v \rangle$ is the rate coefficient. There is a corresponding expression for the other reactions of interest. There is a large difference in the value of cross section for the reactions of interest (Bosch and Hale, 1992), as shown in Fig. 1. A D-T reactor with a lithium blanket is the most attractive because a self-sustaining plasma can be achieved with the lowest plasma temperature ($T > 5 \text{ keV}$) and lowest requirement for the product $n\tau_E^*$, where n is the ion density and $\tau_E^* \equiv W_{\text{TOT}} / (P_{\text{heat}} - P_{\text{breh}})$ where P_{heat} is the heating power and the radiation loss due to Bremsstrahlung, P_{breh} , is explicitly taken into account. $P_{\text{heat}} = P_{\text{aux}} + P_{\text{alpha}}$ where P_{aux} is the auxiliary heating power and P_{alpha} is the alpha heating power used to heat the plasma. In present experiments, the radiation loss due to Bremsstrahlung is typically very small in the power balance

and can be ignored but will be significant when alpha heating becomes the dominant heating mechanism. For a reactor with a uniform, isothermal plasma, the plasma parameters required for a self sustaining fusion reactor can be estimated by equating the plasma heating from the fusion reactions,

$$P_{\alpha} = n_i n_d \langle \sigma v \rangle 3.5 \text{ MeV},$$

to the power required to heat the plasma $[3(n_i T_i + n_e T_e) / 2 \tau_E^*]$. For thermal D-T reactions, $\langle \sigma v \rangle \propto T_i^2$ for $(9 < T_i < 19 \text{ keV})$ and a value of $n_i T_i \tau_E^* > 6 \times 10^{21} \text{ m}^{-3} \text{ keVs}$ is required for ignition when $n_i = n_e$ and $T_i = T_e$ (Furth, *et al.*, 1990). Thus, it has become customary to illustrate technical progress in magnetic fusion in terms of the triple product, $n_{i(0)} T_{i(0)} \tau_E^*$, as shown in Fig. 2. For thermal reactions and steady-state conditions, the ratio of the fusion power to the auxiliary power can be expressed simply as a function of the triple product and temperature. As shown in Fig. 2 in large present experiments, the value of the triple product which has been achieved corresponds to conditions in which for D-T plasmas the fusion power produced would be somewhat less than the auxiliary power required to heat the plasma. Though the relationship of the triple product to fusion power production only applies to D-T experiments which are conducted on JET and TFTR, the highest values of triple product achieved in D experiments on several other devices are shown for comparison. The general considerations given here are for a homogenous, pure, thermal plasma. This analysis has been extended to include effects associated with profile shapes, impurities, non-thermal ion distributions, and $T_i \neq T_e$. Though the precise relationship between the triple product and $P_{\text{fus}}/P_{\text{aux}}$ depends upon these effects, as well as the confinement and thermalization of the alpha particles, these very simple considerations do highlight the important plasma parameters required for substantial fusion power production.

Present deuterium-tritium experiments can address many but not all of the physics issues associated with the use of D-T fuel. Generic issues associated with the use of tritium fuels such as isotope effects on confinement and heating have been studied and these do not depend on the plasma reactivity. The production of substantial rates of fusion reactions enables the detailed study of the confinement and loss of alpha particles (Strachan, *et al.*, 1989). More importantly in present

experiments the effect of alpha particles on plasma stability can be studied. Because these instabilities depend on alpha-particle pressure (as well as other parameters), regimes of operation with high rates of alpha particle production are needed. By operating in regimes in which the ion temperature (or energy) is greater than the electron, it has been possible to achieve fusion power densities comparable to that in a reactor to study this important physics topic even though the ratio of $P_{\text{fus}}/P_{\text{aux}}$ is much less than that in a reactor. In present experiments, alpha heating which depends directly on the ratio of $P_{\text{fus}}/P_{\text{aux}}$ can be detected; however, a comprehensive study requires operation in regimes in which $P_{\alpha} > P_{\text{aux}}$ which has not been obtained in present experiments. In this review, approaches used to increase the plasma reactivity are described because they were an important consideration in the breadth of physics topics which could be studied in present experiments.

In the world tokamak fusion program, two major facilities, JET and TFTR have been designed to study the physics associated with the use of deuterium-tritium fuel. A limited scope, "Preliminary Tritium Experiment" (PTE) was performed on JET in 1991. This experiment utilized a ratio of tritium to deuterium fueling of 13% (JET Team, 1992). A more extensive program is planned to begin in JET in 1997. TFTR has conducted an extensive campaign of high power deuterium-tritium experiments from 1993 to 1996 with a wider range of tritium to deuterium fueling (up to 100%) (Strachan, 1994a; Hawryluk, 1994a). The D-T experiments on JET and TFTR during the past several years have provided important new data on the confinement of D-T plasmas, their heating by radiofrequency waves and energetic neutral beams, and confinement and loss of alpha-particles.

This paper will review the results from the recent D-T experiments from JET and TFTR and highlight remaining issues and scientific opportunities. In preparing this paper, I have benefited from the review papers on alpha-particle and burning plasma physics issues which were written prior to the use of tritium on JET and TFTR by Kolesnichenko (1980), Sigmar (1987), Goloborod'ko, *et al.* (1987), and Furth, *et al.* (1990), as well as several overview papers on the experimental results from both machines (JET Team, 1992; JET Team [presented by Gibson], 1993; Hosea *et al.*, 1994; Strachan *et al.*, 1994b; Bell *et al.*, 1995; Johnson, D. *et al.*, 1995; McGuire *et al.*, 1995; Meade *et al.*, 1995; McGuire *et al.*, 1996; Bell *et al.*, 1996). The experiments on both machines are part of a

worldwide effort to study the physics of high temperature plasmas and rely upon the theoretical and experimental results from this entire effort. In this paper, it is not possible to give a comprehensive review of tokamak physics research. The presentation of results from deuterium-tritium experiments on JET and TFTR should be understood in this broader context.

In addition to these current experiments, there is a major international design study underway to develop a device called the International Thermonuclear Experimental Reactor (ITER) which will be able to sustain a burning plasma for a long duration. This device, which will use deuterium-tritium fuel, is planned to be about three times larger in linear dimension than TFTR or JET and is projected to produce 1500 MW of fusion power. A discussion of the present status of the ITER Project has recently been given by Aymar *et al.* (1996). The design of the ITER device is based on established physics and technology. However, the design process has identified many important issues for burning plasma research. Many of the results in this paper will be presented in terms of the issues and requirements for ITER.

The following major topics will be covered in this review. A brief description of the JET and TFTR devices will be given with particular emphasis on the characteristics of importance to the D-T experiments. The tritium handling system and the radiological consequences of high energy neutrons on machine activation and site-boundary dose will be presented in an Appendix. A key element in the experiments conducted on JET and TFTR has been the development of high performance regimes characterized by high fusion reactivity. In present experiments, these regimes have several distinguishing and common characteristics: reduced levels of plasma transport resulting in enhanced confinement, maximum plasma pressure typically limited by the onset of pressure-driven MHD-activity, and ion temperatures in excess of the electron temperature due to the vigorous application of auxiliary heating. Due to differences between these devices, however, different techniques have been employed to achieve these enhanced regimes of operation. These techniques will be described along with a brief summary of the present understanding of plasma transport and MHD stability limits in these devices. An overview of the fusion power production which has been achieved in these regimes of operation will then be given. Having described the experimental

conditions for deuterium-tritium operation, the effect of D-T fueling on plasma confinement and heating will be discussed. In particular, isotope effects on plasma confinement will be described and the effect of a second ion-resonance on heating by waves in the ion cyclotron range of frequencies will be discussed.

The confinement and thermalization of alpha particles is the key scientific issue for the study of burning plasmas. The confinement of alpha particles in both quiescent and MHD-active discharges will be described. An overview of our present understanding of how alpha particles can in turn destabilize plasma instabilities will be given. Although in present experiments, alpha heating has been small compared with auxiliary plasma heating, initial evidence for alpha heating will be presented. Future research opportunities in the study of D-T plasmas and alpha particle interactions will conclude this review paper.

II. JET AND TFTR DEVICES

Both JET and TFTR are tokamak devices in which a strong toroidal magnetic field together with the self-field produced by a large toroidal plasma current is used to confine and heat the plasma. As shown in Figure 3, the nearly circular TFTR plasma is limited by an inboard limiter composed of graphite and carbon-fiber-composite (CFC) tiles mounted on a water-cooled inconel backing plate. A set of poloidal limiters composed of carbon fiber composite tiles is used to protect RF launchers on the outboard side which are used to heat the plasma. The limiters can withstand heat outflow from the plasma of ~ 30 MW for ~ 1 sec. As shown in Figure 4, the JET vacuum vessel is shaped, enabling plasma formation with an elongation of <1.6 . At the time of the PTE, the heat flux was diverted to a toroidally continuous top target composed of CFC tiles. A continuous inner wall of graphite and CFC tiles, a continuous bottom target clad with beryllium tiles, and a pair of toroidal belt limiters on the outboard side above and below the midplane, the upper one of beryllium and the lower one of carbon, complete the protection of the JET vessel (JET Team, 1992). A comparison of the principal engineering parameters of JET and TFTR is given in Table I. Since the initial D-T experiments were conducted on JET, the machine has been extensively modified with the installation

of a pumped divertor in the bottom of the vessel. Further D-T experiments are planned to be performed in this modified device (JET Team, [presented by Stork] 1994; JET Team, [presented by Jacquinot] 1996).

A. Auxiliary Heating

During the D-T experiments, neutral beam heating has been used on both devices and RF heating in the ion cyclotron range of frequencies (ICRF) has been used on TFTR. In addition an extensive ICRF program was conducted in D discharges on JET.

The TFTR neutral beam system is composed of four beamlines each with three positive-ion sources. The sources extract and accelerate a positive-ion beam which is then neutralized in a gas cell before entering the plasma. The ion sources can operate either in deuterium or in tritium. The maximum operating voltage is 120 kV and a maximum injected power into a D-T discharge has been 40 MW (Grisham *et al.*, 1995; Stevenson *et al.*, 1995). In addition to heating the discharge, the neutral beams are an effective means of fueling the discharge. On TFTR, the fueling has been varied from all deuterium to all tritium. The JET neutral beam heating system is composed of two neutral beamlines with eight positive-ion sources each. For the PTE, two of the ion sources operated in tritium at a voltage of 78 kV to ensure reliable operation. The remaining fourteen sources operated in deuterium, twelve at an operating voltage of 135 kV and two at 75 kV. The injected power into the D-T discharges was 14.3 MW. The tritium fueling rate relative to the total was $\approx 13\%$.

The TFTR ICRF system utilizes four antennas to launch a fast electromagnetic wave into the plasma. The operating frequency has been varied for different experiments. Fast-wave experiments were conducted at 43 MHz utilizing ^3He -minority absorption and second-harmonic tritium absorption, and at 64 MHz utilizing hydrogen-minority absorption. For mode conversion experiments in deuterium-tritium plasmas in which the fast wave is converted into an electrostatic ion Bernstein wave, the frequency is 30 MHz. Mode-conversion experiments were also performed at 43 MHz in D- ^3He -T plasmas.

B. Plasma Diagnostics

New and novel diagnostics have been an important ingredient in developing an understanding of high temperature plasmas. A review of recent diagnostic developments is given by Gentle, 1995. Information about TFTR and JET diagnostics can be found in Hill *et al.* (1990), Young and Johnson (1992), Young (1995), Johnson *et al.* (1996), and Thomas (1996). In modern tokamak experiments, detailed profile measurements of the plasma electron and ion temperature, electron density, current density, and toroidal rotation are routinely available. Measurements of the fluctuations in the plasma are made by a variety of techniques ranging from fast electron cyclotron emission measurements (ECE) of the electron temperature, to x-ray measurements of the chord-averaged x-ray emissivity due to variations in electron temperature and impurity concentration and microwave reflectometer and beam-emission-spectroscopy measurements of the density fluctuations. Table II provides a list of current diagnostics on the TFTR device and the parameter which is measured. In preparation for the D-T experiments, many TFTR diagnostics were modified to cope with the higher radiation fluxes from both the neutrons and gammas during the pulse (Hill *et al.* 1995; Ku *et al.*, 1994). The vacuum systems of the diagnostics were also modified to be tritium compatible. The D-T experiments also provided an opportunity to assess the effect of neutron damage on fiber optics (Morgan, 1992; Adler *et al.* 1995; Ramsey *et al.* 1995; Paul *et al.* 1995).

For the D-T experiments, several new diagnostics were developed to measure the total neutron source strength, the neutron emission profiles, which are a measure of the alpha-particle birth location, and the escaping and confined alpha particles. Since these new measurements are central to the D-T experiments, they will be described below.

1. Neutron Measurements

The neutron emission rates were measured in JET with silicon surface barrier diodes and using ^{235}U and ^{238}U fission chambers (which are not capable of discriminating between 2.5 MeV and 1 MeV neutrons). These detectors were calibrated by comparison with the total time integrated neutron yield measured by the activation of two elemental samples positioned near the vessel. Silicon was used but since the $^{28}\text{Si}(n, p)$ reaction is not well characterized, it was cross-calibrated against the standard dosimetry reaction of $^{63}\text{Cu}(n, 2n)^{62}\text{Cu}$ and $^{56}\text{Fe}(n, p)^{56}\text{Mn}$. The accuracy of the total neutron yield is estimated at $\pm 7\%$. The neutron energy spectrum was measured with a liquid-scintillator spectrometer. Neutron emission profile data were obtained from 19 similar spectrometers arranged in two cameras with orthogonal views (JET Team, 1992; Marcus *et al.* 1993).

TFTR also has an extensive set of fusion neutron detectors (5 fission detectors, 2 surface-barrier detectors, 4 activation-foil stations) (Barnes *et al.*, 1995) and a 10-channel neutron collimator with 25 detectors (including ^4He recoil detectors) to provide time resolution as well as energy discrimination of the D-T and D-D neutron fluxes. The systems were calibrated *in situ* by positioning an intense neutron source at many locations within the vacuum vessel (Barnes *et al.*, 1990; Hendel *et al.*, 1990; Strachan *et al.*, 1990). The yield measured by the fission, surface barrier and ^4He recoil detectors is linear with the yield measured by activation foils over 6 orders of magnitude. The system of multiple measurements has allowed a $\pm 7\%$ determination of the fusion energy production (Jassby *et al.*, 1995; Johnson, *et al.*, 1995; Strachan *et al.*, 1995). The neutron profile and hence the alpha birth location is measured with the neutron collimator.

2. Escaping Alpha Particle Measurements

Fusion product losses from TFTR plasmas are measured by a poloidal array of detectors just behind the limiter shadow. The detectors are situated at poloidal angles 90° , 60° , 45° , and 20° below the outer midplane. The ion $\nabla \mathbf{B}$ drift direction is towards the 90° detector. The 20° detector is mounted on a moveable probe. The detectors are illustrated in Fig. 5. A set of apertures disperses the particles by pitch angle (the escaping particle's angle with respect to the toroidal field) and gyro-

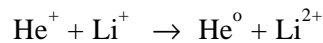
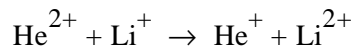
radius onto a planar scintillator. Light from the scintillator is carried by coherent fiber optic bundles to remote detectors which record the two dimensional position on the detector surface, and the total scintillation light versus time (Darrow *et al.*, 1995).

An alternative approach to measure escaping fusion products has been developed by Herrmann *et al.* (1995, 1996) and Chong (1995). Alpha particles escaping from the plasma are implanted in nickel foils located in a series of collimated ports on a vertically moveable probe drive located at 90° below the midplane. Each port accepts particles with a limited range of pitch angles. The Ni foils with the implanted alpha particles are removed from the vessel and analyzed for He content. The alpha energy distribution is deduced by measuring the depth distribution of He in the Ni foils. This diagnostic has better energy resolution than the scintillator detectors but does not have intrinsic time resolution.

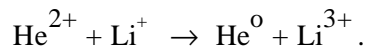
3. Confined Alpha Particle Measurements

Measurements of the confined alpha particles are especially difficult due to the relatively low concentration of alpha particles $n_{\alpha}/n_e \sim 10^{-3}$ and large range in energies, from the birth energy of 3.5 MeV to thermal. These measurements provide important information about the confinement and thermalization of the alpha particles. Two techniques, pellet charge exchange (PCX) and alpha-charge exchange recombination spectroscopy (α -CHERS) have been used on TFTR to study the confined alpha particles.

In the PCX diagnostic, small lithium or boron pellets ($\sim 7 \text{ mm}^3$) are injected radially into TFTR. Upon entering the plasma, the pellet ablates surrounding itself with a dense localized cloud of ionized lithium as it travels through the plasma. This cloud is sufficiently dense that a small fraction of the alpha particles incident on the cloud are neutralized by sequential single electron capture,



and also double capture



By measuring the energy distribution of the resultant helium neutrals escaping from the plasma using a mass and energy resolved neutral particle analyzer (NPA), the energy distribution of the confined alphas can be determined by modeling the fraction of alpha particles which are neutralized in the cloud as a function of alpha energy (Fisher *et al.*, 1995; Medley *et al.*, 1996b). This diagnostic technique is illustrated in Fig. 6. This technique has successfully measured the confined alpha particles from 0.5 to 3.5 MeV with good signal to background ratio. By measuring the radial position of the pellet as a function time using a linear photodiode array situated on the top of the vacuum vessel and the time dependent flux to the neutral particle analyzer, good radial resolution of ~ 5 cm has been obtained (Fisher *et al.*, 1994; Medley *et al.*, 1995, 1996a; Petrov *et al.*, 1995, 1996). Its principal limitations are that it provides a measurement at only one time in the discharge due to the impact of the large increase in density resulting from the Li pellet on the evolution of the discharge, and that its use is typically restricted to the period after high-power heating in order to achieve adequate pellet penetration. Due to the location of the detector, only near-perpendicular energetic ions with $v_{\parallel}/v = -0.048$ are detected. This could, in principle, be changed.

α -CHERS, a charge exchange recombination spectroscopy diagnostic, is designed to observe confined alphas with energies in the range from thermal to ~ 700 keV. A schematic illustration of the diagnostic is shown in Fig. 7 (McKee *et al.*, 1995a). Alpha particles are observed by measuring the Doppler shifted $n=4-3$ transition of He^{+1} near 468.6 nm which is excited by electron exchange reactions between the injected neutral-beam atoms and alpha particles. Analysis of the spectrum yields the spatial density profile and the low energy distribution. This is a very challenging measurement due to the relatively low signal level compared with the background light from Bremsstrahlung and impurity lines emitted by low charge states of carbon. A very high light-throughput system was developed employing a moderate resolution spectrometer, and low-noise, high quantum-efficiency, high dynamic-range detectors to improve the photon counting statistics.

The background light is carefully subtracted from the measured spectrum to give the contribution attributed to alpha particles. During the high-power phase neutron-induced fluorescence in the optical fiber also contributes to the observed signals. As a result, the data is

typically taken after the high-power phase when the population of alpha particles is still high but the neutron flux has decreased substantially. The advantages of this technique are that it can provide time dependent measurements at several radial locations and furthermore, the intensity measurements are absolutely calibrated which allows direct comparison with simulation codes.

III. REGIMES OF OPERATION

Both JET and TFTR operate in a variety of regimes which span a wide range of plasma parameters and which are characterized by differences in plasma transport and stability. The underlying physics responsible for the transport variability will be briefly described, although a comprehensive discussion of this extensive literature is beyond the scope of this paper. Fortunately, there are several papers which provide a good background to these issues which remain under active study in the world-wide program. In this paper, only the regimes of operation which have been studied on JET and TFTR with D-T plasmas will be presented, to provide a background to the results which will be presented in the following sections.

A. L mode

The most easily obtained operating regime is called L mode because it is characterized by comparatively low confinement. In this regime, there is substantial influx of hydrogen and carbon at the limiters and/or divertors. The resulting density profiles are broad and edge ion temperature is low. The electron and ion temperatures are typically comparable especially at high density. An empirical relationship (Yushmanov *et al.*, 1991) has been derived from the world-wide database which describes the confinement time for L-mode plasmas

$$\tau_E^{\text{ITER-89P}} = 0.048 I_P^{0.85} R^{1.2} a^{0.3} n_e^{0.1} B_t^{0.2} (A_{\text{HYD}} \kappa / P)^{0.5}.$$

Where A_{HYD} is the mass of the hydrogenic species, κ is the plasma elongation and P the heating power. The confinement increases with mass of the hydrogenic species, A_{HYD} , as will be discussed in Sec. V. A, and with plasma current and degrades with increasing auxiliary heating power. This

regime of operation has been studied on TFTR in D-T, although relatively briefly, but extensively studied in D.

The empirical observation of transport in TFTR L-mode discharges (Hawryluk *et al.*, 1991 and references therein) has the following features:

- a) The radial transport is governed by turbulent processes such that the electron and ion heat, particle and momentum transport is much larger than predicted by collisional transport theories.
- b) The degradation of thermal τ_E is even stronger $\tau_E^{\text{th}} \sim P^{-0.7}$ (Scott *et al.*, 1996b).
- c) Local transport coefficients electron heat diffusivity (χ_e), ion heat diffusivity (χ_i), and toroidal momentum diffusivity (χ_ϕ) increase strongly with power or temperature (Scott *et al.*, 1990b).
- d) $\chi_i \approx \chi_\phi$ as expected from microturbulence theories.
- e) Degradation is not caused by anomalous loss of fast ions. For a comprehensive review see Heidbrink and Sadler, 1994.
- f) Perturbative measurements of the electron particle transport indicate an adverse temperature scaling.
- g) Toroidal velocity profile measurements following off-axis neutral beam injection can be modeled without introducing an inward momentum pinch.

Significant progress has been made in the understanding of transport process in the core of L-mode discharges. Kotschenreuther *et al.* (1995) utilizing gyrofluid and gyrokinetic nonlinear simulations of the plasma turbulence, have successfully predicted the observed variation of the confinement time and ion and electron temperature profile with plasma current and neutral beam power. The principal transport mechanism in these simulations is low-frequency electrostatic turbulence driven by ion temperature gradients. Over most of the plasma the ion temperature profile is found to be near marginal stability to the mode responsible for the turbulence. Although quite successful for L-mode plasmas, the model used by Kotschenreuther *et al.* (1995) has some important limitations, especially when applied to enhanced confinement regimes. First, the model is not applicable to the edge region (roughly $r/a > 0.85$) and experimental measurements are required to set

the boundary conditions. Also, the electron dynamics which affect particle transport (and hence the heat transport by convection) are known to be important in regimes of operation in which the ion temperature gradient driven turbulence is suppressed and are being incorporated in the model. The effect of shear in the poloidal and toroidal flow velocities is treated in an approximate fashion. This is an especially important mechanism in turbulence suppression and the formation of transport barriers as will be discussed further. Despite these caveats, this model provides a satisfactory prediction of the performance of L-mode discharges within its domain of applicability, and does not require any adjustable parameters.

Another approach has been pursued by Kinsey and Bateman (1996); Bateman *et al.*, (1995, 1996), and Kinsey *et al.*, (1996) using a multi-mode model in which analytic expressions are used to describe the dependence of plasma energy and particle transport in TFTR, JET and DIII-D discharges. In this approach, the numerical factor setting the transport level for each model is obtained by fitting the experimental data and evaluating the overall fit to the data (Kinsey *et al.*, 1995). The edge conditions are not taken from experimental data; however, the influx of neutrals from the edge is adjusted to obtain agreement with the measured density. The transport is predicted to be governed by electrostatic drift-wave turbulence and ballooning modes. The agreement between theory and experiment is satisfactory for a broad range of conditions. Further tests of the model employing both a wider range of data as well as response to plasma perturbations are required to evaluate the range of validity of the multi-mode model.

B. Enhanced Confinement Regimes

The experimental programs on JET and TFTR have focused on operating conditions which produce substantial fusion power and hence can be used to study alpha and other D-T related issues in reactor relevant conditions. Due to the low confinement in the L-mode discharges creating reactor-relevant conditions would require heating powers beyond those available. Thus, nearly all experiments have been conducted in enhanced confinement regimes: H mode, supershot, high- ℓ_i and, mostly recently, enhanced reverse shear discharges.

1. H mode

Since the discovery on the ASDEX diverted tokamak of an enhanced confinement regime known as the H-mode (for its high confinement time) by Wagner *et al.*, (1982) a great deal of research has been conducted on the physics of this regime. In it a transport barrier (i.e. an insulating layer) is established at the edge of the plasma resulting in reduced particle influx, broader density profiles and improved global energy confinement time. The difference between L and H mode discharges is that the core transport is reduced in H-modes. Furthermore, the global empirical scaling relationships for the energy confinement time for H-mode discharges has also an unfavorable scaling with power, implying an unfavorable temperature scaling, and has a favorable scaling with plasma current. H-mode operation has been extended to limiter discharges, albeit under more restrictive conditions.

Edge particle recycling is an important parameter in the degree of confinement improvement with lower recycling yielding improved confinement. Various wall coating and vessel conditioning processes as well as techniques to reduce the neutral influx from the divertors, are used to decrease the edge recycling in the main plasma chamber. On JET, beryllium evaporation was extensively used. Depending upon the density and the heating technique, it is possible to operate in the H-mode with $T_i > T_e$; the term hot-ion H-mode is commonly used for this operating regime. The transport barrier in the edge can suddenly collapse momentarily as a result of edge-localized-modes (ELMs). The transport barrier then can be re-established (or not, depending upon the plasma parameters). This ELM phenomenon is an important consideration for reactor designs because the heat loss to the divertor plates or limiter is suddenly and significantly increased during the relaxation. Under some conditions it is possible to operate without these relaxation events and the discharges are called ELM-free. ELM-free discharges have even better energy confinement though they are transient. The high performance JET D-T experiments were conducted in ELM-free hot-ion H-mode discharges. The plasma parameters for discharges from the JET PTE experiment which achieved the highest fusion power and triple product are given in Table III and the density and temperature profiles are shown in

Fig. 8. H-mode transitions have also been observed in limiter high ℓ_i discharges on TFTR and will be discussed in Sec. III. B.3 and V.A.

The mechanisms responsible for the formation of a transport barrier in the edge region have been reviewed by Ward (1996) and Carlstrom (1996). The basic model underlying many theories of H-mode is that a large radial electric field or electric field gradient is formed in the edge region which reduces the amplitude of the turbulent fluctuations or the correlation between the pressure and potential fluctuations. The parameter of importance in many theoretical studies is the shearing rate, which is the rate at which an ordered structure in the turbulence is pulled apart by $\mathbf{E} \times \mathbf{B}$ rotation shear. Though a comprehensive model of the H-mode has not been established, there is growing agreement on the importance of shear in the radial electric field.

In the core region, the temperature profiles of H-mode plasmas in JET have been successfully simulated by Bateman *et al.* (1996) with the same multi-mode model which describes L-mode plasmas. In these simulations, the measured edge parameters are used as boundary conditions because this model does not simulate the development of the edge transport barrier. The inference from these simulations is that the underlying transport mechanisms within the transport barrier are the same in H and L-mode discharges. In these simulations, the higher edge temperatures resulting from the transport barrier reduce the core transport, because the turbulence is near a condition of marginal stability and attempts to maintain the ion temperature gradient. The reduction in transport in the edge enables the attainment of high confinement times, plasma stored energy and consequently, fusion power. This analysis along with a large experimental literature indicates the importance of edge conditions in plasma confinement.

Transient changes to the transport barrier in the edge by the occurrence of edge localized modes provide interesting tests of transport models. Cordey *et al.* (1995) and Bak *et al.* (1996) analyzed the rapid increase of electron temperature throughout the plasma cross-section following the occurrence of an L \rightarrow H transition and concluded that on JET the transition can not be explained by a sudden reduction in transport in just the edge region only. Much better agreement is obtained by a model in which there is a sudden reduction in transport everywhere outside the $q=1$ region after

the L \rightarrow H transition. Whether these results can be adequately described by the models of Bateman *et al.*, (1996) or Kotchenreuther *et al.*, (1995) is not known. Bak *et al.*, (1996) also have shown that there are three phases in discharges with ELMs. During the ELM (≤ 1 ms), the MHD event modifies the electron temperature not only near the plasma edge, but also far inside the plasma volume. Afterwards, the transport remains large and exceeds the L-mode value for 10-30 ms and then the transport is reduced to the low H-mode level. Thus, in understanding and interpreting H-mode discharges, it is necessary to know the frequency and amplitude of the ELMs as a result of the complex interplay between MHD instabilities at the edge and core transport. A comprehensive model for both the transport barrier formation, change in underlying transport, and relaxation of the barriers due to MHD instabilities does not exist. However, major elements of a model are now emerging.

The maximum stored energy in high performance JET discharges is limited by the occurrence of "X-events." The X-events involve increased MHD activity, loss of confinement and influx of impurities which set operational limits on the maximum stored energy. The phenomena responsible for the degradation in performance are both complex and varied. The JET Team (presented by Thomas) (1996), has identified the importance and interaction between giant ELMs, sawteeth and outer modes. Sawtooth oscillations are a common MHD instability in tokamak discharges and are characterized by a periodic collapse of the pressure of the plasma core and a redistribution of the particles and energy. The so-called outer modes have been identified as saturated low m/n external kinks. The giant ELMs occur when the plasma is calculated to be unstable against kinks and ballooning modes simultaneously. The occurrence of MHD instabilities for a duration short compared with τ_E and the subsequent degradation of the energy confinement time and fusion performance is believed to be associated with the modification of edge conditions, due to the onset of MHD instabilities and possible interaction with the plasma facing components, which in turn affects the core confinement. After the initial onset of MHD instabilities, the plasma does not, in general, regain the high performance condition prior to the degradation even if the activity subsides and remains quiescent for a period longer than the energy confinement time. Very recently, Wesson

and Balet (1996) have inferred an abrupt change in the underlying core transport after the occurrence of these instabilities and prior to a significant change in the plasma parameter. Further work is in progress to understand this seeming irreversible and rapid degradation in confinement in the highest performance discharges.

2. Supershot

Strachan *et al.* (1987) demonstrated that by extensively conditioning the limiters to decrease the influx of deuterium and carbon from the limiters, enhanced confinement discharges are obtained in limiter discharges. These enhanced confinement discharges are characterized by peaked density profiles, $[T_i(0)/T_e(0) \sim 2-4]$, high edge ion temperature, and strong beam particle fueling. These discharges are commonly referred to as supershots and have been extensively studied on TFTR. Recently more effective conditioning techniques involving lithium coating of the limiter have been used to further suppress the influx of deuterium and carbon and to extend the range of operation (Mansfield *et al.*, 1995a,b). Table IV provides a summary of parameters from high performance deuterium-tritium supershot discharges on TFTR. The density and temperature profiles are shown in Fig. 9 for the discharge with the largest triple product and are contrasted with an L-mode discharge.

In TFTR high-performance discharges (supershots, and high ℓ_i), the sawtooth instability is typically stabilized even when the central safety factor, $q(0)$, is less than one. Levinton *et al.* (1994) showed that when the pressure and density profiles are sufficiently peaked compared with the shear in the q -profile, stabilization occurs as predicted by a two-fluid MHD model (Zakharov and Rogers, 1992; Zakharov, Rogers and Migliuolo, 1993; Rogers and Zakharov, 1995).

Core transport in supershot discharges is substantially reduced compared with L-mode discharges. The global parametric confinement scalings which characterize L-mode discharges do not describe the trends in supershot discharges (Bell *et al.*, 1988). In supershots, the confinement time remains approximately constant with both neutral beam heating power and the plasma current, whereas in L- and H-mode discharges the confinement is observed to decrease with power and increase with current. Regressions on the supershot database, as well as dedicated experiments, reveal

a strong adverse dependence of confinement upon the influx rates of carbon and deuterium measured spectroscopically (Strachan 1994). One consequence of an increased influx of carbon and deuterium is to broaden the density profile and reduce the depth of penetration by the neutral beam. H.K. Park (1996) has shown that the energy confinement time is also correlated with central beam fueling.

Local transport studies of supershots indicate that most of the improvement in confinement is associated with the reduction of ion heat conduction (Scott *et al.*, 1990a,b; Zarnstorff *et al.*, 1989a,b) and ion particle transport (Synakowski *et al.*, 1993). Though in L-mode discharges, the ion heat conduction is typically much larger than ion heat convection, in the core of supershots the upper bound for the ratio of $Q_i/\Gamma_i T_i$, where Q_i is the total ion heat transport and Γ_i is the ion particle flux, is only $\sim 3/2$ with balanced injection indicating that conduction is relatively small. In the electron channel, the ratio of $Q_e/\Gamma_e T_e$ is 2. Perturbation experiments by Kissick *et al.*, (1993) also demonstrated that convective heat transport was dominant in the core of supershots. As noted by Zarnstorff *et al.*, (1988a, 1989a) this implies that electron heat transport is not consistent with a strong stochastic particle loss and lends support for the contention that the transport is due to electrostatic driven turbulence. The transport studies also indicate a very different scaling of χ_i and χ_ϕ with T_i . Meade *et al.*, (1991) and Scott (1990b) observed that χ_i and χ_ϕ decreased with T_i in supershot discharges.

The analysis by Kotschenreuther *et al.*, (1995) using the gyrofluid and gyrokinetic models indicates that the reduction in transport is associated with the suppression of ion-temperature-gradient driven modes due to large values of T_i/T_e which at least in part is made possible by the high edge ion temperature and peaked density profiles. However, as noted above, this model did not have a comprehensive treatment of the particle dynamics and, in particular, the convective heat transport in the core and the effect of radial electric field shear stabilization. Thus, these results, while suggestive and supportive, are not conclusive. A general consequence of ion temperature gradient models is that one would qualitatively expect that if the edge temperature were reduced, the ion transport would rapidly increase and that such an edge perturbation would propagate into the plasma. Experiments

10. These modes appear spontaneously, have low frequencies (< 50 kHz), and low poloidal and toroidal wave numbers $m/n = 3/2, 4/3,$ and $5/3$. The $2/1$ mode is rarely observed but is particularly detrimental to confinement. The nonlinear evolution of these modes agrees well with the predictions of neoclassical pressure gradient driven tearing mode theory. The predicted evolution and width of the saturated island is found to be in good agreement with measurements as shown in Fig. 11. Though the present theory predicts several important trends in the data, it does not predict a threshold island width and therefore, when and which modes should grow.

In discharges on TFTR with high toroidal field and plasma current, the neoclassical tearing modes do not appear to be a significant limitation. In these discharges, the maximum stored plasma energy is limited by the onset of a rapidly growing intermediate- n ballooning instability ($n = 10-20$) coupled to a low- n ideal kink mode (Nagayama *et al.*, 1993; Fredrickson *et al.*, 1995a, 1996a). The distortions to the plasma caused by the large low- n ideal mode appear to push the plasma over the ballooning mode stability boundary. The ballooning-mode precursor to the disruption was discovered using two grating polychromators separated toroidally by 126° to measure the electron temperature as shown in Fig. 12. From this data, it is possible to deduce that the ballooning mode is both toroidally and poloidally localized on the outboard midplane. Park *et al.*, (1995) using a three-dimensional nonlinear MHD code have successfully modeled the observed electron temperature fluctuations, as shown in Fig. 13. These simulations indicate that the high- n mode becomes even more localized producing a strong pressure bulge that destroys the flux surfaces, resulting in a thermal quench. This instability limits the maximum fusion power achieved in supershots on TFTR and can result in a plasma disruption.

Operational experience has developed well-defined guidelines for regimes in which the probability of disruption is small. Mueller *et al.*, (1996) have characterized the operation regime of supershots in terms of the parameter β_N and the density peaking parameter, $n_e(0)/\langle n_e \rangle$. The likelihood for disruption increases with both increased values of β_N and $n_e(0)/\langle n_e \rangle$. In TFTR, as a result of aggressive wall conditioning which enables the limiter to pump (absorb) escaping particles, and strong central beam fueling, values of $n_e(0)/\langle n_e \rangle$ up to 4.6 have been attained. Since the

variation in the temperature profile is much less, $n_e(0)/\langle n_e \rangle$ is a useful indicator of the peaking of the pressure profile. (Another important parameter in the MHD stability is the current profile shape as will be discussed below). By restricting the operating range of β_N and $n_e(0) / \langle n_e \rangle$, it is possible to operate with an acceptably low probability of disruption ($\sim 10^{-2}$) for discharges with fusion power about half the highest achievable.

In high-power neutral-beam-heated discharges, the stored energy and neutron flux are observed to decrease with an increase in the influx of hydrogenic and carbon impurities. At the highest power (> 30 MW) rapid influxes of carbon sometimes occur. This phenomenon, which has been observed on both JET and TFTR, is called a "carbon bloom". The influx is attributed to localized regions of the divertor or limiter overheating (Ulrickson *et al.*, 1990). A more common occurrence at lower power is the gradual increase in both deuterium and carbon recycling during neutral beam injection. Li wall conditioning by means of pellet injection is found to significantly reduce carbon and deuterium recycling and improve confinement (Terry *et al.*, 1991; Strachan *et al.*, 1992, 1994c; Mansfield *et al.*, 1995a,b). By means of extensive Li pellet conditioning, the energy confinement time has been increased to 340 ms and the highest fusion-triple product of $n_{HYD}(0) T_i(0) \tau_E^* = 8.0 \times 10^{20} \text{ m}^{-3}\cdot\text{s}\cdot\text{keV}$ where n_{HYD} is the sum of hydrogenic ion densities has been achieved for the condition shown (shot 83546) in Table IV. However, for heating pulse durations significantly greater than τ_E and at high power (> 30 MW) the favorable confinement is observed to decrease during the high power phase. Techniques need to be further developed to extend the duration of the high power enhanced confinement regime.

3. High ℓ_i

Since MHD stability at present limits the maximum fusion power attainable in TFTR supershots, current profile modification has been explored to increase the operational parameter range. Two different operating regimes, high ℓ_i and reversed shear, have been studied.

In present high-performance plasmas, the discharge duration is less than the current relaxation time. Thus by varying the time evolution of the plasma current, it is possible to change the

current profile within the plasma and experimentally evaluate the effect of the current profile on confinement and stability. On TFTR, two approaches have been used to obtain high- ℓ_i discharges: 1) by rapidly decreasing the plasma current or 2) using a novel growth technique to alter the current profile at constant plasma current. By ramping down the plasma current, the peakedness of the current profile and, thus, the plasma internal inductance are transiently increased. Using this technique, the energy confinement and plasma stability are increased relative to a discharge with a relaxed (broad) current profile at the same total plasma current. This regime of operation on TFTR is called the high- ℓ_i (or high- β_p) regime and has been studied in D (Navratil *et al.*, 1991; Sabbagh *et al.*, 1991; Zarnstorff *et al.*, 1991); and D-T discharges (Sabbagh *et al.*, 1995a,b; 1996). In the current rampdown experiments, H-mode transitions were frequently observed which enabled the effects of tritium on H-mode physics to be studied.

More recently, another method has been developed to produce high ℓ_i plasmas at high current (Fredrickson *et al.*, 1996d, Sabbagh *et al.*, 1996). The method involves starting the discharge at very low edge q , $q_a \sim 2.5$, by reducing the minor radius, increasing the current to its final level at constant q_a then expanding the minor radius rapidly to a near full-aperture discharge. This is conceptually similar to the technique of expansion of the plasma elongation developed on DIII-D in which the plasma shape was suddenly changed to alter the current profile distribution (Lao *et al.*, 1993). Since the current profile expands relatively slowly after the plasma motion, the internal inductance is transiently higher. Motional Stark Effect (MSE) measurements of the current profile show that the high ℓ_i plasmas have an increased core current density and an increased radius of the $q = 1$ surface compared with supershot plasmas as shown in Fig. 14. This technique has the advantage that it is not necessary to achieve currents substantially greater than the final current to attain higher values of the internal inductance.

A summary of parameters for the high- ℓ_i discharge which achieved the highest fusion power is given in Table V. In terms of the normalized parameters β_N and $H \equiv \tau_E/\tau_E^{\text{ITER89-P}}$, these discharges access a much broader range of operating space as shown in Fig. 15 than supershots. At present, the maximum fusion power produced in the high- ℓ_i regime is 8.7 MW with a stored energy

of 6 MJ, which is comparable to that achieved in supershots with similar neutral beam powers (Sabbagh *et al.*, 1996) but at higher current and field. At this time, the maximum performance in high- ℓ_i discharges is not limited by MHD stability, but by the confinement time and the occurrence of carbon blooms at high heating power. Further development of limiter wall coatings and power handling techniques is required to evaluate the potential of this regime.

4. Reverse Shear

Theoretical studies including those in support of the design of the SSTR (Ozeki *et al.*, 1993) and the Tokamak Physics Experiment (Kessel *et al.*, 1994, Turnbull *et al.*, 1995) predicted that by creating a plasma core with reversed magnetic shear, i.e. $dq/dr < 0$ over some region of the profile, it would be possible to reduce plasma transport as well as increase MHD stability. The recent development of operational techniques to create this magnetic configuration coupled with new diagnostics to measure the pitch of the magnetic field on TFTR (Batha *et al.*, 1995a; Levinton *et al.*, 1995), DIII-D (Strait *et al.*, 1996), and JT-60U (Fujita *et al.*, 1996) have resulted in rapid progress and exciting new results which have been recently reviewed by Navratil *et al.*, (1996). Very recent and significant work on the effect of modifying the core current profile has been reported by the DIII-D group (Lazarus *et al.*, 1996a,b), JT-60U group (Ushigusa *et al.*, 1996), JET-PD (JET Team [presented by Gormezano] 1996), and TFTR (Levinton *et al.*, 1996; Synakowski *et al.*, 1996a,b).

To create a reverse magnetic shear configuration, the plasma is typically started at full size and the current is ramped up rapidly. Since the current diffusion time is slower than the rise time of the total plasma current, the current density profile, $j(r)$, is hollow during and for some time after the ramp. Low power auxiliary heating is frequently applied during the current ramp which raises the electron temperature, decreasing the plasma resistivity and slowing the inward diffusion of current. This prelude heating is followed by the main heating phase of beam injection as shown for a TFTR discharge in Fig. 16. With variations of beam timing and total current, a range of q -profiles has been produced, with $q(0)$ in the range from 2 to 5 and q_{\min} from 1.8 to 3 according to Motional Stark Effect (MSE) measurements. This is shown in Fig. 17 (Batha *et al.*, 1995a).

The confinement characteristics of reverse shear shots on TFTR in the main heating phase resemble supershots with the same machine parameters. In particular, the global confinement time is enhanced relative to L-mode scaling and convection is important in the core power balance. However, above a power threshold (which depends on machine conditioning and the q-profile) the core transport changes abruptly at 0.2 - 0.3 sec into the main heating phase within the region of reversed shear. In TFTR discharges, the effect is most clearly seen on the central density evolution which can rise by more than a factor of 2 in 0.3 sec as shown in Fig. 18. Since the density outside the reversed shear region changes little, the density profile following the transition became very peaked, reaching values of $n_e(0)/\langle n_e \rangle \sim 5$. This state of improved confinement in the core of reverse-shear plasmas is known as enhanced reverse shear (ERS) in TFTR. Similar improvements in confinement have been observed in reverse shear plasmas in DIII-D, JET, JT-60U and Tore-Supra.

At the transition, the inferred electron particle diffusivity in the region of the steepest gradient drops by a factor of 10 - 50 to near neoclassical levels, while the ion thermal diffusivity falls to levels well below predictions from conventional neoclassical theory (Levinton *et al.*, 1995) as shown in Fig. 19. Similar improvements in the ion momentum diffusivity have also been observed. The region of steepest pressure gradients and where the transport coefficients drop is where a transport barrier is assumed to form. Relatively small changes are observed in the electron heat conductivity. Similar behavior of the transport coefficients in reverse shear plasmas is seen on DIII-D as well, but both JT-60U (Fujita *et al.*, 1996) and Tore Supra (Hoang *et al.*, 1994) have reported significant decreases in χ_e . Possible explanations for the apparent sub-neoclassical ion thermal diffusivity are the violation of the assumptions of standard neoclassical theory, the presence of anomalous electron-ion coupling, or a thermal pinch. Recent calculations by Lin *et al.*, (1996) indicate that a more comprehensive analysis of neoclassical transport which considers orbit dimensions comparable with pressure scale lengths is in better agreement with the data in the enhanced confinement regime. Inasmuch as neoclassical transport is usually thought to be the minimum transport possible, these results represent a dramatic improvement in confinement and performance.

Theories developed to explain the transport barrier formation in H-mode discharges (Biglari *et al.*, 1990; Shaing, *et al.*, 1990; Hahm 1995; Hahm and Burrell, 1995) are being investigated to understand the formation of the transport barrier in ERS discharges (Diamond *et al.*, 1996; Hahm *et al.*, 1996). In TFTR, the inferred shear in the radial electric field increases in the region of the transport barrier after the transitions. This growth in the shear is driven by the increasing pressure gradient in TFTR discharges though in experiments with uni-directional beam injection such as DIII-D toroidal velocity gradients appear to be important. A model for enhanced core confinement is being investigated (Diamond *et al.*, 1996) whose central features are positive feedback between increased pressure gradients, the accompanying growth in electric field shear, and subsequent turbulence decorrelation and confinement improvement. In addition, the gradients in the Shafranov shift of reverse-shear plasmas lead to favorable drift precession of trapped electrons, and subsequent reduction of turbulence-induced flows (Beer, 1996). Recently, Drake *et al.*, (1996) have suggested that local negative shear may be important in the formation of a transport barrier though the particular instability (drift-resistive ballooning modes) is believed to be stable in the core. The ERS transition has been correlated with the suppression of turbulence by the **ExB** shear flow; that is when the shearing rate $\gamma_s \equiv |(\mathbf{R}\mathbf{B}_p/\mathbf{B}) \cdot d/dr (\mathbf{E}_r/\mathbf{R}\mathbf{B}_p)|$ exceeds the plasma turbulence decorrelation rate which is estimated to be about the linear growth rate of the turbulence. After the ERS transition, the fluctuation level in the core is dramatically suppressed according to reflectometer measurements (Mazzucato *et al.*, 1996a,b). Experiments on TFTR indicate that **ExB** shear is necessary to achieve an internal barrier and that the gradient in the Shafranov shift is not sufficient to maintain the barrier (Synakowski *et al.*, 1996a,b; Levinton *et al.*, 1996). Though the agreement between theory and experiment is very promising, further work is in progress to understand why the present models do not adequately describe the dependence of the power threshold on the toroidal field and neutral beam induced rotation. Also, it is unclear whether the higher power threshold for ERS discharges in T versus D can be readily reconciled with simple **ExB** mechanisms (Scott *et al.*, 1996b). Another topic requiring further investigation is the apparent decoupling of the electron and ion heat diffusivity, perhaps suggesting that more than one mechanism is important in core transport.

The MHD stability in ERS discharges is an active area of investigation due to the potential for increased performance. In the region of reversed shear, MHD activity is absent in ERS discharges as measured by the four channel reflectometer, suggesting that, as predicted by theory, reversed shear plasmas may indeed have greater local MHD stability. The local pressure gradient in flux coordinates in enhanced reversed shear discharges on TFTR is larger, by a factor of 3-5, than that in typical supershots with monotonic q profiles, which very often have low- n MHD modes in the core. However, as the transport barrier moves into the weak or positive shear region and as the radius of the minimum value of a q (r_{\min}) moves to the core region, a rapidly growing MHD instability is observed. The maximum pressure appears to be limited in this region by the ideal infernal mode. Comparison of the structure of the observed and calculated mode as shown in Fig. 22 is in good agreement, and the threshold is in reasonable agreement (Hender *et al.*, 1996; Manickam *et al.*, 1996). In at least one case, the infernal mode was coupled to a moderate n , toroidally localized ballooning mode, similar to what occurs in the supershot disruption (Park *et al.*, 1996). The MHD behavior in both the prelude and postlude phases is even more complex with the occurrence of double tearing modes which can also disrupt the plasma (Chang *et al.*, 1996a).

In most present experiments, the current and pressure profiles are not actively controlled but evolve towards a resistive equilibrium. The evolution of the current profile is due not only to the formation technique which creates an initially hollow current profile, but also to the generation of bootstrap currents which are driven by the strong pressure and density gradients due to the improved confinement. Kikuchi and Azumi (1995) have recently reviewed the work on bootstrap current. Bootstrap currents were first theoretically predicted by Galeev (1970) and Bickerton *et al.*, (1971) and experimentally inferred to exist on a tokamak (TFTR) by Zarnstorff *et al.*, (1988b), and subsequently on JET (Challis *et al.*, 1989) and JT-60 (Kikuchi *et al.*, 1990). The bootstrap current reduces the auxiliary current drive requirement and facilitates the development of a steady state reactor concept. In present experiments, the bootstrap current generated by the pressure profile is not well-aligned with the current profile required for MHD stability. New techniques, such as the application of ion Bernstein waves (Biglari, Diamond and Terry, 1990; Craddock and Diamond,

1991; Biglari *et al.*, 1992; Craddock *et al.*, 1994) to control the internal transport barrier location and hence the pressure profile, have been demonstrated on the PBX-M tokamak (Ono, 1993) and are under development to control the evolution of the bootstrap current. In lower β_p discharges, the bootstrap current is smaller and hence, less important. Under these conditions, Ide *et al.*, (1996) have demonstrated that it is possible to sustain the reversed shear configuration non-inductively by using lower hybrid waves. Extension of this technique to higher β reversed shear discharges in which the evolution of the bootstrap current is substantial will be an important demonstration of combining improved MHD stability and enhanced confinement.

IV. FUSION POWER PRODUCTION

The fusion power in TFTR D-T and D discharges increases nonlinearly with the plasma stored energy ($P_{\text{fus}} \propto W_{\text{tot}}^{1.7}$) as shown in Fig. 21. This illustrates the motivation for developing enhanced confinement regimes with increased MHD stability to increase the plasma stored energy.

The discharges with the highest fusion power produced are shown in Figures 22 and 23 for JET and TFTR. In both devices, the decrease in fusion power during the high power heating phase is triggered by MHD instabilities followed by carbon blooms. In the JET D-T experiments, a sawtooth collapse coupled to an ELM, led to a carbon bloom. In the TFTR high power discharge shown in Fig. 23, a minor disruption terminates the high performance phase. The total fusion yield from a single plasma pulse has reached 6.5 MJ on TFTR. The fusion power densities achieved at the center of high-performance TFTR supershots, up to 2.8 MWm^{-3} are comparable to, or greater than, those expected in ITER. The fusion power density in the JET discharges was 0.08 MWm^{-3} . The value of $P_{\text{fus}}/P_{\text{aux}}$ reached 0.12 in JET and 0.27 in TFTR. The fusion power density in the JET discharges was suppressed by the relatively low concentration of tritium compared with deuterium in their initial experiments. The JET Team (1992) has projected that for the parameters of their D-T discharges, the fusion power would have increased from 1.7 MW to 4.6 MW with an optimum fuel mix and the ratio of $P_{\text{fus}}/P_{\text{aux}}$ would have increased to 0.32.

In the literature, the quantity Q_{DT} which in steady-state discharges is defined as $Q_{DT} = P_{fus}/P_{aux}$, where $P_{aux} = P_{\Omega} + P_b + P_{RF}$, P_{Ω} is the ohmic heating power, P_b the neutral beam heating and P_{RF} the RF heating power, is often used to describe the fusion performance of plasma discharges. Though Q_{DT} has very limited engineering usefulness *per se*, it is commonly used as a figure of merit to illustrate technical progress. In discharges in which there are significant effects associated with the time variation in stored energy or heating power, several different definitions of Q_{DT} have been used. The TFTR group adopted the convention that $Q_{DT} = P_{fus}/P_{aux}$ during the high power phase. This definition provides a simple figure of merit for the performance of high power discharges relative to the auxiliary heating system but cannot be extended to transient conditions such as when the heating power is turned off or decreased to a lower value. (An example of such an experiment is the postlude phase shown in Fig. 16). The JET Team, (1992) has defined it as the sum of separate terms arising from thermal-thermal, Q_{tt} , beam-thermal, Q_{bt} and beam-beam, Q_{bb} reactions:

$$Q_{DT} = Q_{tt} + Q_{bt} + Q_{bb}$$

where $Q_{tt} = P_{tt}/(P_{loss} - 0.2 P_{tt})$

$$Q_{bt} = P_{dt}/(P_b - P_{st})$$

$$Q_{bb} = P_{bb}/(P_b - P_{st})$$

P_{tt} , P_{bt} , and P_{bb} are the fusion powers, respectively from thermal-thermal, beam-thermal and beam-beam reaction, $P_{loss} = P_b + P_{\Omega} - P_{st} - dW/dt + P_{\alpha i} + P_{\alpha e}$ where $P_{\alpha i}$, $P_{\alpha e}$ is the alpha heating power to the ions and electrons and P_{st} is the neutral beam “shinethru” power which is not absorbed by the plasma but impinges on the protective armor beyond the plasma. This definition excludes part of the inefficiency associated with the neutral beam heating system by ignoring the shinethru power. In hot-ion discharges such as those achieved on TFTR (McGuire *et al.*, 1996) and JT-60U (Ushigusa *et al.*, 1996) and to a lesser extent on JET (the JET Team, presented by Jacquinot, 1996), in which the central ion temperature is approaching 2/3 of the mean energy of the beam injected ions the distinction between thermal and beam-thermal reactions is somewhat arbitrary and depends on when a thermalized beam ion is considered part of the thermal distribution. However, under the definition

used by JET, the value of Q_{DT} does depend upon this distinction, since the term dW/dt is included in the thermal component. Another issue with this definition of Q_{DT} is that it does not take into account the effect of how the heating power affects the plasma transport. This may be especially important if the high power phase creates a transport barrier (or reduces transport) which can not be sustained in the lower power phase for time durations long compared with the core energy and particle confinement time, such as in the “postlude” phase. In the literature, factors of 1.6 can be found due to differences in the definition of Q_{DT} .

The usefulness of the parameter Q_{DT} is further complicated because, with the exception of the TFTR and JET experiments, measurements are made in D discharges and then extrapolated to what would occur in D-T. In the literature, the term Q_{DT}^{Equiv} is commonly used for such a projection. The extrapolation is typically performed by using computer codes though both the JET Team (1992) and Jassby *et al.*, (1996) have utilized trace tritium experiments in conjunction with computer modeling to extrapolate to an optimum D-T mix. The extrapolation from D to D-T depends on various assumptions which will be discussed below and only recently have the codes and assumptions been benchmarked, in actual D-T conditions. A more consistent technique for comparing the performance of deuterium discharge is to compare the ratio of P_{fus}/P_{aux} with the caveats and limitations described above; however, as with the definition of Q_{DT} , there are differences in viewpoint within the community.

Simulations of the neutron production on JET and TFTR have been performed using the TRANSP data analysis code (Hawryluk, 1980; Goldston *et al.*, 1981; Budny 1994a; Budny *et al.*, 1995). This code uses the measured electron density and temperature profiles, ion temperature profile, and visible Bremsstrahlung measurements in conjunction with other diagnostic and engineering data, such as the beam heating power and source divergence, to calculate the neutron source rate from thermal, beam-thermal, and beam-beam reactions. The ratio of thermal reactions to those from beam-thermal and beam-beam reactions depends upon the density, electron temperature and beam parameters. The overall agreement for both the time dependence of the D-T neutron emission and the neutron emissivity profile is well described by the TRANSP code as shown in Figs.

24 and 25 for JET (JET Team, 1992) and TFTR supershot discharges (Budny *et al.*, 1995) respectively. Typical results are shown in Fig. 26 for TFTR supershot discharges for the neutron emissivity profile and good agreement is found in the radial profile (Budny *et al.*, 1995). Bell *et al.*, (1994) have noted, however, that despite the reasonable agreement in deuterium-tritium discharges, there appears to be a small but consistent difference in the TFTR results for similar D-only plasmas. The TRANSP code predicts the neutron emission in deuterium discharges to be lower than the measured values by approximately 20%. The cause for this relatively small discrepancy is not understood.

Since experiments on most fusion devices utilize only deuterium fuel, computer codes such as TRANSP are used to extrapolate from deuterium experiments the fusion power in deuterium-tritium experiments. In these codes, the expected fusion reactivity enhancement in D-T plasma over their deuterium counterparts can be estimated from the ratio of the velocity-weighted fusion cross-section for DT and DD reactions. For fixed fuel density and temperature, the ratio of P_{DT}/P_{DD} from purely thermal reactions reaches an idealized maximum of ~ 223 for $T_i \sim 12$ keV but the ratio decreases to ~ 150 at $T_i = 30$ keV. For discharges in which the reactivity is enhanced due to non-thermal reactions, the ratio of P_{DT}/P_{DD} also decreases for T_i above 15 keV. Experimentally in high performance supershots on TFTR, the ratio of P_{DT}/P_{DD} is ~ 115 if plasmas with the same stored energy are compared (Bell *et al.*, 1994; McGuire *et al.*, 1996; Bell *et al.*, 1996). This ratio is especially relevant if the stored energy is constrained by β -limiting disruptions. When comparing plasmas with the same heating power, the stored energy in D-T plasmas is typically higher than similar D-only plasmas due to a favorable isotope effect (which is discussed in the next section) as well as the increased stored energy from the beam injected tritons and alpha particles. As a result, the power ratio P_{DT}/P_{DD} is ~ 140 at constant beam power. This value is experimentally relevant when, for example the heat flux to the plasma facing components limits the heating power. On TFTR, it is possible to increase the neutral beam heating power by operating the beam sources in tritium due to its higher neutralization efficiency. As a result of the increased beam power, the highest fusion power in TFTR D-T discharges is ~ 165 times greater than in D discharges. This was achieved by increasing

the plasma stored energy from 5.6 MJ in the D-plasma to 6.9 MJ in the D-T plasma, which required operating at higher magnetic field and plasma current.

Another practical consideration is that the ratio of n_D/n_T is determined not only by the ratios of the beam fueling rate, P_b^T/P_b^D , but also by the recycling and influx of hydrogenic species from plasma facing components (Bell *et al.*, 1994). A striking result of the TFTR experiments was the low level of tritium recycling at the limiters. Even in hot-ion mode supershot discharges without supplementary gas injection at the edge of the plasma (gas puffing), wall recycling is an important factor in fueling the plasma. The exchange of hydrogenic species at the limiters and walls is important in determining the mix of deuterium and tritium in the plasma. Fabry-Perot interferometer was used to measure the Balmer H_α , D_α , and T_α transitions from the plasma edge (Skinner *et al.*, 1995a,b) and Monte Carlo neutral transport simulation to interpret the measured line shapes (Stotler *et al.*, 1996). On a particular day, the T_α fraction was typically undetectable on the first D-T neutral beam fueled discharge [$T_\alpha/(H_\alpha + D_\alpha + T_\alpha) < 2\%$] and then increased by about 1% per discharge (Skinner *et al.*, 1996b). The maximum was 11% after 8 D-T neutral beam fueled discharges indicating that the incident tritium flux is being exchanged with the imbedded deuterium and hydrogenic species in the limiter. Only as a result of extensive gas puffing to fuel the discharge in support of L-mode experiments did the ratio increase to 75% (Skinner *et al.*, 1996b). To compensate for the influx of deuterium from the limiters and walls, the fusion reactivity was optimized in supershot discharges by increasing the tritium beam power (and hence fueling rate) relative to deuterium beam power (Bell *et al.*, 1994).

These practical considerations illustrate some of the issues in projecting from D to D-T operation. In addition, the results depend also on the operating density and temperature as well as the plasma response to changes in isotopic concentration and heating power deposition. For example, since the density in many low recycling conditions such as the supershot regime on TFTR and the hot-ion H-mode on JET is determined largely by beam fueling and wall recycling, it is difficult to optimize the plasma reactivity by independently varying the density, for the overall confinement is affected. In principle such an optimization and projection from one operating point to another is

possible but requires a very detailed understanding of how the underlying transport is affected by changes in the edge conditions associated with the influx of gas to fuel the discharge. As will be discussed in the next section, the confinement changes with isotopic concentration and needs to be incorporated in the projection. In addition, the tritium neutral beams do not penetrate as well resulting in slightly broader density profiles. In future long pulse devices, the accumulation of He ash must also be incorporated into the simulation. The integration of these various issues and operational constraints determines the observed ratio of P_{DT}/P_{DD} and differences in assumptions (explicit and implicit) account for the large variation in this parameter in the literature. This discussion also highlights some of the important physics issues of confinement, stability, power handling and fuel mix associated with projecting the performance of future machines and the need for a detailed characterization and understanding of the underlying physics.

V. CONFINEMENT IN D-T DISCHARGES

Previous experiments on a large number of devices and operating regimes have shown that the confinement in D discharges is different than in H discharges as discussed by Bessenrodt-Weberpals *et al.* (1993) and references therein, as well as in more recent experiments in the literature. The scaling of confinement time with isotopic mass is important for not only projecting the performance of future devices operating in D-T, but also as a test of different transport models. It was immediately apparent in the initial TFTR D-T experiments that the global energy confinement in supershots is significantly better in D-T plasmas than in comparable D plasmas (Hawryluk *et al.*, 1994a). This favorable result was also evident in high- ℓ_i plasmas including those with H-mode transitions. Recent D-T experiments in L-Mode plasmas on TFTR have shown that the global and thermal plasma energy confinement scale at least as favorably with average ion mass as the $\tau_E \propto \langle \text{AHYD} \rangle^{0.5}$ dependence embodied in the ITER-89 L-Mode scaling. Most transport models scale as gyro-Bohm with $\chi \propto \chi_B \rho^*$ where $\chi_B = cT/eB$, $\rho^* \equiv \rho/a$ and ρ is the ion Larmor radius and would predict an unfavorable scaling with ion mass. The favorable dependence of confinement upon ion mass is opposite to the ρ^* scaling predicted theoretically and observed in B-field scans and thus presents fertile ground for benchmarking theoretical models of transport. Due to the low concentration of tritium in the JET experiments as well as limited number of shots, no affect in the energy transport could be attributed to the presence of tritium (Balet *et al.*, 1993). The D-T discharges in JET had a higher ion thermal conductivity (poorer confinement) than the D discharge used for comparison but were similar to many other D discharges studied.

A. Isotope Effects on Energy Confinement

The initial D-T experiments in the supershot regime indicated an increase of up to 20% in τ_E between D and 50:50 D-T under identical external conditions (R , B_t , I_p , P_b held constant) (Hawryluk *et al.*, 1994a). The increase of global energy confinement time, τ_E , with average ion mass including more recent data is shown in Fig. 27. For higher heating power, 60-80% of the increase in W_{tot} between D and D-T plasmas is due to changes in the thermal plasma. An

improvement in thermal energy confinement with ion mass is observed for both supershots, limiter H-modes, high ℓ_i , and L-mode plasmas in TFTR.

Ion temperature measurements by charge exchange recombination spectroscopy show that the central ion temperature increased from 30 to 37 keV in going from D to ~50:50 D-T shown in Fig. 28. Since the central electron and ion densities remained approximately constant, $n_i(0) T_i(0) \tau_E^*$ increased by about 55% between D and ~ 50:50 D-T plasmas. In some cases, up to 80% improvements in the triple product have been obtained. Detailed profile measurements show that the effective ion thermal diffusivity (including conduction and convection) improves throughout the confinement region ($r/a < 0.75$) in a 50:50 D-T plasma relative to a D plasma as shown in Fig. 29 (Scott *et al.*, 1995, 1996a).

The inferred scalings in supershot plasmas with average isotopic mass are quite strong, with $\tau_E \propto \langle A \rangle^{0.82 \pm 0.06}$, $\tau_E^{\text{thermal}} \propto \langle A \rangle^{0.89 \pm 0.1}$, $\chi_i^{\text{tot}} \propto \langle A \rangle^{-2.6 \pm 0.3}$ and $D_e \propto \langle A \rangle^{-1.4 \pm 0.2}$ at fixed P_b . At fixed T_i , $\chi_i^{\text{tot}} \propto \langle A \rangle^{-1.8 \pm 0.2}$ is obtained so the observed isotopic variation of χ_i^{tot} cannot be explained by a simple dependence on T_i/T_e or by its previously observed correlation $\chi_i \sim T_i^{-1}$ in the supershot regime. When the isotopic scaling of χ_i is combined with the correlation with T_i^{-1} , this implies that roughly $\chi_i \propto A^{-1} \rho_i^{-2}$ (for fixed B) opposite to the gyro-Bohm dependence (Zarnstorff *et al.*, 1995). In both the supershot (Synakowski *et al.*, 1995b) and L-mode (Scott *et al.*, 1996b) regimes, matched density and temperature profiles were obtained with D and D-T plasmas by injection ~ 25% less beam power in D-T than in D. The matched pairs thus have the same β and v^* but different ρ^* , with the larger ρ^* in D-T corresponding to improved confinement as shown in Fig. 30 for an L-mode discharge. This trend is opposite to that inferred in ρ^* scans performed with a single isotope by varying the B-field.

H-mode plasmas produced on TFTR in high- ℓ_i D-T plasmas have energy confinement enhancements > 4 relative to the ITER-89P scaling while corresponding D plasmas had enhancements of ~3.2 as shown in Fig. 31 (Sabbagh *et al.*, 1995a,b; Bush *et al.*, 1994, 1995). The ion heat conductivity was improved across the plasma profile during the D-T H-mode as shown in Fig. 32. The edge localized modes are much larger and exhibit a lower frequency during the D-T H-modes

and may suggest that reactor D-T plasmas are more susceptible to giant ELMs than inferred from D only experiments. The power threshold for the transition to an H-mode is similar in D and D-T TFTR discharges. Due to the limited experimental campaign on JET, isotope scaling in diverted H-mode plasmas has not been established. Further experiments in the divertor JET configuration are planned and are necessary to extend the TFTR results.

A number of auxiliary-heating L-mode studies in both small and large tokamaks have demonstrated improved global energy confinement in deuterium versus hydrogen plasmas, typically scaling as $\tau_E \propto \langle A \rangle^{0.3-0.4}$ when neutral beams are used for auxiliary heating. Although some of this improvement can be attributed to purely classical differences in beam stored energy, higher central electron temperatures are consistently observed in the D plasmas, clearly indicating improvement in thermal electron energy confinement. A consensus regarding changes in ion heat and momentum confinement in L-mode H versus D plasmas has not emerged among the various tokamaks. TFTR L-mode experiments in H versus D with $P_b \leq 7$ MW (Barnes, *et al.*, 1996) observed $\tau_E \propto \langle A \rangle^{0.41 \pm 0.12}$, $\tau_E^{th} \propto \langle A \rangle^{0.26 \pm 0.11}$, small increases in $T_e(0)$, and no apparent change in thermal ion heat or momentum transport. Similar experiments in JET H versus D L-mode plasmas obtained results in reasonable agreement with the TFTR experiment, $\tau_E \propto \langle A \rangle^{0.32}$ and $\tau_E^{th} \propto \langle A \rangle^{0.20}$ (Tibone *et al.*, 1993). A fairly weak isotope effect on τ_E was also observed between D versus D-T plasmas in TFTR L-mode experiments at low beam power (~8 MW). Similar to the experience in D-T supershot plasmas, the isotope effect in the D-T L-mode regime appeared to increase with heating power, and at $P_b = 18$ MW, the confinement scaling was somewhat stronger than $\tau_E \propto \langle A \rangle^{0.5}$.

In addition to neutral beam heating, ICRF hydrogen minority heating in D and D-T L-mode plasmas, has been studied (Rogers *et al.*, 1996). The advantage of this technique is that the heating profile does not change. The observed increase in stored energy is consistent with $\tau_E \propto \langle A \rangle^{0.35-0.5}$. In these experiments clear evidence of a favorable scaling of electron heat diffusivity with mass was observed.

The favorable isotope scaling of energy confinement in supershot, H-mode, high ℓ_i and L-mode plasmas is a serious constraint to the models used to predict the heat and particle flux and

hence the energy confinement time. To resolve this discrepancy, several different effects are being investigated. Scott *et al.*, (1996b), have shown that the model of shear flow modification to the ion-temperature gradient turbulence reproduces the observed isotope effect in L-mode plasma. In addition, the role of multi-ion species (D, T, and C) is being invoked as possibly altering the turbulence and giving an apparently favorable scaling with ion mass. This remains an important area of investigation and the ramifications for the performance of larger devices have not been resolved.

Interestingly, in the TFTR reversed shear regime as well as the enhanced reverse shear, the isotope scaling with mass is absent (Scott *et al.*, 1996b). This result is especially surprising in the reversed shear plasmas whose profiles are similar to supershots. Why changes in the current profile should affect the isotope scaling remains to be clarified. In the ERS discharges, the power threshold for the formation of an internal transport barrier was significantly higher in a D-T discharge compared with a D discharge. Further work is required to assess the implication of this result for the new models of transport barrier formation.

B. Particle Transport

Due to the large differences in the nuclear reaction cross-sections between D-D and D-T reactions, tritium transport in a deuterium plasma can be inferred from profile measurements of the 14 MeV neutron source strength using the multi-channel neutron collimator diagnostic (Balet *et al.*, 1993; Johnson *et al.*, 1994). This was proposed by Strachan, Chrien and Heidbrink (1983) and now provides direct measurements of the transport of the hydrogenic species in a tokamak plasma. Inversion of the neutron source strength provides local measurements of the tritium density as shown in Fig. 33 following a small gas puff into a supershot discharge on TFTR. Analysis of the evolution of the profile indicates that the trace tritium particle diffusivity in supershot discharges is comparable to the electron diffusivity and to the ion thermal diffusivity as shown in Fig. 34. The tritium trace particle convection velocities are found to be small (Efthimion *et al.*, 1995a,b). Similar results were inferred from neutron profile measurements in JET experiments which utilized beam fueling using trace quantities of tritium injected into a deuterium hot-ion mode discharge (Marcus *et al.*,

1993). The evolution of the neutron profile after the turn-off of the beams was simulated using the TRANSP code. Balet *et al.*, (1993) concluded that the effective tritium diffusivity is similar to the effective deuterium diffusivity observed in similar pure deuterium discharges and to the effective helium diffusivity observed during the He beam injection into a deuterium plasma. This approach has been used to exclude various models for particle transport and to place constraints on the models, but does not determine the diffusivity and convection velocities separately as can be achieved by gas puffing experiments.

Recently, the transport of tritium has been studied in the steady-state “postlude” phase of ERS discharges on TFTR. The tritium profile remains hollow for a long time > 0.15 s and does not peak on axis. The results are qualitatively different from those in supershot discharges. In comparisons with reverse shear plasmas with similar q-profiles, but no transition, the tritium particle diffusivity is nearly one order of magnitude smaller inside the reverse shear region, while they are comparable outside the region. In the ERS case, the diffusivity drops an order of magnitude in going from r/a  0.45 to 0.35, a clear indication of a particle transport barrier. These lower diffusivities within the reverse shear region are consistent with neoclassical particle transport predictions for tritium. These results are qualitatively similar to those observed in the study of He transport. He gas puffing studies in the “postlude” phase show a rapid He density rise up to the barrier and a slow increase in He density within the barrier.

VI. HEATING OF D-T DISCHARGES

Neutral beam injection is used to heat and fuel JET and TFTR D-T discharges and RF heating in the ion cyclotron range of frequencies has been used to heat and drive localized currents on TFTR.

A. Neutral Beam Heating

Neutral beam injection has been extensively studied on a large number of tokamaks and is well understood. By injecting short pulses of high power D-T beams into TFTR and analyzing the evolution of the neutron profile, Ruskov *et al.* (1996) have studied the radial transport of the beam ions in TFTR in a set of 28 D and D-T discharges. Analysis of these discharges indicates that for 26 of the 28 the radial diffusion coefficient for the fast beam particles, D_f , is $< 0.2\text{m}^2/\text{s}$ as shown in Fig. 35 and implies that radial transport for the beam ions is not important. The two exceptions were in discharges with larger major radius in which the ripple in the toroidal field is greater. Stochastic ripple diffusion, which will be discussed in the Sec. VII.B.2, is believed to be responsible for the increased radial transport.

B. ICRF Heating

ICRF heating and current drive have been studied in D-T plasmas on TFTR. ICRF wave physics in D-T plasmas is complicated by the possibility of multiple, spatially separated resonances and by alpha particle damping which can compete with electron absorption in the fast-wave current-drive regime. A promising scenario for heating D-T plasmas is fast wave absorption at the second harmonic of the tritium cyclotron frequency, which is degenerate with the ^3He fundamental. By selectively heating a majority ion species rather than a minority ion species, potential difficulties with ICRF driven fast-ion excitation of MHD instabilities, such as toroidal Alfvén eigenmodes (TAE) instabilities, may be avoided. Though core damping is predicted to be acceptable, off-axis absorption near the deuterium fundamental and ion-ion hybrid layer is predicted to compete with the second harmonic tritium core damping in tokamaks with moderate aspect ratio. In TFTR supershot plasmas, with the second harmonic tritium ($2\Omega_T$) layer coincident with the Shafranov-shifted axis at 2.82 m,

the $2\Omega_D/\Omega_H$ layer is out of the plasma on the low field side, but the Ω_D layer is in the plasma on the high field side at $R \sim 2.1$ m for $B_t = 5.66$ T. Experiments have been performed utilizing combined ICRF heating and neutral beam injection in D-T plasmas (Taylor *et al.*, 1995, 1996a; Wilson *et al.*, 1995). These experiments have focused on the RF wave coupling and damping physics associated with D-T plasmas. Second harmonic tritium heating with ~ 5.5 MW (with a 2% He^3 minority) in a plasma with 23.5 MW of neutral beam injection (60% in T) has resulted in an increase of the ion temperature from 26 to 36 keV as shown in Fig. 36. The electron temperature increased from 8 to 10.5 keV due to direct electron damping and ^3He minority tail heating. Similar results were obtained in discharges in which no ^3He was added. Because of significant D (and minimal T) wall recycling, n_T/n_e was only $\sim 25\%$ - 30% in these plasmas. Despite this relatively low T concentration, as much as 70% of the RF power was absorbed by the ions. Comparisons with two independent full wave codes (PICES and TRANSP) show reasonable agreement with the observed ratio of ion to electron absorption as shown in Fig. 37 (Phillips *et al.*, 1995). In these experiments, the power is modulated and the local heating measured to determine the absorption mechanism.

Second harmonic ICRF heating experiments have also been performed in D-T L-mode plasmas which are not heated by neutral beams. The development of an ion tail has been measured using the pellet charge exchange diagnostic. A tritium tail temperature of ~ 350 keV has been obtained and shows localized heating within 0.2 m from the resonance locations (Duong *et al.*, 1996b). Despite the low single pass absorption due to the low ion temperature in this case, second harmonic tritium heating of an L-mode plasma has been demonstrated to be an effective technique to heat the plasma which is relevant to the startup phase of ITER. The increase in stored energy is the same as that obtained by injection of neutral beams into comparable plasmas (Rogers *et al.*, 1996).

Majeski *et al.*, (1994) have proposed a novel technique using the mode-converted ion Bernstein wave excited at the ion-ion hybrid layer in a multiple ion species plasma (such as D-T) for electron heating or for generating localized electron currents. In more conventional ICRF heating schemes, fast magnetosonic waves launched by antennas on the low-field side of the magnetic axis propagate into the core, where absorption by minority and/or majority ions occurs with or without

some mode conversion to IBW. In plasmas consisting of a majority ion species plus a low concentration minority ion species, the RF power absorbed by ions near the cyclotron resonance is enhanced by the presence of the nearby ion-ion hybrid layer. The ion-ion hybrid layer is located approximately, where $n_{\parallel}^2 = S$, where S is the familiar cold plasma dielectric tensor element and n_{\parallel} is the parallel component of the wave vector, k_{\parallel} , normalized to the free-space wavelength, ω/c , with ω equal to the wave frequency. At sufficiently high minority concentration, the fast wave can be cut off in the narrow region between the cyclotron layer and the hybrid layer, so the incident waves must tunnel through a cutoff region to reach the mode conversion layer and the high-field side of the discharge. High concentrations of a “minority” ion can be utilized to move the mode conversion/cutoff region outside of the Doppler-broadened ion cyclotron resonance region so that ion heating is minimized, while mode conversion of the incident fast waves to IBW is maximized. The “minority” species can be D in D-T plasmas, with mode conversion occurring near the D-T ion-ion hybrid layer, or ^3He in either D-T- ^3He or D- ^4He - ^3He plasmas, with the mode conversion occurring near the D- ^4He - ^3He ion-ion hybrid layer. For an isolated ion-ion hybrid layer, the maximum mode conversion that can be attained is approximately 25%. However, if the species mix, plasma density, toroidal magnetic field, and k_{\parallel} are chosen carefully, then the fast wave cutoff on the high toroidal side of the plasma (small R), which usually occurs in the low-density edge regions, can be moved into the high-density regions near the mode conversion/cutoff layers. This leads to a closely spaced “cutoff-resonance-cutoff” triplet and an increase in the mode conversion efficiency by a factor of 4 (i.e. approaching 100%) over the isolated hybrid layer can result due to constructive interference effects (Phillips *et al.*, 1995). Experiments on TFTR in D- ^3He plasmas demonstrated strong highly localized electron heating in multiple ion species plasmas as shown in Fig. 38, with > 80% of the ICRF power coupled to electrons near the mode conversion surface achieving temperatures of ~ 10 keV (Majeski *et al.*, 1995, 1996). The experimentally observed single-pass absorption efficiency for mode conversion heating can exceed the single pass absorption for direct fast wave electron heating by more than an order of magnitude. Efficient heating has been

demonstrated at radii over the range $0 < r/a < 0.5$, by changing either the toroidal field or ion species mix to move the mode conversion layer as shown in Fig. 39 (Majeski *et al.*, 1996).

Current drive has been demonstrated as well using the mode-converted ion Bernstein wave by phasing the antenna. This technique has been used to drive 130 kA of on-axis and off-axis current in a D-⁴He - ³He discharge. The experimentally observed non-inductive current (Majeski *et al.*, 1996) is in good agreement with the estimated driven current based on the Ehst and Karney (1991) parametrization as shown in Fig. 40. The combination of high single pass absorption and ability to drive localized off-axis currents, may make mode-conversion current drive MCCD a potentially attractive current drive technique.

Very recent mode-conversion heating experiments have been performed in D-T plasmas by lowering the source frequency to 30 MHz. The fraction of heating power going to the electrons decreased to $< 30\%$ (Rogers *et al.*, 1996). This low efficiency is believed to be due to competition from ⁷Li minority heating. ⁷Li is the most common isotope of Li (92.5% of natural Li) and is used to condition the vessel walls in TFTR. Calculations indicate that a concentration of 0.5% of ⁷Li would be sufficient to reduce the mode converted power to the electrons to the observed level. This can be avoided by using ⁶Li for wall conditioning or eliminating the use of Li. However, plasma facing components using beryllium would result in a similar problem due to the presence of ⁹Be in the plasma if the ⁹Be concentration is $> 0.1\%$. In this case, a suitable alternate isotope does not exist.

VII. ALPHA PARTICLE

The behavior of alpha particles from D-T reactions is a fundamental consideration for the performance of a future D-T reactor. If a significant fraction of the alpha particles is not confined, then the $nT\tau$ requirements for ignition will increase; however, the confinement of the resultant alpha ash must be sufficiently short to avoid quenching the reaction. Also, if a small unanticipated fraction (a few percent) of the alpha particles is lost in a reactor such as ITER and the resulting heat flux is localized, damage to first-wall components could result. Thus, a detailed knowledge of alpha particle

loss processes is vital to design the plasma facing components to avoid damage by energetic alpha particles.

In a tokamak, there are two generic classes of particles, those with passing orbits and those with banana orbits which mirror between the high field portions of the orbit as illustrated in Fig. 41. The loss of alpha particles to the plasma facing components is due to three generic mechanisms. The first mechanism is single particle effects due to the structure of the confining magnetic field. The main examples of such losses are (a) first orbit losses, due to particles born on fat banana orbits which intersect the wall, (b) ripple trapping losses, where particles are mirror trapped between toroidal field coils and drift out of the confinement region, and (c) stochastic toroidal field ripple diffusion, where trapped particles with their banana tips in certain regions can diffuse to the wall due to stochasticity brought on by toroidal field ripple. The second mechanism is alpha particle interactions with MHD instabilities and radio frequency waves, and the third is alpha particle interactions with MHD instabilities which are driven by the presence of alpha particles

A. Single Particle Effects

Single particle effects are the best understood theoretically and the losses can be evaluated by following orbits of individual particles numerically. Monte Carlo techniques are commonly used to calculate orbit trajectories in analysis such as TRANSP. Recent experiments provide a detailed test of the theoretical models.

1. First Orbit Loss Scaling

An extensive study of fusion product losses in deuterium experiments was conducted on TFTR prior to beginning D-T experiments (Zweben *et al.*, 1990; 1991; 1993a,b; 1994; Boivin *et al.*, 1993). Zweben *et al.*, (1995) have summarized the results from the deuterium experiments on TFTR using the escaping fusion product detectors described in Sec. II. B.2:

- (a) For MHD- quiescent R= 2.6m plasmas the loss to the 90^o detector was consistent with the expected first orbit loss over the plasma current range $I_p = 0.6 - 2.0$ MA.

- (b) An additional anomalous delayed loss was seen at 90° for $R = 2.45$ m plasmas at $I_p = 1.4$ - 2.5 MA.
- (c) During large coherent MHD activity there was an increase up to a factor of 3 in the losses at the 90° and 20° detectors.
- (d) The pitch angle distribution of the loss at 60° and 45° agreed reasonably well with the first orbit model at $I_p = 1.2$ MA.
- (e) There was a large non-first-orbit loss component in the 20° detector, which was consistent with the expected loss due to stochastic TF ripple diffusion.

The alpha flux measured in the 90° detector from quiescent discharges on TFTR is in good agreement with the first orbit loss model over the entire range of plasma current as shown in Fig. 42. Similarly good agreement is found in the pitch angle variation with current for the 90° detector (Zweben *et al.*, 1995; Darrow *et al.*, 1996a). Global losses in TFTR are calculated to vary from 3% of the total source rate at $I_p = 2.7$ MA to about 50% at $I_p = 0.6$ MA.

In contrast with the deuterium fusion product experiments, an additional delayed loss was not observed on the escaping alpha detector during D-T experiments. Zweben *et al.*, (1995) have suggested that this may be due to the different collisionality of 3.5 MeV alphas and the 1 MeV tritons. The tritons from D-D reactions have three times longer slowing down times which may make them more susceptible to being scattered into loss orbits either by collisions (pitch angle scattering) or MHD effects. Recent foil deposition measurements using an alpha collector probe by Chong (1995) and Herrmann *et al.*, (1996) are in good agreement with the 90° detector measurements at 1.0 MA but show a significant loss of partially thermalized ions in 1.8 MA plasmas similar to the delayed loss feature observed in D discharges. The difference between these two measurements has not been fully reconciled; however, the alpha collector probe indicates that the enhanced loss varies strongly with radial probe position. It is possible that the poloidal limiter in TFTR or other obstacles removes the partially thermalized alpha particles before they strike the scintillator detector. Several possible mechanisms to explain this have been examined by Herrmann *et al.*, (1996). One of the more promising is charge exchange loss, in which the previously confined alpha orbits transition to

prompt loss orbits as a result of electron capture from H-like carbon impurities. Further work is required to test this hypothesis; however, the observed strong radial dependence does not appear consistent with the large step-size diffusion that would be associated with this mechanism. Since the mechanism for the delayed loss is not understood, its impact on the design of first wall components in a reactor can not be estimated.

2. Stochastic Ripple Diffusion

Due to finiteness of the number of toroidal field coils ($N = 32$ in JET and 20 in TFTR), the variation in the magnetic field strength along a field line is in the range of $< 0.1 - 1\%$. Although this ripple is usually too small to cause significant ripple trapping, a more subtle form of “stochastic ripple diffusion” has been predicted by Goldston, White and Boozer (1981) which can result in rapid energetic ion loss when the ripple exceeds a threshold, γ , that is approximately given by

$$\gamma = (r/R \pi Nq)^{3/2} / 2 \rho q'$$

where q' is the local derivative of the safety factor. The ripple causes radial diffusion of banana orbits whose turning points lie within a certain zone. For alphas in TFTR, that zone is roughly $0.5 < r/a < 1$. Subsequently, a Hamiltonian coordinate guiding center code has been developed to simulate the transport of alpha particles in the presence of toroidal field ripple, including collisions, and first orbit loss (Redi *et al.*, 1995a). These guiding center codes which take into account the ripple in the toroidal field are typically relatively time consuming; however, there has been recent progress in developing a more rapid algorithm (White *et al.*, 1996). In the transport interpretative code, TRANSP, a simple stochastic domain model for TF ripple loss is used to simulate the alpha particle behavior which has been benchmarked against the more accurate guiding center model (Redi *et al.*, 1995b). As mentioned above, previous studies of fusion product loss on the 20° detector in TFTR deuterium discharge by Boivin *et al.*, (1993) were at least partially consistent with the predictions of stochastic TF ripple loss.

Measurements of D-T alpha particle loss near the outer midplane of TFTR are similar to those observed in D discharges (Zweben *et al.*, 1995). Several questions remain to be resolved before the

midplane measurements can be interpreted by a quantitative model for TF ripple loss of alpha particles (Zweben *et al.*, 1996c). One of the unresolved questions is the role of shadowing effects due to the outer limiter and the detector itself which complicates the interpretation of the data and may contribute to the lack of quantitative understanding (Wang and Zweben, 1996).

Recently, sensitive infrared camera measurements on JT-60U have been reported by Ikeda *et al.*, (1996). These measurements indicate a localized loss of neutral beam ions in good agreement with code simulations of the stochastic TF ripple loss. In ICRF discharges on JT-60U, enhanced loss, attributed to stochastic TF ripple diffusion, is also observed; however, a self-consistent simulation of RF heating and orbit trajectories has not been performed.

Tobita *et al.*, (1996) have studied the confinement of tritium produced by D-D reactions in JT-60U. The subsequent “burnup” of the triton by D-T reactions is measured to evaluate the confinement of tritons in both normal shear and reversed shear discharges. The tritons are found not to be as well confined in reversed shear discharges. The confinement of tritons is well described by Monte Carlo orbit calculations which include first orbit and stochastic ripple diffusion as well as collisional ripple loss.

3. Passing-trapped Particle Boundary Effects Due to ICRF

Coupling of the ICRF power to the fusion products has been observed in the TFTR D experiments (Darrow *et al.*, 1996d) and in D-T experiments (Rogers *et al.*, 1994). Fig. 43 shows the alpha particle loss signal from the escaping fast ion probe at the bottom of the vessel as a function of the toroidal field. The observed gyroradius of the alpha particles ejected during the RF implies energies equal to or slightly greater than the 3.5 MeV birth energy. RF heating of the alpha particles caused a fraction of the particles to cross the passing-trapped particle boundary and go onto loss orbits. When the toroidal magnetic field was below 3.6 T or above 4.5 T no RF-induced losses were seen. The shading in Fig. 43 indicates the range of toroidal field for which marginally passing alpha particles can be in Doppler shifted resonance with the RF wave, i.e. for which $\Omega_{\alpha} = \omega - k_{\parallel} v_{\parallel}$. This coincides with the range of fields for which losses are seen, supporting the hypothesis that these losses

arise from transforming marginally passing particles to lost banana orbits. Heating of these particles by the RF wave gives them sufficient additional v_{\perp} that they then mirror on the high field side of their orbit and are lost. At toroidal fields outside the range shaded, some alpha particles are still being heated, but are not being put into loss orbits.

B. Confined Alpha Particles

The distribution function of the confined alpha particles on TFTR has been measured using the pellet-charge-exchange diagnostics and charge exchange recombination measurements, which are described in Sec. II.B.3. The pellet-charge exchange diagnostic has obtained data when a boron pellet has been fired into a 1.6 MA D-T supershot, 0.2s after neutral beams were turned off. The measured shape of the energy spectrum of the alphas in the range from 3.5 MeV down to 0.9 MeV is in good agreement with TRANSP calculations of the predicted spectrum as shown in Fig. 44 where the data has been normalized to the TRANSP calculations (Fisher *et al.*, 1995; Petrov *et al.*, 1995; Medley *et al.*, 1995, 1996a). The alpha population in the lower energy range, 0.1 - 0.6 MeV, has been detected by absolutely-calibrated spectrometry of charge-exchange recombination emission (McKee *et al.*, 1995b, 1996). The measured spectrum agrees with TRANSP predictions both in the absolute intensities (within experimental error of 30%) and the spectral dependence, assuming classical collisional slowing down and neoclassical confinement as shown in Fig. 45 (McKee *et al.*, 1995b). Measurements of the spatial profile agree with TRANSP, and constrain the value of any anomalous radial diffusion coefficient to less than $0.03 \text{ m}^2/\text{s}$, in addition to the neoclassical coefficient which is estimated to be $0.01\text{-}0.05 \text{ m}^2/\text{s}$.

1. Sawtooth Instabilities

The effect of the sawtooth instability on the confined alpha particles has been studied on TFTR. As noted before, during the high performance phase on TFTR, the instability is typically stabilized. Thus the studies of alpha particle redistribution in TFTR are performed after the neutral beam heating power is decreased during which time the density and pressure profile relax and the

sawtooth instability reappears. Comparison of pellet charge exchange measurements in the presence and absence of sawteeth in the period following the D-T heating phase indicate that the sawtooth activity transports trapped fast alphas radially outward as shown in Fig. 46 (Petrov *et al.*, 1995; Petrov *et al.*, 1996). In these sawtooth cases, no enhanced alpha loss appears on the edge scintillator probes, indicating that the redistribution is primarily within the plasma. Gorelenkov *et al.*, (1996), Kolesnichenko and Yakovenko (1996), and Zhao and White (1996) have shown it is necessary to include the helical perturbed perpendicular electric field during the sawtooth crash to understand the rapid radial expulsion of the trapped alpha particles and the change in their energy spectrum. The model of Gorelenkov *et al.*, (1996) includes the amplitude of the electric field as an adjustable parameter and for reasonable electric field values is in good agreement with PCX measurements of the trapped alpha particles in D-T TFTR plasmas as shown in Fig. 46. In addition, charge-exchange-recombination-spectroscopy has been used to measure the alpha particles with energies up to 600 keV in a D-T pulse soon after the T-beams have been turned off, but with D-beams remaining on to allow the measurement. As shown in Fig. 47, the signal from these intermediate energy alpha particles is observed to be smaller in a discharge where a sawtooth occurred prior to the observation compared to one with a sawtooth after the observation period (Stratton *et al.*, 1996). The effect of the sawtooth instability on these lower energy passing alpha particles has also been modeled and found to be in reasonable agreement with the measurements using the model by Kolenichenko *et al.*, (1992) which does not incorporate the helical electric field.

A more internally consistent model of fast particle redistribution has been developed by Kolesnichenko and Yakovenko (1996) and Zhao and White (1996). A comparison of the data with the model by Kolesnichenko *et al.*, (1996a) has not as yet been performed. Zhao and White (1996) investigated alpha particle redistribution during the sawtooth crash by using the Hamiltonian guiding center model. Once again reasonable agreement with experiment is achieved; however, the simulation corresponding to the trapped alpha particles measured by the pellet charge exchange analyzer suffers from poor statistics and possibly incorrect treatment of the electric field in the nonlinear stage, indicating the need for perhaps an improved model for the sawtooth crash.

2. Stochastic Ripple Diffusion

The PCX diagnostic has also been used to test the predictions of the stochastic ripple diffusion models which predict that in certain regions of the plasma the nearly perpendicular particles, which PCX measures, will be lost. As shown in Fig. 48, PCX results are in reasonable agreement with the energy and q scaling of the simplified Goldston-White-Boozer formalism for the ripple loss threshold (Duong *et al.*, 1996b). Initial modeling of the radial dependence of the alpha particle density using TRANSP is in good agreement with PCX data (Redi *et al.*, 1995b). Work is in progress to compare PCX data with the more accurate predictions of orbit following codes (White *et al.*, 1996).

C. He Ash

The production, transport, and removal of helium ash are issues that have a large impact in determining both the size and cost of a future reactor such as ITER. In previous L-mode and supershot deuterium experiments, helium transport was studied using gas puffing to determine particle diffusivities, and convection velocities (Synakowski *et al.*, 1993). These results have been compared with transport of trace quantities of tritium in supershot discharges fueled by deuterium. (See Sec. V.B) The quantitative results are that the helium and tritium particle confinement times (ignoring recycling) are comparable to the energy confinement time, and that the helium and tritium particle and heat diffusivities are comparable across the profile. The well-conditioned bumper limiter serves as a particle pump in a supershot. The resultant effective helium particle confinement time in previous gas puffing experiments is 5 - 7 times the energy confinement time, well within the acceptable limits for ITER or for a D-T reactor.

D-T operation provides a unique opportunity to measure alpha ash production and transport. Measurements of radial ash profiles have been made using charge-exchange recombination spectroscopy. Differences between similar D and D-T supershots in the time history and amplitude of the thermal helium spectrum enable the alpha ash profile to be deduced. These measurements

have been compared to predictions from the TRANSP code, using transport coefficients from earlier gas puffing experiments in deuterium plasmas and the TRANSP calculation of alpha particle slowing-down and transport upon thermalization. The ash profiles are consistent with the TRANSP modeling, indicating that the ash readily transports from the central source region to the plasma edge as shown in Fig. 49. These results confirm that the thermalization of the alpha particles down to thermal energies is in agreement with the TRANSP modeling. These measurements provide evidence that, even with a central helium ash source, helium transport from the plasma core will not be a fundamental limiting factor for helium exhaust in a reactor with supershot-like transport (Synakowski *et al.*, 1995a). Further work is required to assess He ash retention in discharges with internal transport barriers such as the enhanced reverse shear regime or ELM-free H-mode.

D. Interaction with MHD

With the exception of the discussion regarding the effect of sawtooth instabilities on alpha particles, the above results have been in MHD quiescent discharges. MHD instabilities as noted earlier can enhance the transport of the background plasma. Thus, the effect of MHD instabilities on alpha particles has been investigated.

1. Disruptions

Both minor and major disruptions produce substantial losses of alpha particles. In major disruptions, losses of energetic alphas estimated to be up to 20% of the alpha population have been observed to occur in ~2 ms during the thermal quench phase while the total current is still unperturbed (Janos *et al.*, 1996). The alpha particle losses are observed to occur prior to the start of the thermal and current quench as shown in Fig. 50. The start of the alpha losses occurs with the start of the rapid growth of the ballooning mode. Three dimensional nonlinear MHD simulations predict that the flux surfaces become stochastic from the distortion caused by the ballooning modes. This onset of stochasticity could explain the sudden loss of alpha particles. Such losses, which were observed mainly on the 90°-detector and hence localized, could have a serious impact on first-wall

components in a reactor. Additional measurements which view a larger fraction of the first wall components are required to assess the degree of localization and reproducibility of the heat flux from alpha particles during disruptions.

2. Low m-n modes

In both D and D-T experiments, MHD activity with low toroidal and poloidal mode numbers is observed to increase the loss of fusion products. The alpha particle loss is sometimes observed to be well correlated with the phase of the modes as shown in Fig. 51 during the presence of neoclassical tearing modes in a TFTR plasma. Once again because these modes can persist in the plasma, albeit resulting in a degradation in plasma performance, they can also increase the heat load to first wall components.

3. Kinetic Ballooning Modes

The first direct evidence of alpha particle loss induced by an MHD mode was due to a kinetic ballooning mode (KBM) in TFTR D-T experiments as shown in Fig. 52 (Chang *et al.*, 1996b). The kinetic ballooning modes are driven by sharp gradients in the plasma pressure profile. Note that these modes are different from the ideal ballooning modes observed in TFTR before high- β disruptions, which are toroidally localized and have larger radial extents. In general, the kinetic ballooning modes have only a small effect on plasma confinement. The frequency of the mode is close to the ion-diamagnetic frequency. The observed toroidal mode number is $n=6$. These modes are localized near the peak plasma pressure gradient and have largest amplitude on the large major radius side of the magnetic axis. An enhancement of up to a factor of three in the alpha particle loss to the 90° detector was correlated with a bursting KBM (Darrow *et al.*, 1996a). The resonant interaction of the waves with the alpha particles results in the increased alpha particle loss by moving marginally passing alpha particles onto lost banana orbits. This has been simulated using a guiding center code. Numerical simulations of alpha particle loss associated with ballooning modes agree well with experimental measurements (Park *et al.*, 1996). Similar KBMs are observed in D

discharges; so the modes are not driven by the alpha particles but by the pressure gradients in the plasma.

VIII. COLLECTIVE EFFECTS

The effect of MHD instabilities driven by the background plasma on alpha particle confinement has been discussed in the previous section. Energetic particles such as alphas can also destabilize (or in some cases stabilize) MHD modes. A comprehensive review of this work in H and D discharges has been given by Heidbrink and Sadler, 1994. This is a potentially important topic due to the coupling between alpha-heating and MHD stability in a reactor, as well as the loss of alpha particles to first wall components due to the induced collective instabilities. In this paper, the effect of alpha particles on the stability of Toroidal Alfvén eigenmodes (TAE) and Alfvén cyclotron instabilities (also called magnetoacoustic cyclotron instabilities) will be discussed. The alpha parameters achieved in present experiments on JET and TFTR are summarized in Table VI.

A. Toroidal Alfvén Eigenmodes

Toroidal Alfvén eigenmodes have been shown to exist with discrete frequencies located inside the shear Alfvén continuum gaps created due to toroidal coupling of different poloidal harmonics (Cheng, Chen and Chance, 1985; Cheng and Chance, 1986). These modes were predicted to be driven unstable by energetic particles through wave-particle resonances by tapping the free energy associated with the energetic alpha pressure gradient (Cheng *et al.*, 1989; Fu and Van Dam 1989; Cheng 1991). Since this initial theoretical work, a large theoretical literature has developed which includes additional important effects, both in the analysis of the instability criteria as well as in the nonlinear saturation mechanisms. Experiments on TFTR (Wong *et al.*, 1991, 1992; Durst *et al.*, 1992; Wilson *et al.*, 1993; Fredrickson, 1995b; Wong *et al.*, 1996b), JET (Fasoli *et al.*, 1994; 1995, 1996; JET Team [presented by Start] 1996) JT-60U (Saigusa *et al.*, 1995) and DIII-D (Heidbrink *et al.*, 1991; Strait *et al.*, 1993) have shown that the toroidal Alfvén eigenmode could be destabilized by the energetic ion populations created either by neutral beam injection or ICRF heating. These

instabilities, as shown in Fig. 53, can be sufficiently strong to eject a large fraction of the fast particles (Darrow *et al.*, 1996b) and to damage first wall components (White *et al.*, 1995a).

The initial D-T experiments in TFTR in supershot and L-mode discharges, however, showed no signs of alpha-driven instability in the TAE frequency range, and the alpha-particle loss rate remained a constant fraction of the alpha production rate as the alpha pressure increased, suggesting that deleterious collective alpha instabilities were not being excited (Batha *et al.*, 1995b; Chang *et al.*, 1996c; Zweben *et al.*, 1996b). Theory has since shown that, although TFTR achieves levels of the alpha-particle driving terms nearly comparable to those of a reactor, the damping of the mode in TFTR is generally stronger than the alpha-particle drive (Cheng *et al.*, 1994; Fu *et al.*, 1995). Two approaches have been successfully used to study the role of alpha particles in exciting the TAE. The first was to destabilize the plasmas using ICRF minority heated ions, and the second was to alter the magnetic configuration to decrease the threshold requirements. Experiments with ICRF H-minority heating have found that the RF power threshold for the TAE instability is 20% lower in D-T plasmas compared with similar D shots as shown in Fig. 54 (Wong *et al.*, 1996a). Calculations indicate that the reduction in threshold power is consistent with the alpha particles contributing 10%-30% of the total drive in a D-T plasma with 3 MW of peak fusion power.

Recent theoretical calculations have shown that the predicted alpha-driven TAE threshold is sensitive to the q-profile (Spong *et al.*, 1995; Fu *et al.*, 1996a,b; Berk *et al.*, 1996). This is potentially important in advanced tokamak configurations in which the current profile is modified to achieve higher stability. In experiments with weak magnetic shear on TFTR, TAE driven by energetic alpha particles have been observed in D-T plasmas (Nazikian *et al.*, 1996a,b; Chang *et al.*, 1996d). These modes are observed only after the end of the high power heating phase when the beam ion density and plasma pressure are decaying more rapidly than the alpha pressure as shown in Fig. 55. The fusion power threshold is ~ 1.0 MW with $\beta_{\alpha}(0) \sim 10^{-4}$ for $q(0) \simeq 2.4$ which is much lower than obtained in high powered supershots discharges with $q(0) \leq 1$ and monotonically increasing q-profile and which were observed to be stable. The onset of mode activity is generally consistent with NOVA-K linear stability calculations (Fu *et al.*, 1996a) though the poloidal mode structure remains to be

clarified (Chang *et al.*, 1996d). The mode amplitude increases with the increasing fusion power as shown in Fig. 56.

So far, the amplitude of this mode is very small and no loss of alpha particles has been detected. This is consistent with the general arguments presented by White (1995b) which indicate that little radial transport would occur due to a weak single mode. In larger machines, higher values of the mode number can be excited and overlapping modes may result in stochastic diffusion and perhaps increased transport. This recent experimental progress has clarified the threshold criteria for alpha driven TAE instability; however, further experimental work is required, with larger amplitude modes and perhaps with overlapping modes, to test the nonlinear saturation mechanisms and alpha transport physics due to these instabilities.

B. Ion Cyclotron Instabilities

In both JET (Cottrell *et al.*, 1993) and TFTR (Arunsalam and Greene, 1993, Cauffman *et al.*, 1995) experiments, ion cyclotron emission (ICE) has been observed during both D and D-T discharges. On JET, ICE is detected using the ICRF antennae, and on TFTR by rf probes located near the top and bottom of the machine. The ICE spectra contains superthermal, narrow, equally spaced emission lines which correspond to successive cyclotron harmonics of deuterium or alpha particles at the outer midplane near to the last closed flux surface. The emission is inferred to arise from alpha particles which are born in the core but whose large orbits intersect the edge of the plasma. As a result, the alpha-particle distribution function in the plasma edge is very anisotropic and provides the free-energy required to drive the instability. In pure deuterium and mixed D-T JET discharges, the time averaged ICE power increases linearly with the total neutron flux over a wide range of six decades in signal intensity as shown in Fig. 57. The emission is strongly affected by edge localized modes in the plasma edge. The results on TFTR are similar to those on JET but also have some striking differences. In TFTR supershot discharges, emission at the alpha cyclotron harmonic is observed only for approximately 100 - 250 ms. However in discharges with broad density profiles, the emission is observed to persist.

The emission has been studied theoretically by several groups (Coppi, 1993; Arunsalam and Green, 1993; Arunsalam, Greene and Young, 1994; Dendy *et al.*, 1994, 1995; Gorlenkov and Cheng 1995a,b; McClements *et al.*, 1996; Kolesnichenko *et al.*, 1996c; Arunsalam 1996a,b). The Alfvén cyclotron instability is driven by the anisotropic alpha distribution function. The results on JET and TFTR are in qualitative agreement with numerical calculations of growth rates due to the magnetoacoustic cyclotron instability (Cauffman *et al.*, 1995). Furthermore, the theory predicts that the instability is sensitive to the ratio of n_{α}/n_e , the anisotropy in the distribution function, and $V_{\alpha 0}/V_A$ in the edge region where $V_{\alpha 0}$ is the alpha birth velocity and V_A is the Alfvén velocity. Thus in TFTR supersonic discharges with low edge density, $V_{\alpha 0}/V_A$ is < 1 and the growth rate is reduced. Whereas in JET H-mode and TFTR L-mode discharges with broader density profiles, $V_{\alpha 0}/V_A$ is > 1 which results in a larger growth rate.

Cottrell *et al.*, (1993) suggested that, due to the strong correlation between fusion power and ICE, this could be used as an alpha particle diagnostic. The results on TFTR indicate that the interpretation of the emission depends upon the details of the edge parameters as well as the alpha particle density which will hamper the use of this interesting observation as a diagnostic technique.

IX. ALPHA HEATING EXPERIMENT

In the highest performance D-T discharges produced so far, the alpha-particle heating is a relatively small fraction of the total power heating the plasma, making its detection difficult. Nevertheless, the electron temperature rise in TFTR D-T shots during beam injection is greater than in D-only or T-only shots (Hawryluk *et al.*, 1994a; Budny *et al.*, 1994b; Taylor *et al.*, 1996b). During the initial TFTR D-T experiments, Hawryluk *et al.*, (1994a) reported that within $r/a < 0.25$, the ratio of the alpha heating power, $P_{\alpha e}$, to the total heating power to the electrons $P_{\alpha e}/(P_{\alpha e} + P_{be} + P_{ie} + P_{oh})$ was less than 15%. However, in these experiments there were similar changes in the ion-electron coupling, P_{ie} , and collisional beam heating P_{be} . The observed increase of T_e measured by electron cyclotron emission was roughly twice that expected from alpha heating and the changes in P_{be} and P_{ie} assuming fixed electron thermal diffusivity, suggesting that both alpha heating and other isotope effects were important.

Recent analysis based on a larger data set confirms that the change in electron temperature requires including both alpha-heating and isotope effects (Taylor *et al.*, 1996b). When the database is constrained to take into account the change in electron temperature associated with confinement, the residual change has been determined to be in reasonable agreement with the predicted alpha heating as shown in Fig. 58. Further experiments with a higher ratio of alpha heating to beam heating power will be required to evaluate the efficiency of alpha heating.

X. FUTURE DIRECTIONS

In this section, future research opportunities motivated by the results from the JET and TFTR experiments as well as the accompanying theoretical work in support of those experiments will be discussed. As with active areas of research, future opportunities will largely be defined by theoretical and experimental insights yet to be identified.

A. Alpha Heating

Experimental determination of the alpha heating effectiveness remains an important topic due to its crucial importance for reactor design. Though a great deal has been learned about both the confined and escaping alpha particles, it must be kept in mind that the present diagnostics sample only part of the distribution function (Zweben *et al.*, 1996a). Thus direct measurements of the alpha-particle heating effectiveness are important to check the validity of the computational modeling. As discussed in the previous section, although the TFTR experiments have shown that alpha heating is in reasonable accord with expectations, the observed heating is small and hence the uncertainty in the heating effectiveness is large. To obtain a clearer demonstration requires larger values of $P_{\alpha e}/P_{\text{heat},e}$ and $P_{\alpha e}/P_{ie}$. The JET Team (1992) has projected higher values of $P_{\text{fus}}/P_{\text{heat}}$ than achieved to date on TFTR, albeit in transient discharges with relatively large values of $(dW/dt)/P_{\text{heat}}$. Higher values of $P_{\text{fus}}/P_{\text{heat}}$ offer the possibility of reducing the experimental uncertainty in the alpha heating efficiency though the interpretation may be complicated due to the transient behavior and possible changes in the underlying transport coefficients.

B. Alpha Channeling

Several techniques have been proposed to use alpha particle-wave interactions to more effectively utilize the alpha particles in a reactor (Fisch and Rax, 1992; Mynick and Pomphery, 1994; Hsu *et al.*, 1994; Fisch, 1995; Fisch *et al.*, 1994, 1996; Fisch and Herrmann, 1995, Herrmann and Fisch, 1996). By coupling the alpha particle energy to a plasma wave which then deposits its energy in the plasma it is theoretically possible to: 1) transfer the energy of alpha particles preferentially to the ions and thereby increase the plasma reactivity and reduce the alpha pressure; 2) radially redistribute the alpha particles for alpha-ash control; 3) control the alpha-heating profile which may enable pressure profile control in a tokamak; 4) control the alpha-pressure profile which may further reduce the drive for adverse alpha-particle instabilities; 5) transfer momentum to the electrons for current drive. While it may not be possible to achieve all of these objectives simultaneously in a reactor, this concept offers additional flexibility which may be important to the operation of an

advanced tokamak reactor which utilizes self-sustaining pressure and current profile control while requiring as little auxiliary power as possible.

Experiments on TFTR have focused on understanding the physics of energetic particle interaction with plasma waves which is a central issue for these approaches. The experiments have utilized a mode-converted fast-wave to interact with the energetic ions. In D-³He plasmas, strong interaction between the mode-converted wave and beam ions has resulted in strong beam-ion heating. The escaping energetic ions, shown in Fig. 59, are in reasonable agreement with the alpha particle-wave model when applied to fast beam ions (Fisch *et al.*, 1996).

RF-induced alpha-particle cooling in which the energy in the alpha particle is transferred to the wave has been predicted for a specific phasing between alphas and high k_{\parallel} ion Bernstein waves which could then damp on the ions (Valeo and Fisch, 1994). The value of k_{\parallel} of the fast wave is predicted to change sign after undergoing mode conversion for waves either above or below the midplane. Experiments on TFTR have demonstrated that in D-³He plasmas the loss of deuterium beam ions is correlated with the direction of the rf wave and is in agreement with the rf model which predicts a dependence on the direction of the wave, thus, confirming an important element of the theory (Fisch *et al.*, 1996).

The experimental results (Darrow *et al.*, 1996c) to date support some of the underlying assumptions in the models which predict the feasibility of alpha channeling; however, much more experimental and theoretical work is required to establish this novel approach. Numerical simulations indicate that for a reactor size plasma it will be necessary to excite both TAE and mode-converted IBW to extract more than half the energy from the alpha particles (Fisch and Herrmann, 1995; Herrmann and Fisch 1996). Evaluation of the interaction of energetic particles with TAE which have been directly driven by beat waves or saddle coil antennae (Fasoli *et al.*, 1995; The JET Team [presented by Start] 1996) is an important element in establishing the underlying physics. Ultimately, combining the two waves and demonstrating energy transfer from the alpha particles to the waves and then damping of the waves will be required to evaluate this concept.

In the theoretical work by Fisch and Rax (1992) stochastic wave-particle interactions diffuse the particle orbits in a preferred direction by the appropriate choice of wave numbers and wave direction. Another approach, relying upon frequency sweeping of the wave has been proposed by Mynick and Pomphrey, (1994) and Hsu *et al.*, (1994). This mechanism can move particles with a selected parallel velocity in a non-diffusive fashion from one specified radius to another. A perturbed single-harmonic wave induces an island in the particle drift surfaces having the same m, n number as the wave. As the wave frequency is slowly varied, a particle starts inside a drift island called a “bucket” and moves adiabatically with that island. By varying the frequency of the wave, it is possible to consecutively transport part of the alpha distribution with the wave. This technique may be used to control the density of He ash especially in regimes of operation such as the enhanced reversed shear in which alpha ash accumulation may be important inside the transport barrier. This technique also requires experimental tests to evaluate the efficiency of removing a significant part of the distribution function.

C. Isotope Effects in Diverted H-mode Plasmas

The isotope effect has been studied in a wide range of plasma operating regimes on TFTR as discussed in Sec. V. However, one important operating regime, diverted H modes, which is the planned operating mode for ITER, has not been explored. Isotopic scaling of the energy confinement time and the threshold power for the transition from L- to H-mode remains to be established. The results from limiter H-modes on TFTR indicate that the confinement time has a favorable isotope scaling but the threshold power for the transition is unchanged. In enhanced reverse shear discharges with an internal transport barrier on TFTR, the confinement time does not exhibit a favorable isotope scaling and the threshold power appears to be higher in D-T discharges. These differences motivate a thorough study of isotope scaling in diverted H-mode plasmas as are planned on JET.

1. Divertor Operation

Particle and heat removal is an important issue for future devices operating at much higher powers and for longer pulse durations. In this regard, the ITER device will employ a divertor. Fueling of a diverted tokamak plasma, including control of the ratio of n_T/n_D , while minimizing tritium inventory are issues remaining to be studied. The use of pellet injection and advanced fueling techniques, such as a compact toroid injection is under study.

D. Ignition Devices

In present experiments, the pressure profile, current profile and the rotation profile are largely determined by the application of auxiliary heating, inductive and non-inductive current drive and the applied torque. The current profile is largely determined by the applied external flux and the plasma conductivity. The internally driven bootstrap currents can be significant and can affect the current profile and the plasma stability, although most present high performance experiments are performed in regimes with small bootstrap current fractions or with heating pulse durations which are short compared with the current diffusion time. Thus, the current profile is largely (externally) inductively driven. The rotation profile and the accompanying radial electric field profile is in most experiments determined by the external application of torque (almost always by neutral beam injection). Only recently in the enhanced reverse shear regime on TFTR has the pressure gradient as a result of intense heating been sufficiently large in the plasma core to significantly change the radial electric field shear. In present D-T experiments, alpha heating has had a small effect on the pressure profile. While this external control of profiles has facilitated the study of the underlying transport and plasma stability in present day experiments, it is not representative of conditions in an ignited plasma.

In an ignition device, the operating temperature cannot be simply controlled because the heating power cannot be controlled externally. Simple considerations of the energy balance equation and the temperature dependence of the rate coefficients indicate that ignition at low temperatures can be thermally unstable but that at high temperature a thermally stable operating point exists (Borrass *et*

al., 1986). Thus, just from these considerations it may be required to introduce additional loss mechanisms to obtain a stable operating point.

The problem becomes more complex when one considers the constraints on an economically attractive tokamak device operating in steady state. The self-generated internal processes become dominant for $P_{\alpha} \sim P_{\text{loss}} \gg P_{\text{aux}}$. The alpha heating profile is then a sensitive function of the ion pressure profile. In a steady-state machine, the fraction of bootstrap current is expected to be large, otherwise the power required for external current drive using present techniques would be too large (Ozeki *et al.*, 1993). (An alternative approach is to design a pulsed device similar in concept to present machines; however as discussed by Bathke *et al.*, (1994) this may be more expensive). The rotation profile and, hence, the radial electric field would be largely defined by the plasma pressure gradients because to drive significant plasma flows, the power required would be too large using neutral beam injection. In future ignited machines, the role of the external heating and current drive, as well as applied torque, will be to control and modify the plasma either through the alpha particles, such as by alpha channeling, or by altering the underlying transport mechanisms. In addition, the interaction between the pressure, current and rotation profiles can become much greater, especially in regimes with higher values of β . A couple of examples will be given for illustration. In an ignited plasma, the pressure profile will determine the heating profile, the bootstrap current, and a significant component of the radial electric field. The bootstrap current modifies the current profile which in turn modifies the radial electric field shear due to the change in the poloidal magnetic field. The radial electric field shear may decrease the radial transport, increasing the plasma pressure, which in turn increases the alpha-heating. Hence, it is not certain that a self-consistent stable operating point exists, for the processes are highly nonlinear and require a detailed knowledge of the underlying transport mechanisms beyond what has so far been developed. Furthermore, the problem becomes even more complex when MHD stability, which is sensitive to the current and pressure profiles, is taken into account. Controlling the operating point of a burning plasma with a minimum of auxiliary power for the control systems (such as local fueling or heating or momentum input) is both a major scientific and technological challenge.

Though the control of a burning plasma is a significant issue, the evolving understanding of the underlying transport mechanisms, MHD stability and wave-particle interactions in both D and D-T experiments is providing the tools necessary for this task. Advanced computational techniques are being developed and benchmarked on present experiments both to evaluate these issues and develop new concepts to control a burning plasma. Throughout this paper, the results of the D-T experiments have been placed in the context of this evolving understanding of the plasma science because this has not only enabled the successful execution of the present experiments but also provides a basis for designing future experiments. With this increased understanding, new concepts have emerged ranging from reverse-shear magnetic configurations, to more efficient use of the alpha particles by means of alpha channeling, to the formation of internal transport barriers by use of IBW. Further experimental and theoretical work will determine the viability of these new concepts.

XII. CONCLUSIONS

The first series of high power D-T experiments on JET and TFTR have provided important new information in fusion technology and science. This is a significant step towards the development of higher power and higher performance fusion devices. In support of fusion technology development, safe and extended operation of a deuterium-tritium facility has been demonstrated. Tritium handling and processing, tritium retention in plasma facing components, and neutron shielding have been successfully accomplished. Remote handling, use of low activation materials, and large scale tritium processing remain to be demonstrated in future facilities.

In addition to the large increase in fusion power which occurred with the introduction of D-T fuels, several important scientific issues associated with the use of tritium and with the production of alpha particles from D-T reactions have been studied. Significant enhancements in plasma confinement have been obtained in TFTR supershot, limiter H-mode, high ℓ_1 and L-mode discharges, but not in reversed shear discharges to date. Furthermore, the power required to obtain an internal transport barrier is greater in D-T discharges. The favorable scaling with isotopic mass observed in most TFTR regimes imposes a significant constraint on transport models which would tend to predict

an adverse scaling with mass. This as well as the different behavior observed in the reverse shear regime, remain important problems to be understood.

The use of tritium enables the direct measurement of the transport of hydrogenic species in a plasma. The transport of tritium is comparable to that of electrons and helium gas injected at the edge. More importantly the transport of particles is comparable in radial dependence and magnitude to the transport of heat and toroidal momentum placing an important constraint on turbulent transport models for the plasmas. The transport of tritium in enhanced reverse shear plasmas is much less within the internal transport barrier qualitatively similar to the changes observed in the ion heat transport.

Heating by tritium beams is found to be similar to the heating by deuterium beams when the differences associated with charge-exchange and ionization cross-sections, as well as thermalization, are taken into account. The introduction of a second ion resonance into the plasma with D-T fuels provides additional flexibility in heating a plasma with ICRF waves. Second harmonic tritium absorption has successfully been used to heat the plasma in accordance with expectations. In D-³He plasmas, mode conversion was found to heat the electrons locally with high efficiency, and effective current drive was demonstrated. However, when this approach was applied to D-T plasmas on TFTR, the heating efficiency was decreased due to direct absorption by ⁷Li impurities. This may be especially important in future experiments in which ⁹Be from the plasma facing components could provide a competing resonance. Further experiments in which the concentration of ⁷Li impurities is decreased by replacement with ⁶Li are required to confirm the role of ⁷Li absorption and evaluate mode-conversion heating and current drive efficiency in a D-T plasma.

Due to the low concentration of alpha particles $n_{\alpha}/n_e \sim 10^{-3}$ and their large energy range, diagnosis of alpha particles, especially in a high radiation environment, is a formidable challenge. The study of the confinement and loss of alpha particles has been made possible by the successful development of new diagnostic techniques namely pellet-charge-exchange analysis, charge-exchange recombination spectroscopy and collector probes. The confined alpha particles behave classically in quiescent MHD plasmas. Sawtooth instabilities redistribute alpha particles in the plasma core. Loss

of alpha particles due to stochastic ripple diffusion has been observed. The study of confined alpha particles has been conducted principally in discharges with monotonic q profiles. Further work is required to evaluate the confinement and transport in reverse shear discharges. In quiescent discharges, the loss of alpha particles to the collectors near the bottom of the vessel is in generally good agreement with first orbit loss calculation. Further work is in progress to obtain a quantitative evaluation of the loss due to stochastic ripple diffusion. Loss of alpha-particles due to sawtooth events, low- m , n MHD instabilities, plasma disruptions and RF waves has been observed. These may be an important design consideration in future devices due to the localized heat loss to plasma facing components. The thermalized alpha particles from fusion reactions have been detected. The radial transport of the alpha ash is comparable to that of the electrons and ions, so accumulation of alpha ash should not be a problem in discharges with supershot-like transport properties. However, the transport of alpha ash has not been studied in discharges with internal transport barriers, and the need for active techniques to remove the ash remains to be determined.

The destabilization of MHD instabilities, including the toroidal Alfvén eigenmodes and the Alfvén cyclotron instabilities, by alpha particles have been observed. The stability of the TAE has been found to be sensitive to the current profiles, as predicted by theory. In TFTR discharges with monotonic q -profiles, the mode was observed to be stable. Only in discharges with weak shear and higher values of $q(0)$ was the mode found to be weakly unstable after the termination of the high-power phase, when beam-ion Landau and continuum damping of the mode was decreased. Further experiments with larger amplitude instabilities are required to evaluate the effect of these instabilities on the confinement of the alpha particles. The Alfvén cyclotron instability is found to interact with alpha particles in the edge of the plasma by creating ion cyclotron emission. Good agreement between theory and experiment is found. Unlike the TAE instability which can theoretically eject significant fractions of alpha particles, the impact of this instability appears to be small.

In TFTR experiments, small temperature excursions have been identified to be due to alpha heating. Further experiments in which the alpha heating power approaches the loss power are

required to establish the efficiency of alpha heating and the effect, if any, of alpha heating on plasma transport.

Recent theoretical work on alpha particle-wave interactions to more effectively use the confined particles to heat the plasma and drive the current has stimulated basic experiments. These experiments lend support to the underlying physics of alpha particle-wave interactions, however, further work is required to establish this concept.

As with all active research, despite the rapid progress during the past three years of D-T experiments, many questions remain. Some of these will be addressed in the current generation of facilities, but others will only be answered on a burning plasma device operating near ignition conditions.

Acknowledgments:

This work is the product of a great deal of effort by scientists, engineers and technical staff on both TFTR and JET and is but a brief summary of their work and accomplishments. I would like to express my appreciation to R. Davidson, H.P. Furth and D. Meade for their steadfast support and encouragement of the TFTR D-T experiments. The author would like to thank M. Bell, R. Budny, C. Bush, Z. Chang, C.Z. Cheng, G Cottrell, D. Darrow, P. Efthimion, N. Fisch, E. Fredrickson, G.Y. Fu, A. Gibson, L. Grisham, J. Hosea, D. Johnson, F. Levinton, K. McGuire, R. Majeski, D. Meade, S. Medley, D. Mueller, R. Nazikian, M. Petrov, C.K. Phillips, G. Rewoldt, E. Ruskov, S. Sabbagh, S. Scott, C. Skinner, E. Synakowski, J. Strachan, B. Stratton, W. Tang, G. Taylor, A. von Halle, M. Williams, J.R. Wilson, K.L. Wong, K. Young, M. Zarnstorff, S. Zweben, for providing figures and valuable input to this paper. The preparation of this manuscript would not have been completed without the support by P. Shangle and C. Such.

This work was performed under US DOE Contract No. DE-AC02-76-CH03073.

Appendix: TRITIUM AND ACTIVATION CONSIDERATIONS

Deuterium-tritium experiments impose additional requirements on the facility to accommodate the use of tritium which is radioactive and the increased machine activation from the D-T reactions (Huguet *et al.*, 1992; Hawryluk *et al.*, 1994b).

A. Tritium Systems

The full JET tritium system was not available for the initial D-T experiments (Hemmerich *et al.*, 1992). To collect and measure the injected tritium, the normal torus pumping system was replaced by a cryogenic gas collection system as shown in Fig. A1. During operation, the gas flow from the torus or neutral beamlines condensed on a tubular cryopanel containing activated charcoal at liquid helium temperature. Subsequently, the condensed tritium, together with larger amounts of deuterium, was transferred to uranium storage beds. Approximately 7.4×10^{13} Bq (2 kCi) of tritium were used in the JET initial D-T experiments.

The TFTR tritium gas handling system is restricted to 1.85×10^{15} Bq (50 kCi) in-process tritium (Hawryluk *et al.*, 1994b; Anderson *et al.*, 1994, 1995). By restricting the tritium inventory, the accident potential is reduced to personnel working on-site as well as to the general public. The tritium gas is brought on site in a shipping canister and is transferred to a uranium bed, where it is stored as shown in Fig. A2. The uranium bed is heated to transfer the gas to the neutral beam or torus injection systems. The gas is then injected into the torus or neutral beams, and pumped by the cryopanel in the beam boxes. During plasma operation, some of the gas is retained in the graphite limiter in the vacuum vessel. Outgasing of tritium from the vacuum vessel walls and limiters is pumped by a combination of neutral beamline cryopanel as well as the dedicated vessel pumping system. The gas on the cryopanel and from the pumping systems is transferred to the Gas Holding Tank. The gas in the Gas Holding Tank is oxidized by the Torus Cleanup System and absorbed onto molecular sieve beds. These beds are shipped off site for reprocessing. More than 3.2×10^{16} Bq (860 kCi) of tritium have been processed from November 1993 to August 1996. Since initial operation, a low-inventory cryodistillation system (Busigin *et al.*, 1995; Raftopoulos *et al.* 1995) has

been developed to repurify the tritium on site and decrease the number of off-site shipments of oxidized tritium. This system has been successfully commissioned. In future larger D-T experiments, on-site reprocessing will be required.

1. Tritium Retention

Some of the tritium introduced into the vacuum vessel is retained on the graphite limiter and co-deposited layers on the walls. Retention of tritium in the vacuum vessel walls and components is important for two reasons. The first is associated with regulatory considerations (Bell *et al.*, 1992; DeLooper, 1994). The quantity of tritium retained must be accounted for since special controls are imposed on the handling of tritium (LaMarche *et al.*, 1994; Saville, *et al.*, 1995, Nagy *et al.*, 1996). On TFTR, the quantity of tritium permitted in the vessel is restricted to $< 7.4 \times 10^{14}$ Bq (20 kCi) to limit release to the environment in the event of a major vacuum leak and simultaneous failure of tritium containment systems. The second reason is that the interaction of the plasma with the limiter and walls results in the exchange of the hydrogenic species in the plasma with the species embedded in the limiters and walls. This can affect the concentration of tritium and deuterium in the discharge, as discussed in Sec. IV.

Saibene *et al.*, (1992) and Andrew *et al.*, (1993) reported that by a combination of extensive JET operation in deuterium high power discharges (>1000 shots with and without auxiliary heating), disruptive discharges, glow discharge cleaning and a deuterium soak of the limiters it was possible to reduce the tritium in the vessel to as little as 3% of the injected tritium of 2×10^{12} Bq or 54 Ci. A study of the effectiveness of the different techniques was performed. This was aided by having a short concentrated operating phase with tritium followed by an extensive campaign in deuterium to study the evolution of the tritium in the discharge. In TFTR, operation with D-T and D discharges were interspersed for a longer period of time (over 2 years) and a larger number of high power D-T (> 841 shots) and D shots (>19700). Two dedicated campaigns were performed on TFTR to remove the retained tritium in October 1995 and August 1996. The following are results from the first campaign (Skinner *et al.*, 1996a,c; Mueller *et al.*, 1996). At the start of the removal effort which

followed a series of experiments in which large quantities of T gas were puffed into the plasma, about 50- 75% of the injected tritium (6×10^{14} Bq or 16 kCi) was retained in the vessel. This was in general agreement with the results of previous deuterium retention studies on TFTR and is in contrast with a smaller retention fraction on JET of about 16% (Coad, 1995) in deuterium discharges. Removal of tritium from the TFTR vessel was accomplished by glow discharge cleaning with deuterium and He-O₂ mixtures, followed by a moist air purge of the vessel. The tritium retention was reduced from 16 kCi to about 8 kCi. It would have been possible to reduce the tritium further with additional time. One difference between the two devices is that JET operates with the vacuum vessel walls at about 300⁰ C whereas TFTR operates at room temperature. In addition both devices use wall coatings, Be in JET and Li in TFTR, to reduce the influx of impurities.

Both devices studied the release of tritium due to exposure of the vessel to air. In JET with the walls initially at 300⁰ C, Andrew *et al.*, (1993), reported that as a result of an air leak about 10% of the tritium in the vessel 7×10^9 Bq (0.2 Ci) was liberated. In a planned moist air purge experiment on TFTR about 15% of the tritium was released from the vessel surfaces 7.8×10^{13} Bq (2.1kCi) and subsequently processed by the cleanup system (Skinner, 1996c). The experience on TFTR has shown that it is possible to control the quantity of tritium in the vessel within stringent regulatory requirements.

B. D-T Neutronics

The production of D-T neutrons has been used to study the effectiveness of shielding and machine activation. Apart from its practical importance to present operation, this is important to the design of future D-T tokamak reactors.

1. Shielding

Due to the complexity of the tokamak structure and the surrounding hardware, including the neutral beamlines and diagnostics, accurate simulations of the effectiveness of machine shielding are difficult to perform. The approach taken on TFTR was to augment the shielding calculations with an

extensive set of real time measurements during deuterium operation to characterize the shielding and the consequent dose both within the facility and at the site boundary (Kugel *et al.*, 1994, 1995). The results were then compared with existing shielding calculations assuming a relatively simple model for the machine structure which was then revised to take into account the additional equipment in the Test Cell. The results of the comparison of the original neutronics modeling with the experimental measurements indicated that the calculations were conservative (Ku and Liew, 1994). Prior to the D-T experiments, supplementary local shielding (especially for sensitive diagnostic equipment) was installed; however, the installation of a complex “igloo” shield around the tokamak was found to be unnecessary, resulting in significant cost savings as well as facilitating maintenance of the machine. The requirement for the design of the shielding for TFTR is that the dose at the site boundary from all sources (direct dose due to gammas and neutrons as well as from tritium and activated air) be less than 100 μSv per year. The dose from all pathways has been $< 3 \mu\text{Sv}$ per year. For the JET experiments, the results from passive dosimetry outside of the biological shield are generally indistinguishable from background (Caldwell-Nichols *et al.*, 1992).

2. Machine Activation

Activation of the machine by high energy neutrons imposes operational constraints in present machines on maintenance and machine modification (Caldwell-Nichols *et al.*, 1992; Stencel *et al.*, 1994; Kugel *et al.*, 1996). The scope of the JET D-T experiments was limited to permit subsequent hands-on modifications of the components within the vessel (Huguet *et al.*, 1992). In TFTR, the radiation level decreases rapidly with distance from the vacuum vessel enabling routine hands-on maintenance on nearly all components in the Test Cell except those very close to the vessel. From November 1993 to August 1996, 4.8×10^{20} D-T neutrons were produced on TFTR resulting in a integrated yield of 1.4 GJ. After a week of cooldown for the short-lived isotopes in the stainless steel vessel, the contact dose of the vacuum vessel decreased to 1-2 mSv/hour. Neutronics simulations of the activation of the vessel were benchmarked on TFTR and are in agreement (within a factor of 2) with the measured activation level and have provided a reliable guide for planning and design. This

level of machine activation in TFTR experiments has enabled limited hands-on maintenance of components on the vessel with considerable attention being given to reducing the duration of the tasks and providing local shielding. In the future, one of the main technological tasks will be to develop remote handling techniques for a fusion reactor. For the next series of D-T experiments on JET, remote handling tools have been developed to remove the divertor cassettes (Pick *et al.*, 1996).

For the long-term, one of the most challenging tasks for fusion energy development will be to develop low activation materials for a reactor. The use of either stainless steel or inconel alloys, which are used extensively on present experiments (including TFTR and JET), would result in a large waste disposal problem for a fusion reactor. Presently, it is difficult to obtain reliable calculations of the nuclear cross-sections for reactions producing long lived half-lives due to large uncertainties on fitted nuclear-model parameters. Experiments on TFTR have benchmarked the codes used to predict the level of activation, and specific experiments have been performed to document the activation of other possibly lower activation materials for the future (Kumar *et al.*, 1996 a,b; Kugel *et al.*, 1996). In summary, the JET and TFTR D-T experiments have demonstrated that it is possible to safely operate these facilities with tritium. Whereas these experiments provide valuable technical data for the design of the next generation of D-T reactors, those machines will encounter much more challenging requirements due to higher neutron fluences and tritium inventory.

- Adler, H.G., K.W. Hill, A.T. Ramsey, W. Tighe, 1995, Rev. of Scientific Instruments, **66**, 904.
- Anderson, J.L. *et al.*, 1994, 3rd International Symposium on Fusion Nuclear Technology, Los Angeles.
- Anderson, J.L. *et al.*, 1995, in *Plasma Physics and Controlled Nuclear Fusion Research: Proceedings of the 15th International Conference Seville, Spain, 1994* (IAEA, Vienna) **2**, 681.
- Andrew, P. *et al.*, 1993, Nucl. Fusion **33**, 1389.
- Artsimovich, L.A., 1972, Nucl. Fusion **12**, 215.
- Arunasalam, V. and G.J. Greene, 1993, Phys. Rev. Lett. **71**, 3119.
- Arunasalam, V., G.J. Greene, K.M. Young, 1994, Nuclear Fusion **34**, 927.
- Arunasalam, V. 1996a, Journal of Plasma Physics (in press).
- Arunasalam, V. 1996b, Journal of Plasma Physics (in press).
- Aymar, R. *et al.*, 1996, in *Proceedings of the Sixteenth IAEA Fusion Energy Conference, Montreal, 7-11 October 1996*, IAEA-CN-64/01-1.
- Bak, P., B. Balet, A. Cherubini, J.G. Cordey, N. Deliyianakis, M. Erba, V.V. Parail, L. Porte, E.M. Springmann, A. Taroni, G. Vayakis, 1996, Nucl. Fusion, **36**, 321.
- Balet, B. *et al.*, 1993, Nucl. Fusion **33**, 1345.
- Barnes, C.W., M.G. Bell, H.W. Hendel, D.L. Jassby, D. Mikkelsen, A.L. Roquemore, S.D. Scott, J.S. Strachan, M.C. Zarnstorff, 1990, Rev. Sci. Instrum. **61**, 3151.
- Barnes, C.W., A.R. Larson, G. LeMunyan, M.J. Loughlin, 1995, Rev. of Scientific Instruments, **66**, 888.
- Barnes, C.W. *et al.*, 1996, Phys. Plasmas **3**, 4521.
- Bateman, G., J. Weiland, H. Nordman, J. Kinsey, C. Singer 1995, Physica Scripta **51**, 597.
- Bateman, G., J.E. Kinsey, A.H. Kritz, A.J. Redd, J. Weiland, 1996, in *Proceedings of the Sixteenth Fusion Energy Conference, Montreal, 7-11 October 1996*, IAEA-CN-64.
- Batha, S.H., F.M. Levinton, M.C. Zarnstorff, and G.L. Schmidt, 1995a, 22nd European Physical Society Conference on Controlled Fusion & Plasma Heating, Bournemouth, United Kingdom (European Physics Society, Petit-Lancy, Switzerland) Part **II**, 113.
- Batha, S.H., F.M. Levinton, D.A. Spong, R.V. Budny, Z.Y. Chang, D.S. Darrow, E.D. Fredrickson, G.Y. Fu, E. Mazzucato, R. Nazikian, S.J. Zweben, 1995b, Nucl. Fusion, **35**, 1463.
- Bathke, C.G. and the Aries Research Team, 1994, Fusion Technology, **26**, 1163.
- Beer, M. 1996, submitted to Phys. Plasmas.
- Bell, A.C., M. Wykes, B.J. Green, Fusion Engineering and Design **19**, 169.

- Bell, M.G. *et al.*, 1988, in *Plasma Phys. Control. Nuclear Fusion Research : Proceedings of the Twelfth International Conference Nice, 1989* (IAEA, Vienna), **I**, 27.
- Bell, M.G. *et al.*, 1994, in *Plasma Physics and Controlled Nuclear Fusion Research: Proceedings of the 15th International Conference, Seville, 1994* (IAEA, Vienna) **1**, 171.
- Bell, M.G. *et al.*, 1995, Nucl. Fusion **35**, 1429.
- Bell, M.G. *et al.*, 1996, submitted to Phys. Plasmas.
- Berk, H.L. *et al.*, 1996, in *Proceedings of the Sixteenth IAEA Fusion Energy Conference, Montreal, 7-11, October 1996*, IAEA-CN-64/D2-5.
- Bessenrodt-Weberpals, M. *et al.*, 1993, Nucl. Fus. **33**, 1205.
- Bickerton, R.J. *et al.*, 1971, Nature Phys. Sci. **224**, 110.
- Biglari, H., P.H. Diamond, P.W. Terry, 1990, Phys. Fluids B **2**, **1**.
- Biglari, H., M. Ono, P.H. Diamond and G.G. Craddock, 1992, in *Proceedings of the Ninth Topical Conference on Radio-Frequency Power in Plasmas*, Charleston, AIP Conference Proceedings 244 (New York) 376.
- Boivin, R.L. *et al.*, 1993, Nucl. Fusion **33**, 449.
- Borrass, K., 1986, Phys. Scr., **T16**, 107.
- Bosch, Hans-Stephan, G.M. Hale, 1992, Nucl. Fusion **32**, 611.
- Budny, R.V., 1994a, Nucl. Fusion **34**, 1247.
- Budny R.V. *et al.*, 1994b, in *Proceedings of the 21st EPS Conference on Controlled Fusion and Plasma Physics*, Montpellier, edited by E. Joffrin, P. Platz, P.E. Stott (EPS, Geneva) **1**, 82.
- Budny, R.V. *et al.*, 1995, Nucl. Fusion **35**, 1497.
- Bush, C.E. *et al.*, 1994, in *Proceedings of the 21st EPS Conference on Controlled Fusion and Plasma Physics*, Montpellier, edited by E. Joffrin, P. Platz, P.E. Stott (EPS, Geneva) **18B**, 354.
- Bush, C.E. *et al.*, 1995, Phys. Plasmas **2**, 2366.
- Bush, C.E. *et al.*, 1996, in *Proceedings of the Plasma Surface Interaction Conference*, May 1996, PPPL Report 3207.
- Busigin A., C.J. Busigin, J.R. Robins, K.B. Woodall, D.G. Bellamy, C. Fong, K. Kalyanam, S.K. Sood., 1995, Fusion Technol. **28**, 1312.
- Caldwell-Nichols, C.J., R.M. Russ, A.C. Bell, N. Davies, A.D. Haigh, H.D. Jones and L. Serio, 1992, Fusion Engineering and Design **19**, 149.
- Carlstrom, T.N., 1996, Plasma Physics and Controlled Fusion **38**, 1149.

- Cauffman, S. R. Majeski, K.G. McClements R.O. Dendy, 1995, Nucl. Fusion **35**, 1597.
- Challis, C.D. *et al.*, 1989, Nucl. Fusion **29**, 563.
- Chang, Z. *et al.*, 1994, Nucl. Fusion **34**, 1309.
- Chang, Z., J.D. Callen, E.D. Fredrickson, R.V. Budny, C.C. Hegna, K.M. McGuire, M. Zarnstorff, 1995, Phys. Rev. Lett. **74**, 4663.
- Chang, Z. *et al.*, 1996a, Phys. Rev. Lett. **77**, 3553.
- Chang Z. *et al.*, 1996b, Phys. Rev. Lett. **76**, 1071.
- Chang, Z. *et al.*, 1996c, Nucl. Fusion **35**, 1469.
- Chang, Z. *et al.*, 1996d, submitted to Phys. Plasmas.
- Cheng, C.Z., L. Chen, M.S. Chance, 1985, Ann. Phys. **161**, 21.
- Cheng, C.Z. , M.S. Chance, 1986, Phys. Fluids **29**, 3695.
- Cheng, C.Z., G.Y. Fu, J.W. Van Dam, 1989, Theory of Fusion Plasmas (Proc. Joint Varenna - Lausanne Int. Workshop, Chexbres, Switzerland, 1988), Editrice Compositon, Bologna, 259.
- Cheng, C.Z., 1991, Phys. Fluids **B3**, 2463.
- Cheng, C.Z. *et al.*, 1994, in *Plasma Physics and Controlled Nuclear Fusion Research: Proceedings of the 15th International Conference, Seville, 1994*(IAEA, Vienna) **3**, 373.
- Chong, G.P., 1995, "Measurement of Helium in Nickel Foils from the TFTR Alpha Collector Probe" MS Thesis (University of Toronto).
- Coad, J.P., 1995, Journal of Nuclear Material **220**, 156.
- Coppi, B. 1993, Phys. Lett. **A 172**, 439.
- Cordey, J.G., D.G. Muir, S.V. Neudachin, V.V. Parail, E. Springmann, and A. Taroni, 1995, Nucl. Fusion **35**, 101.
- Cottrell, G.A., V.P. Bhatnagar, O. DaCosta, R.O. Dendy, J. Jacquinet, K.G. McClements, D.C. McCune, M.F.F. Nave, P. Smeulders, D.F.H. Start, 1993, Nucl. Fusion **33**, 1365.
- Craddock, G.G., P.H. Diamond, 1991, Phys. Rev. Lett. **67**, 1535.
- Craddock, G.G., P.H. Diamond, M. Ono, H. Biglari, 1994, Phys. Plasmas **I**, 1944.
- DIII-D Team, 1995, in *Plasma Physics and Controlled Nuclear Fusion Research: Proceedings of the 15th International Conference Seville, 1994* (IAEA, Vienna) **1**, 83.
- Darrow, D.S., H.W. Herrmann, D.W. Johnson, R.J. Marsala, R.W. Palladino, S.J. Zweben, 1995, Rev. of Scientific Instruments **66**, 476.
- Darrow, D.S. *et al.*, 1996a, Phys. Plasmas **3**, 1875.

- Darrow, D.S., 1996b, "Observation of Neutral Beam and ICRF Tail Ion Losses Due to Alfvén Modes in TFTR," PPPL Report 3160, submitted to Nucl. Fusion.
- Darrow, D.S. *et al.*, 1996c, Nuclear Fusion **36**, 509.
- Darrow, D.S. *et al.*, 1996d, Nuclear Fusion **36**, 1.
- DeLooper, J., 1994, Fusion Techn. **31**, 1051.
- Dendy, R.O. *et al.*, 1994, Phys. Plasmas **1**, 1918.
- Dendy, R.O., C.N. Lashmore-Davies, K.G. McClements, G.A. Cottrell, R. Majeski, and S. Cauffman, 1995, Nucl. Fusion **35**, 1733.
- Diamond, P.H. *et al.*, 1996, submitted to Phys. Rev. Lett.
- Drake, J.F., Y.T. Lau, P.N. Guzdar, A.B. Hassam, S.V. Novakovski, B. Rogers, and A. Zeiler, 1996, Phys. Rev. Lett. **77**, 494.
- Duong, H.H., R. Fisher, S. Medley, M. Petrov, N. Gorelenkov, R. Budny, D. Mansfield, J. McChesney, P. Parks, A. Roquemore, R. White, S. Zweben, 1996a, Nucl. Fusion (in press).
- Duong, H.H., R.K. Fisher, J.M. McChesney, P.B. Parks, S.S. Medley, D.K. Mansfield, A.L. Roquemore, M.P. Petrov 1996b, Rev. Sci. Instruments (in press).
- Durst, R.D. *et al.*, 1992, Phys. Fluids B **4**, 3707.
- Efthimion, P.C. *et al.*, 1995a, Phys. Rev. Lett. **75**, 85.
- Efthimion, P.C. *et al.*, 1995b, in *Plasma Physics and Controlled Nuclear Fusion Research: Proceedings of the 15th International Conference Seville, 1994* (IAEA, Vienna) **1**, 289.
- Ehst, D.A. and C.F.F. Karney, 1991, Nucl. Fusion **31**, 1933.
- Ernst, D.R. *et al.*, 1995, Annual Meeting of the APS/DAP, Louisville, KY, November 7-11, 1995, Poster 9P31.
- Ernst, D. R., S.D. Scott, and the TFTR Group, 1996, 1996 International Sherwood Fusion Theory Conference, Philadelphia, PA, March 18-20, Poster 1C38.
- Equipe Tore Supra, 1996 in *Proceedings of the Sixteenth IAEA Fusion Energy Conference*, Montreal, Canada, October 7-11, 1996, IAEA-CN-64/02-2.
- Fasoli, A. *et al.*, 1994, Phys. Rev. Lett **75**, 645.
- Fasoli, A. *et al.*, 1995a, Nucl. Fusion **35**, 1485.
- Fasoli, A. *et al.*, 1995b, in *Plasma Physics and Controlled Nuclear Fusion Research: Proceedings of the 15th International Conference, Seville, 1994* (IAEA, Vienna) **1**, 405.
- Fasoli, A. *et al.*, 1996, Phys. Rev. Lett. **76**, 1067.
- Fisch, N.J., J.-M. Rax, 1992, Phys. Rev. Lett. **69**, 612.

- Fisch, N.J., E.J. Valeo, C.F.F. Karney, R. Majeski, 1994, 21st EPS Conference on Controlled Fusion and Plasma Physics, Montpellier, edited by E. Joffrin, P. Platz, P.E. Stott (EPS, Geneva) **2**, 640.
- Fisch, N.J., 1995, *Phys. Plasmas* **2**, (6), 2375.
- Fisch, N.J., M.C. Herrmann, 1995, *Nucl. Fusion* **35**, 1753.
- Fisch, N.J., M.C. Herrmann, D.S. Darrow, H.P. Furth, R.F. Heeter, H.W. Herrmann, J.C. Hosea, R. Majeski, C.K. Phillips, J. Rogers, G. Schilling, S.J. Zweben, 1996, in *Proceedings of the Sixteenth IAEA Fusion Energy Conference, Montreal, 7-11, October 1996*, IAEA-CN-64/A2-3.
- Fisher, R.K., J.M. McChesney, P.B. Parks, H.H. Duong, S.S. Medley, A.L. Roquemore, D.K. Mansfield, R.V. Budny, M.P. Petrov, R.E. Olson, 1995, *Phys. Rev. Lett.* **75**, 846.
- Fredrickson, E.D., K.M. McGuire, Z. Chang, A. Janos, M. Bell, R.V. Budny, C.E. Bush, H. Manickam, H. Mynick, R. Nazikian, G. Taylor, 1995a, *Phys. Plasmas* **2**, 4216.
- Fredrickson, E.D. *et al.*, 1995b, *Nucl. Fusion* **35**, 1457.
- Fredrickson, E.D., K.M. McGuire, Z.Y. Chang, A. Janos, J. Manickam, G. Taylor, 1996a, *Physics of Plasmas* (in press), PPPL Report 3149.
- Fredrickson, E.D. *et al.*, 1996b, submitted to *Phys. of Plasmas*.
- Fu, G.Y., J.W. Van Dam, 1989, *Phys. Fluids* **B1**, 1949.
- Fu, G.Y., C.Z. Cheng, R. Budny, Z. Chang, D.S. Darrow, E. Fredrickson, E. Mazzucato, R. Nazikian, S. Zweben, 1995, *Phys. Rev. Lett.* **75**, 2336.
- Fu, G.Y., *et al.*, 1996a, in *Proceedings of the Sixteenth IAEA Fusion Energy Conference, Montreal, Canada, 7-11, October 1996*, IAEA-F1-CN-64/D2-6.
- Fu, G.Y. *et al.*, 1996b, *Phys. Plasmas* **3**, 4036.
- Fujita, T. *et al.*, 1996, submitted to *Phys. Rev. Lett.*
- Furth, H.P., R.J. Goldston, S.J. Zweben, D.J. Sigmar, 1990, *Nucl. Fusion* **30**, 1799.
- Furth, H.P., 1975, *Nucl. Fusion* **15**, 487.
- Galeev, A.A., 1970, *Zh. Eksp. Teor. Fiz.* **59**, 1378 (*Sov. Phys. - JETP*) **32**, 752
- Gentle, K.W., 1995, *Rev. of Modern Phys.* **67**, 809.
- Goldston, R. *et al.*, 1981, *J. Comput. Phys.* **43**, 61.
- Goldston, R.J., R. B. White, A.H. Boozer, 1981, *Phys. Rev. Lett.*, **47**, 647.
- Goloborod'ko, V. Ya.I. Kolesnichenko, V.A. Yavorskij, 1987, *Phys. Scr.* **T16**, 46.
- Gorelenkov, N.N., C.Z. Cheng, 1995a, *Phys. Plasmas* **2** (6) 1961.

- Gorelenkov, N.N. and C.Z. Cheng, 1995b, Nucl. Fusion **35**, 1743.
- Gorelenkov, N.N. *et al.*, 1996, "Modeling of α -Particle Redistribution by Sawteeth in TFTR using FPPT Code", PPPL Report 3184.
- Grisham, L. *et al.*, 1995, Nuclear Instruments and Methods in Phys. Res., **B99**, 353.
- Hahm, T.S., 1995, Phys. Plasmas **1**, 2940.
- Hahm, T.S. and K. Burrell, 1995, Phys. Plasmas **2**, 1648.
- Hahm, T.S., M. Artun, M.A. Beer, G.W. Hammett, W.W. Lee, X. Li, Z. Lin, H.E. Mynick, S.E. Parker, G. Rewoldt, W.M. Tang, 1996, in *Proceedings of the Sixteenth IAEA Fusion Energy Conference, Montreal, Canada, 7-11, October 1996* IAEA-F1-CN-64/D1-2.
- Hawryluk, R.J., 1980, in *Physics of Plasmas Close to Thermonuclear Condition*, edited by B. Coppi, G.G. Leotta, D. Pfirsch, R. Pozzoli and E. Sindoni (Pergoma, New York) (CEC, Brussels) **1**, 19.
- Hawryluk, R.J. *et al.*, 1991, Plasma Physics and Controlled Fusion, **33**, 1509.
- Hawryluk, R.J. *et al.*, 1994a, Phys. Rev. Lett. **72**, 3530.
- Hawryluk, R.J. *et al.*, 1994b, Phys. Plasmas **1**, 1560.
- Hawryluk, R.J. *et al.*, 1995, in *Plasma Physics and Controlled Nuclear Fusion Research: Proceedings of the 15th International Conference Seville, Spain, 1994* (IAEA, Vienna), **1**, 11.
- Heidbrink, W.W. *et al.*, 1991, Nucl. Fusion **31**, 1635.
- Heidbrink, W.W., G.J. Sadler, 1994, Nucl. Fusion **34**, 535.
- Hemmerich, J.L. R. Lasser and T. Winkel, 1992, Fusion Engineering and Design **19**, 161.
- Hendel, H.W. *et al.*, 1990, Rev. Sci. Instrum. **61**, 1900.
- Hender, T.C. *et al.*, 1996, to be published in the Proceedings of the European Physical Society Meeting, Kiev, Ukraine.
- Herrmann, H., D.S. Darrow, J.R. Timberlake, S.J. Zweben, G.P. Chong, C.S. Pitcher, R.G. Macauley-Newcombe, 1995, Rev. of Scientific Instruments, **66**, 351.
- Herrmann, H., S. Zweben, D. Darrow, J. Timberlake, G. Chong, A. Haasz, CV. Pitcher, R. Macauley-Newcombe, 1996, Nucl. Fusion (in press).
- Herrmann, M.C. and Fisch, N.J., 1996, submitted to Phys. Rev. Lett.
- Hill, K.W., K.M. Young, L.C. Johnson, 1990, PPPL Report 2690.
- Hill, K.W., H. Adler, M. Bitter, E. Fredrickson, S. von Goeler, H. Hsuan, A. Janos, D. Johnson, A.T. Ramsey, G. Renda, 1995, Rev. Sci. Instrum. **66**, 913.

- Hoang, G.T. *et al.*, 1994, Nucl. Fusion, **34**, 75.
- Horton, W., D. Lindberg, J.Y. Kim, J.Q. Dong, G.W. Hammett, S.D. Scott, M.C. Zarnstorff, S. Hamaguchi, 1992, Phys. Fluids B **4**, 953.
- Hosea, J. *et al.*, 1994, Fusion Technol., **26**, 389.
- Hsu, C.T., C.Z. Cheng, P. Helander, D.J. Sigmar, R. White, 1994, Phys. Rev. Lett. **72**, 2503.
- Huguet, M. *et al.*, 1992, Fusion Engineering Design **19**, 121
- Ide, S., T. Fujita, O. Naito, M. Seki, 1996, Plasma Phys. Control. Fusion **38**, 1645.
- Ikeda, Y., K. Tobita, K. Hamamatsu, K. Ushigusa, O. Naito, H. Kimura, 1996, Nucl. Fusion **36**, 759.
- Janos, A.C. *et al.*, 1996, Nucl. Fusion **36**, 475.
- Jassby, D.L., C.W. Barnes, L.C. Johnson, A.L. Roquemore, J.D. Strachan, D.W. Johnson, S.S. Medley, K.M. Young, 1995, Rev. of Scientific Instruments **66**, 891.
- Jassby, D.L., *et al.*, 1996, submitted to Nucl. Fusion.
- JET Team, 1992, Nucl. Fusion **32**, 187.
- JET Team, (presented by A. Gibson), 1993, in Plasma Physics and Controlled Nuclear Fusion Research, Fourteenth Conference Proceedings, Würzburg, Germany, 1992 (IAEA, Vienna) **1**, 99.
- JET Team (presented by D. Stork) 1995, in *Plasma Physics and Controlled Nuclear Fusion Research: Proceedings of the 15th International Conference Seville, Spain, 1994* (IAEA, Vienna) **I**, 51.
- JET Team (presented by P.R. Thomas) 1996, in *Proceedings of the Sixteenth IAEA Fusion Energy Conference, Montreal, Canada, 7-11, October 1996* IAEA-CN-64/A3-2.
- JET Team (presented by J. Jacquinet) 1996, in *Proceedings of the Sixteenth IAEA Fusion Energy Conference, Montreal, Canada, 7-11, October 1996* IAEA-CN-64/01-4.
- JET Team, (presented by D.F. Start) 1996, in *Proceedings of the Sixteenth IAEA Fusion Energy Conference, Montreal, Canada, 7-11, October 1996* IAEA-CN-64/A2-6.
- JET Team (presented by C. Gormezano) 1996, in *Proceedings of the Sixteenth IAEA Fusion Energy Conference, Montreal, Canada, 7-11, October 1996* IAEA-CN-64/A5-5.
- Johnson, D. *et al.*, 1995, Plasma Phys. Control Fusion **37**, A69.
- Johnson, L.C., P.C. Efthimion, J.D. Strachan, E. Synakowski, M. Zarnstorff, D. McCune, A.L. Roquemore, M. Loughlin, C.W. Barnes, 1994, 21st EPS Conference on Controlled Fusion and Plasma Physics, Montpellier, edited by E. Joffrin, P. Platz, P.E. Stott (EPS, Geneva) **1**, 182.
- Johnson, L.C., C.W. Barnes, H. Duong, W.W. Heidbrink, D.L. Jassby, M.J. Loughlin, A.L. Roquemore, E. Ruskov, J.D. Strachan, 1995, Rev. of Scientific Instruments **66**, 894.

- Johnson, L.C. *et al.*, 1996, in *Diagnostics for Experimental Thermonuclear Fusion Reactors*, (Plenum Press, New York) p369.
- Kessel, C. *et al.*, 1994, Phys. Rev. Lett. **72**, 1212.
- Kikuchi, M. *et al.*, 1990, Nucl. Fusion **30**, 343.
- Kikuchi, M. *et al.*, 1995, in *Plasma Physics and Controlled Nuclear Fusion Research: Proceedings of the 15th International Conference, Seville, Spain, 1994* (IAEA, Vienna) Vol. **1**, 31.
- Kikuchi, M., M. Azumi, 1995, Plasma Phys. Control. Fusion **37**, 1215
- Kinsey, Jon, C. Singer, T. Djemil, D. Cox, G. Bateman, 1995, Phys Plasmas **2**, 811.
- Kinsey, Jon E. and G. Bateman, 1996, Phys. Plasmas, **3**, 3344.
- Kinsey, Jon E., G. Bateman, A. Kritiz, A. Redd, 1996, Phys. Plasmas, **3**, 561.
- Kissick, M.W. *et al.*, 1993, Phys. Fluids, B, **5**, 3618.
- Kolesnichenko, Ya.I., 1980, Nucl. Fusion **20**, 727.
- Kolesnichenko, Ya.I. *et al.*, 1992, Phys. Rev. Lett. **68**, 3881.
- Kolesnichenko, Ya.I., *et al.*, 1996a, 23rd EPS Conference on Controlled Fusion and Plasma Physics, Kiev.
- Kolesnichenko, Ya.I., Yu. V. Yakovenko, 1996b, Nucl. Fusion, **36**, 159.
- Kolesnichenko, Ya.I., D. Anderson, T. Fülöp, M. Lisak, 1996c, in *Proceedings of the Sixteenth IAEA Fusion Energy Conference, Montreal, Canada, 7-11, October 1996* IAEA-CN-64/F1-CN-64/D3-5.
- Kotschenreuther, M., W. Dorland, M. Beer, G. Hammett, 1995, Phys. Plasmas **2**, 2381.
- Ku, L.P., D.W. Johnson, S.L. Liew, 1994, Fusion Technol. **26**, 933.
- Ku, L.P., S.L. Liew, 1994, in Proceedings of the 8th International Conference on Radiation Shielding, (ANS, LaGrange Park, IL) 1062.
- Kugel, H.W. *et al.*, 1994, Fusion Technol, **31**, 302.
- Kugel, H.W. *et al.*, 1995, Third International Symposium on Fusion Nuclear Technology, Los Angeles, CA, Fusion Engineering and Design **28**, 534.
- Kugel, H.W., G. Ascione, S. Elwood, K. Rule, 1996, in *Proceedings of the Twelfth American Nuclear Society Topical Meeting on the Technology of Fusion Energy, June 16 - 20, Reno, NV.*
- Kumar, A., H.W. Kugel, G. Ascione, 1996a, in *Proceedings of the Twelfth American Nuclear Society Topical Meeting on the Technology of Fusion Energy, June 16 - 20, Reno, NV.*
- Kumar, A., H.W. Kugel, G. Ascione, 1996b in *Proceedings of the Sixteenth IAEA Fusion Energy Conference, Montreal, Canada, October 7-11, IAEA-CN-641GP-6.*

- LaMarche, P.H. *et al.*, 1994, *Fusion Technology*, **26**, 427.
- Lao, L.L. *et al.*, 1993, *Phys. Rev. Lett.* **70**, 3435.
- Lazarus, E.A. *et al.*, 1996a, *Phys. Rev. Lett.* **77**, 2714.
- Lazarus, E.A. *et al.*, 1996b, in *Plasma Physics and Controlled Nuclear Fusion Research: Proceedings of the Sixteenth IAEA Fusion Energy Conference, Montreal, Canada* IAEA/CN/64-A1-2.
- Levinton, F.M., L. Zakharov, S.H. Batha, J. Manickam, M.C. Zarnstorff, 1994, *Phys. Rev. Lett.* **72**, 2895.
- Levinton, F.M. *et al.*, 1995, *Phys. Rev. Lett.* **75**, 4417.
- Levinton, F.M., *et al.*, 1996, in *Proceedings of the Sixteenth IAEA Fusion Energy Conference, Montreal, Canada, 7-11, October 1996* IAEA-CN-64/A1-3.
- Lin, Z., W. Tang, W.W. Lee, 1996, *Phys. Rev. Lett.* **78**, 456.
- McClements, K.G., R. Dendy, C. Lashmore-Davis, G. Cottrell, S. Cauffman, R. Majeski, 1996, *Physics of Plasmas* **2**, 1623.
- McGuire, K.M. *et al.*, 1995, *Phys. Plasmas* **2**, 2176.
- McGuire, K.M., *et al.*, 1996, in *Proceedings of the Sixteenth IAEA Fusion Energy Conference, Montreal, Canada, 7-11, October 1996* IAEA-F1-CN-64/01-2.
- McKee, G.R., R.J. Fonck, T.A. Thorson, B.C. Stratton, 1995a, *Rev. Sci. Instrum.* **66**, 643.
- McKee, G.R. *et al.*, 1995b, *Phys. Rev. Lett.* **75**, 649.
- McKee, G.R. *et al.*, 1996, submitted for publication to *Nuclear Fusion*.
- Majeski, R. *et al.*, 1994, *Phys. Rev. Lett.* **73**, 2204.
- Majeski, R. *et al.*, 1995, in *Plasma Physics and Controlled Nuclear Fusion Research: Proceedings of the 15th International Conference, Seville, Spain, 1994* (IAEA, Vienna) **1**, 443.
- Majeski, R. *et al.*, 1996, *Phys. Rev. Lett.* **76**, 764.
- Manickam, J., *et al.*, 1996, in *Proceedings of the Sixteenth IAEA Fusion Energy Conference, Montreal, Canada, 7-11, October 1996* IAEA-CN-64/A5-2.
- Mansfield, D.K., *et al.*, 1995a, *Phys. Plasmas* **3**, 1892.
- Mansfield, D. K. *et al.*, 1995b, *Phys. Plasmas* **2**, 4252.
- Marcus, F.B., J.M. Adams, B. Balet, D.S. Bond, S.W. Conroy, P.J.A. Howarth, O.N. Jarvis, M.J. Loughlin, G.J. Sadler, P. Smeulders, N. Watkins, 1993, *Nucl. Fusion* **33**, 1325.
- Mazzucato E. *et al.*, 1996a, *Phys. Rev. Lett.* **77**, 3145.

- Mazzucato, E., *et al.*, 1996b, in *Proceedings of the Sixteenth IAEA Fusion Energy Conference, Montreal, Canada, 7-11, October 1996* IAEA-CN-64/AP2-16.
- Meade, D.M. *et al.*, 1991, in *Plasma Physics and Controlled Nuclear Fusion Research: Thirteenth Conference Proceedings*, Washington, US (IAEA, Vienna) **1**, 9.
- Meade, D.M., 1995, *Fusion Engineering and Design* **27**, 17.
- Medley, S.S., R.K. Fisher, A.V. Khudoleev, D.K. Mansfield, J.M. McChesney, P.B. Parks, M. P. Petrov, C.K. Phillips, A.L. Roquemore, K.M. Young, 1995, 22nd European Conference on Controlled Fusion and Plasma Physics, Bournemouth, Contributed Papers edited by B.E. Keen, P.E. Stott, J. Winter (EPS, Geneva) **1**, 409.
- Medley, S.S., R.V. Budny, D.K. Mansfield, M.H. Redi, A.L. Roquemore, R.K. Fisher, H.H. Duong, J.M. McChesney, P.B. Parks, M.P. Petrov, N.N. Gorelenkov, 1996a, *Plasma Phys. Controlled Fusion* **38**, 1779.
- Medley, S.S., H. Duong, R. Fisher, N. Gorelenkov, A. Khudoleev, D. Mansfield, J. McChesney, P. Parks, M. Petrov, A. Roquemore 1996b, *Rev. Sci. Instrum.* **67**, 3122.
- Morgan, P.D., 1992, in *Proceedings of the 17th Symposium on Fusion Technology*, Rome Italy, Edited by C. Ferro, M. Gasparotto, H. Knoepfel (Elsevier, Amsterdam) 722.
- Mueller, D. *et al.*, 1996, in *Proceedings of the Twelfth American Nuclear Society Topical Meeting on the Technology of Fusion Energy*, June 16 - 20, Reno, NV.
- Mueller, D. *et al.*, 1996, *Fusion Technol* **30**, 251.
- Mynick, H.E. and N. Pomphery, 1994, *Nucl. Fusion* **34**, (9), 1277.
- Nagayama, Y. *et al.*, 1993, *Phys. Fluids* **B5**, 2571.
- Nagy, A. *et al.*, 1995, in *Proceedings of the 16th IEEE/NPSS Symposium on Fusion Engineering*, Champaign, IL, edited by G. Miley, C. Elliott (IEEE, Piscataway, NJ) Vol. **2**, 573
- Navratil, G. *et al.*, 1991, in *Plasma Physics and Controlled Nuclear Fusion Research: Proceedings of the 13th International Conference, Washington, DC, 1990* (IAEA, Vienna) **1**, 209.
- Navratil, G., *et al.*, 1996, presented at the European Physical Society Meeting in Kiev, Ukraine, 1996, to be published in *Plasma Physics and Controlled Fusion*.
- Nazikian, R. *et al.*, 1996a, in *Proceedings of the Sixteenth IAEA Fusion Energy Conference, Montreal, Canada, 7-11, October 1996* IAEA-CN-64/A2-4.
- Nazikian, R., *et al.*, 1996b, submitted to *Phys. Rev. Lett.*
- Ono, M., 1993, *Phys. Fluids B* **5**, 241.
- Ozeki, T. *et al.*, 1993, in *Plasma Physics and Controlled Fusion Research: Proceedings of the Fourteenth International Conference, Würzburg* (IAEA Vienna) **2**, 187.
- Park, H.K. 1996, submitted to *Phys. of Plasmas*.

- Park, W., E.D. Fredrickson, A. Janos, J. Manickam, W.T. Tang, 1995, *Phys. Rev. Lett.* **75**, 1763.
- Park, W., Z. Chang, E. Fredrickson, G.Y. Fu, N. Pomphrey, 1996, in *Proceedings of the Sixteenth IAEA Fusion Energy Conference, Montreal, Canada, 7-11, October 1996*, IAEA-CN-64/D2-2.
- Paul, S.F., J.L. Goldstein, R.D. Durst, R.J. Fonck, 1995, *Rev. of Scientific Instruments*, **66**, 1252.
- Petrov, M.P., R.V. Budny, H.H. Duong, R.K. Fisher, N.N. Gorelenkov, J.M. McChesney, D.K. Mansfield, S.S. Medley, P.B. Parks, M.H. Redi, A.L. Roquemore, 1995, *Nucl. Fusion* **35**, 1437.
- Petrov, M.P., *et al.*, 1996, in *Proceedings of the Sixteenth IAEA Fusion Energy Conference, Montreal, Canada, 7-11, October 1996* IAEA-CN-64/A2-2.
- Phillips, C.K. *et al.*, 1995, *Phys. Plasmas* **2**, 2427.
- Pick, M. *et al.*, 1996, 1996, in *Proceedings of the Twelfth American Nuclear Society Topical Meeting on the Technology of Fusion Energy, June 16 - 20, Reno, NV*
- Raftopoulos, S., R. Scillia, P. Sichta, L. Dudek, G. Labik, J. Satkofsky, J. Langford, D. Voorhees, 1995, in *Proceedings of the 16th IEEE/NPSS Symposium on Fusion Engineering, Champaign, IL, edited by G. Miley, C. Elliott (IEEE, Piscataway, NJ)* **1**, 581.
- Ramsey, A.T., 1995, *Rev. of Scientific Instruments*, **66**, 871.
- Redi, M.H., M.C. Zarnstorff, R.B. White, R.V. Budny, A.C. Janos, D.K. Owens, J.F. Schivell, S.D. Scott, S.J. Zweben, 1995a, *Nucl. Fusion* **35**, 1191.
- Redi, M.H. *et al.*, 1995b, *Nucl. Fusion* **35**, 1509.
- Rogers, B., L. Zakharov, 1995, *Phys. Plasmas*, **2**, 3420
- Rogers, J.H., D. Darrow, R. Majeski, M. Murakami, C.K. Phillips, D.A. Rasmussen, G. Schilling, J. Stevens, G. Taylor, J.R. Wilson, K.L. Wong, 1994, *21st EPS Conference on Controlled Fusion and Plasma Physics, Montpellier*, edited by E. Joffrin, P. Platz, P.E. Stott (EPS, Geneva) **2**, 988.
- Rogers, J.H., *et al.*, 1996, in *Proceedings of the Sixteenth IAEA Fusion Energy Conference, Montreal, Canada, 7-11, October 1996* IAEA-CN-64/EP-2.
- Ruskov, E., W.W. Heidbrink, R.V. Budny, 1995, *Nucl. Fusion* **35**, 1099.
- Sabbagh, S.A. *et al.*, 1991, *Phys. Fluids B* **3**, 2277.
- Sabbagh, S.A. *et al.*, 1995a, in *Plasma Physics and Controlled Nuclear Fusion Research: Proceedings of the 15th International Conference Seville, Spain*, 1994 (IAEA, Vienna) **1**, 663.
- Sabbagh, S.A. *et al.*, 1995b, Tokamak Concept Improvement, in *Proceedings of the Workshop held at the 1994 International School of Plasma Physics, Varenna, Italy* edited by S. Bernabei, N. Sauthoff, E. Sinloni, Editrice Compositori, Italy.

- Sabbagh, S.A., *et al.*, 1996, in *Proceedings of the Sixteenth IAEA Fusion Energy Conference, Montreal, Canada, 7-11, October 1996* IAEA-CN-64/AP2-17.
- Saibene, G., R. Sartori, P. Andrew, J. How, Q. King, and A.T. Peacock, 1992, *Fusion Engineering and Design* **19**, 133
- Saigusa, M., *et al.*, 1995, *Plasma Physics Controlled Fusion* **37**, 295.
- Saville, C., G. Ascione, S. Elwood, A. Nagy, S. Raftopoulos, R. Rossmassler, J. Stencel, D. Voorhees, C. Tilson, 1995, *Fusion Technol.* **28**, 1078.
- Scott, S. *et al.*, 1990a, *Phys. Rev. Lett.* **64**, 531
- Scott, S. *et al.*, 1990b, *Phys. Fluids B* **2**, 1300.
- Scott, S.D. *et al.*, 1995, *Phy. Plasmas* **2**, 1994.
- Scott, S.D. *et al.*, 1996a, *Phys. Scr.* **51**, 394.
- Scott, S.D., *et al.*, 1996b, in *Proceedings of the Sixteenth IAEA Fusion Energy Conference, Montreal, Canada, 7-11, October 1996* IAEA-F1-CN-64/A6-6.
- Shaing, K.C., E.C. Crume, Jr., and W.A. Houlberg, 1990, *Phys. Fluids B* **2**, 1492.
- Sigmar, D.J., 1987, *Phys. Scr.* **T16**, 6.
- Skinner, C., H. Adler, R.V. Budny, J. Kamperschroer, L.C. Johnson, A.T. Ramsey, D.P. Stotler, 1995a, *Nucl. Fusion* **35**, 143.
- Skinner, C.H., D.P. Stotler, H. Adler, A.T. Ramsey, 1995b, *Rev. of Scientific Instruments* **66**, 646.
- Skinner, C.H. *et al.*, 1996a, *J. Vac. Sci. Technol.* **A14**, 3267.
- Skinner, C.H., J. Kamperschroer, D. Mueller, A. Nagy, J. Stotler, 1996b, *J. Nucl. Mater.* (in press).
- Skinner, C.H. *et al.*, 1996c, *J. Nucl. Mater.* (in press).
- Spong, D.A., C.L. Hedrick, B.A. Carreras, 1995, *Nuclear Fusion* **35**, 1687.
- Stencel, J.R., J.D. Gilbert, J.D. Levine, G. Ascione, 1994, *Journal of Applied Health Physics*, **11**, 27.
- Stevenson, T., T. O'Connor, V. Garzotto, L. Grisham, J. Kamperschroer, B. McCormack, R. Newman, M. Oldaker, S. Ramakrishnan, A. von Halle, K. Wright, 1995, 16th IEEE/NPSS Symposium on Fusion Engineering, Champaign, IL, edited by G. Miley, C. Elliott (IEEE, Piscataway, NJ) **1**, 537.
- Stotler, D.P., C.H. Skinner, R.V. Budny, A.T. Ramsey, 1996, *Phys. Plasmas* **3** (11), 4084.
- Strachan, J.D., R.E. Chrien, W.W. Heidbrink, 1983, *J. Vac. Sci. Technol. A*, **1**, 811.
- Strachan, J.D. *et al.*, 1987, *Phys. Rev. Lett.* **58**, 1004.

- Strachan, J.D. *et al.*, 1989, in *Proceedings of the 10th International Conference on Plasma Physics and Controlled Nuclear Fusion Research*, Nice (IAEA, Vienna) **1**, 257.
- Strachan, J.D. *et al.*, 1990, *Rev. Sci. Instrum.* **61**, 3501.
- Strachan, J.D. *et al.*, 1992, *J. Nucl. Mat.* **96**, 28.
- Strachan, J.D., 1994, *Nucl. Fusion* **34**, 1017.
- Strachan, J.D. *et al.*, 1994a, *Phys. Rev. Lett.* **72**, 3526.
- Strachan, J.D. *et al.*, 1994b, *Plasma Physics and Controlled Fusion* **36**, B3.
- Strachan, J.D. *et al.*, 1994c, *J. Nucl. Mat.* **217**, 145.
- Strachan, J.D., C.W. Barnes, M. Diesso, D. Jassby, L. Johnson, M. Loughlin, S. McCauley, T. Munsat, A.L. Roquemore, 1995, *Rev. of Sci. Instrum.*, **66**, 1247.
- Strait, E. J. *et al.*, 1993, *Nucl. Fusion* **33**, 1849.
- Strait, E. J. *et al.*, 1996, *Phys. Rev. Lett.* **75**, 4421.
- Stratton, B., R. Fonck, G. McKee, R. Budny, Z. Chang, F. Wising, A. Ödholm, 1996, *Nucl. Fusion* **36**, 1586.
- Synakowski, E.J. *et al.*, 1993, *Phys. Fluids, B*, **5**, 2213.
- Synakowski, E.J. *et al.*, 1995a, *Phys. Rev. Lett.* **75**, 3689.
- Synakowski, E.J. *et al.*, 1995b, in *Proceedings of the 22th European Conference on Controlled Fusion and Plasma Physics* (Bournemouth, U.K., 1995), volume 19C of Europhysics Conference Abstracts, pp. 13-16, Petit-Lancy, Switzerland, 1995, EPS, Part III.
- Synakowski, E.J. *et al.*, 1996a, submitted to *Phys. Plasmas*.
- Synakowski, E.J. *et al.*, 1996b, submitted to *Phys. Rev. Lett.*
- Taylor, G. *et al.*, 1995, in *Plasma Physics and Controlled Nuclear Fusion Research: Proceedings of the 15th International Conference, Seville, Spain, 1994* (IAEA, Vienna) **1**, 431.
- Taylor, G. *et al.*, 1996a, *Plasma Phys. Control Fusion* **38**, 723.
- Taylor, G. *et al.*, 1996b, *Phys. Rev. Lett.* **76**, 2722.
- Terry, J.L. *et al.*, 1991, in *Proceedings of the 11th International Conference on Plasma Physics and Controlled Nuclear Fusion Research*, Washington, D.C., (International Atomic Energy Agency, Vienna), **1**, 393.
- Thomas, P.R., 1996, “*Divertor Diagnostics for JET*” in *Diagnostics for Experimental Thermonuclear Fusion Reactors* (Plenum Press, New York, 1996) 531.
- Tibone, F. 1993, *Nucl. Fusion* **33**, 1319.

- Tobita, K. *et al.*, 1996, in *Proceedings of the Sixteenth IAEA Fusion Energy Conference, Montreal, Canada, 7-11, October 1996* IAEA-CN-64/A5-6.
- Troyon, F., R. Gruber, H. Saurenmann, S. Semenzato, S. Succi, 1984, *Plasma Physics and Controlled Fusion* **26**, 209.
- Turnbull, A.D. *et al.*, 1995, *Phys. Rev. Lett.* **74**, 718.
- Ulrickson, M. *et al.*, 1990, *J. Nucl. Mater.* **176/177**, 44.
- Ushigusa, K. and the JT-60 Team, 1996, in *Proceedings of the Sixteenth IAEA Fusion Energy Conference, Montreal, Canada, 7-11, October 1996* IAEA-CN-64/F1-CN-64/01-3.
- Valeo, E.J., N.J. Fisch, 1994, *Phys. Rev. Lett.* **73**, 3536.
- Wagner, F. *et al.*, 1982, *Phys. Rev. Lett.* **49**, 1408.
- Wang, S., S.J. Zweben, 1996, "Model of Alpha Particle Diffusion in the Outer Limiter Shadow of TFTR", PPPL-3186.
- Ward, D.J., 1996, *Plasma Phys. and Controlled Fusion* **38**, 1201.
- White, R.B., E. Fredrickson, D. Darrow, M. Zarnstorff, R. Wilson, S. Zweben, K. Hill, Y. Chen, G. Fu, 1995a, *Phys. Plasmas* **2**, 2871.
- White, R.B., Y. Wu, Y. Chen, E.D. Fredrickson, D.S. Darrow, M.C. Zarnstorff, J.R. Wilson, S.J. Zweben, K.W. Hill, G.Y. Fu, 1995b, *Nucl. Fusion* **35**, 1707.
- White, R.B., *et al.*, 1996, *Phys. Plasmas* (in press).
- Williams, M.D. and the TFTR Group, 1996, Symposium on Fusion Technology, September 16-20, 1996 (Lisbon, Portugal) to be published in *Fusion Engineering and Design*.
- Wilson, J.R. *et al.*, 1993, in *Plasma Physics and Controlled Nuclear Fusion Research, Fourteenth Conference Proceedings, Würzburg, Germany, 1992* (IAEA, Vienna) **1**, 661.
- Wilson, J.R., *et al.*, 1995, *Phys. Rev. Lett.* **75**, 842.
- Wong, K.L., *et al.*, 1991, *Phys. Rev. Lett.* **66**, 1874.
- Wong, K.L. *et al.*, 1992, *Phys. Fluids B* **4**, 2122.
- Wong, K.L. *et al.*, 1996a, *Phys. Rev. Lett.* **76**, 2286.
- Wong, K.L. *et al.*, 1996b, "Evolution of Toroidal Alfvén Eigenmode Instability in TFTR", PPPL-3204, submitted for publication.
- Young, K.M., D.W. Johnson, 1992, *Plasma Phys. and Controlled Fusion* **34**, 2001.
- Young, K.M. 1995, "Advanced Tokamak Diagnostics", *Proceedings of the 7th International Conference on Plasma Physics and Controlled Nuclear Fusion*, December 1995; (in press).
- Yushmanov, P.N., T. Takizuka, K.S. Riedel, O.J.W.F. Kardaun, J.G. Cordey, S.M. Kaye and D.E. Post, 1991, *Nuclear Fusion* **30**, 1999.

- Zakharov, L., B. Rogers, 1992, Phys. Fluids B **4**, 3285.
- Zakharov, L. B. Rogers, and S. Migliuolo, 1993, Phys. Fluids B **5**, 2498.
- Zarnstorff, M.C. *et al.*, 1988a, *15th European Conference on Controlled Fusion and Plasma Heating*, Dubrovnik, Contributed Papers edited by S. Pesic, J. Jacquinet, 1988, (EPS) **12B**, Part 1, 95.
- Zarnstorff, M.C. *et al.*, 1988b, Phys. Rev. Lett. **60**, 1306.
- Zarnstorff, M.C. *et al.*, 1989a, in *Plasma Physics and Controlled Nuclear Fusion Research: Proceedings of the Twelfth International Conference Nice, Oct. 12-19, 1988* (IAEA, Vienna) **1**, 183.
- Zarnstorff, M.C. *et al.*, 1989b, *Controlled Fusion and Plasma Physics, Proceedings of the Sixteenth European Conference, Venice 1989*, **13B**, Part 1, 35.
- Zarnstorff, M.C. *et al.*, 1990, *Controlled Fusion and Plasma Heating, Proceedings of the Seventeenth European Conference, Amsterdam, 1990*, Vol. **14B**, Part 1, 42.
- Zarnstorff, M.C. *et al.*, 1991 in *Plasma Physics and Controlled Nuclear Fusion Research: Proceedings of the Thirteenth International Conference, Washington, 1990* (IAEA, Vienna), Vol. **1**. 109.
- Zarnstorff, M.C. *et al.*, 1995, in *Plasma Physics and Controlled Nuclear Fusion Research: Proceedings of the 15th International Conference, Seville, Spain, 1994* (IAEA, Vienna) **1**, 183.
- Zhao, Y., and R. White, 1996, "Simulation of α -Particle Redistribution due to Sawteeth on TFTR," PPPL Report 3219, submitted for publication.
- Zweben, S.J. *et al.*, 1990, Nucl. Fusion **30**, 1551.
- Zweben, S.J. *et al.*, 1991, Nucl. Fusion **31**, 2219.
- Zweben, S.J. *et al.*, 1993a, Nucl. Fusion **33**, 705.
- Zweben, S.J. *et al.*, 1993b, in *Plasma Physics and Controlled Nuclear Fusion Research: Proceedings of the 14th International Conference, Würzburg, 1992* (IAEA, Vienna) **1**, p.363.
- Zweben, S.J. *et al.*, 1994, Phys. Plasmas **1**, 1469.
- Zweben, S.J., *et al.*, 1995a, Nucl. Fusion, **35**, 893.
- Zweben, S.J., D.S. Darrow, H.W. Herrmann, M.H. Redi, J.F. Schivell, R.B. White, 1995b, Nucl. Fusion **35**, 1445.
- Zweben, S.J. *et al.*, 1996a, Invited Paper at ICPP Conf. Nagoya, Sept. 1996, submitted to Plasma Phys. & Controlled Fusion.
- Zweben, S.J. *et al.*, 1996b, "Search for Alpha-Driven TAE Modes at Lowered Ion Temperature in TFTR D-T Discharges", PPPL-3154.

Figure Caption

- Fig. 1 Cross sections for fusion reactions of importance in magnetic fusion are plotted versus energy.
- Fig. 2 The achieved product $n_{\text{HYD}} T_i(0) \tau_E^*$ where n_{HYD} is the sum of all hydrogenic densities versus $T_i(0)$ for various tokamak devices. In present devices, P_{breh} is small compared with P_{aux} and ignored. For comparison, an estimate of the criteria for $P_{\text{fus}}/P_{\text{aux}} = 1$ and ignition in which the alpha heating sustains the plasma is given.
- Fig. 3 The interior of the TFTR vacuum vessel is shown. The carbon-composite and graphite tiles on the inner wall limits the plasma and protects the vacuum vessel wall.
- Fig. 4 Interior of the JET vacuum vessel (JET Team, 1992).
- Fig. 5 Four lost alpha detectors are located behind the limiter shadow. Schematic diagram of the TFTR lost alpha detector. The escaping alphas enter a pair of apertures that disperse them in pitch angle and gyroradius (Darrow *et al.*, 1996a).
- Fig. 6 Illustration of the pellet charge exchange diagnostic to measure confined alpha particles (Medley *et al.*, 1996b).
- Fig. 7 Alpha-CHERS sightlines and beam viewing geometry (McKee *et al.*, 1995a, 1996).
- Fig. 8 Radial profiles of the ion and electron temperature and electron density for JET pulse number 26148 (JET Team, 1992).
- Fig. 9 Radial profiles of the ion and electron temperature and electron densities for TFTR pulse number 83546, a high performance supershot, is contrasted with a comparable L-mode discharge with similar plasma current and heating power.
- Fig. 10 (a) Comparison of stored energy deterioration ($\delta W/W$) theory and experiment due to neoclassical tearing modes. (b) The energy deterioration is proportional to the island width as predicted by the theory and simulation (Chang *et al.*, 1994).
- Fig. 11 Comparison of the measured magnetic island evolution with the nonlinear neoclassical driven tearing mode theory for (a) the $m/n=3/2$ mode case and (b) the $4/3$ mode case (Chang *et al.*, 1994).
- Fig. 12 a) Electron cyclotron emission measurements of the evolution of the electron temperature prior to a disruption. An $n = 1$ kink mode is observed to precede the destabilization of a ballooning mode (Fredrickson *et al.*, 1995a, 1996c).
b) Contours of the electron temperature evolution at one toroidal location. The ballooning mode is observed on the outer midplane.
c) Contours of the electron temperature evolution toroidally separated by 126° from the previous set of measurements.
- Fig. 13 a) Three dimensional nonlinear simulation of equi-pressure contours of the MHD instability.
b) Simulations of the electron cyclotron emission measurements of the electron temperature reproduce the observation of the ballooning mode shown in Fig. 12

being destabilized by a low-n kink mode with the largest displacement on the outboard side of the plasmas (Park *et al.*, 1995). Since the plasma rotates toroidally, the calculations versus toroidal angle are related to the measurements versus time.

- Fig. 14 Motional Stark Effect measurements of the $j(r)$ and $q(r)$ profiles in a high ℓ_i discharge are contrasted with a supershot discharge (Sabbagh *et al.*, 1996).
- Fig. 15 Operating range of high ℓ_i discharges in terms of the enhancement in energy confinement time, $H = \tau_E/\tau_E^{\text{ITER89-P}}$ and β_N is compared with the operating range of supershot discharges (Sabbagh *et al.*, 1994b, 1996).
- Fig. 16 Hollow current profiles are achieved by rapidly ramping the plasma current and heating the plasma in the “prelude” phase prior to the “high power” heating phase. Subsequently, the power is decreased in the “postlude” phase to study the evolution of the plasma transport (Levinton *et al.*, 1996).
- Fig. 17 Motional Stark Effect measurements of the safety factor, q , which illustrate the effect of applying heating power during the “prelude” phase. The magnetic equilibrium reconstruction analysis is shown for comparison. The normalized minor radius of the minimum of the safety factor is denoted r_{\min} and the corresponding value of the safety factor is denoted q_{\min} (Levinton *et al.*, 1996).
- Fig. 18 Comparison of the evolution of two reverse shear discharges near the threshold power for a transition. Shown is the (a) central electron density, (b) the central electron temperature, (c) the central ion temperature, and (d) the total neutral beam power waveform. In the enhanced reverse shear discharge, the development of an internal transport barrier and reduced core transport results in a large increase in the central density and core pressure. In this ERS plasma, the loss of good core confinement in the 14 MW “postlude” period of injection is correlated with a reduction in the radial electric field magnitude \mathbf{ExB} shearing rate γ_s , induced by opposing contributions from co-rotation and the plasma pressure (Synakowski *et al.*, 1996a) After the back transition, the plasma confinement properties return to those in the reverse-shear discharge without the transport barrier.
- Fig. 19 The inferred ion thermal diffusivity (a) and particle diffusivity (b) is observed to decrease dramatically in the enhanced reversed shear discharges (Levinton *et al.*, 1995). For comparison, the standard calculation of neoclassical ion heat conductivity is shown as well as the recent calculations by Lin *et al.* (1996).
- Fig. 20 a) ECE measurements of the displacement of the magnetic surfaces are in good agreement with the predictions of ideal MHD theory for reverse shear TFTR discharges (Manickam *et al.*, 1996). b) The corresponding q -profile.
- Fig. 21 Dependence of the peak D-T fusion power (averaged over a 40ms interval) on total plasma energy in high-current (≥ 2.0 MA) supershots [squares] and high- ℓ_i plasmas at 2.0 - 2.3 MA produced by cross-section expansion of low- q ($q_a \approx 2.5$) discharges [diamonds]. All plasmas have approximately the same volume ($\sim 38\text{m}^3$) and a nearly optimal mixture of D and T in the reactive region produced by neutral beam injection (Bell *et al.*, 1996).
- Fig. 22 Time dependence of the central electron and ion temperatures, the volume averaged electron density, the line average, Z_{eff} , the plasma diamagnetic energy, the D_α emission, the total neutron rate, and the neutral beam and radiated power for pulse No. 26148 (JET Team, 1992).

- Fig. 23 Evolution of the central electron density, ion temperature, electron temperature, stored energy and fusion power for TFTR shot No. 80539.
- Fig. 24 Neutron source strength measurements and TRANSP simulation of the total neutron rate on JET pulse No. 26148 (JET Team., 1992).
- Fig. 25 Neutron source strength measurement and TRANSP simulation of the total neutron rate for TFTR pulse No. 76778 with $P_b = 33.9$ MW (Budny *et al.*, 1995).
- Fig. 26 Neutron emission profile as measured by the neutron collimator are compared with a TRANSP simulation. The contributions from thermal-thermal, beam-thermal and beam-beam reactions are shown (Budny *et al.*, 1995).
- Fig. 27 The ratio of the energy confinement in a D-T discharge is compared with that in a companion D-discharge versus the average hydrogenic ion mass, $\langle A \rangle = \sum n_i A_i / \sum n_i$, where n_i is the hydrogenic density (Scott *et al.*, 1995, 1996a).
- Fig. 28 Comparison of electron density, ion and electron temperature profiles for a D and a companion D-T discharge (Scott *et al.*, 1996a).
- Fig. 29 Comparison of the ion thermal diffusivity in a D-T plasma heated by tritium beam with a companion D discharge. The thermal mix of the background ions is approximately a 50:50 D-T mix. (Scott *et al.*, 1996a).
- Fig. 30 Kinetic profiles in D and D-T L-mode ‘isotope ρ^* -scaling’ plasmas matched in density, temperature, β , v^* , B_t , I_p , Z_{eff} , and v_{*e} . Contrary to gyroBohm expectations, the D plasma with smaller ρ^* requires $\sim 30\%$ more heating power to sustain the temperature (Scott *et al.*, 1996b).
- Fig. 31 Evolution of a) $\tau_E/\tau_E^{\text{ITER-89-P}}$ and b) D_α for a D-T discharge and a companion D discharge on TFTR (Bush *et al.*, 1995).
- Fig. 32 Comparison of the effect of H-mode transition in a D and D-T limiter discharge on TFTR (Bush *et al.*, 1995).
- Fig. 33 Evolution of a) D-T neutron emissivity and b) the inferred tritium density profiles following a small tritium gas puff into a supershot discharge on TFTR (Johnson *et al.*, 1994; Efthimion *et al.*, 1995a).
- Fig. 34 The tritium particle diffusivity following a small tritium gas puff is comparable with the electron particle diffusivity as well as the He diffusivity (Efthimion *et al.*, 1995a).
- Fig. 35 The measured neutron source strength of 14 MeV neutrons by a Si diode detector due to a short pulse of high power neutral beam injection is in good agreement with simulations which assume a small radial diffusivity ($D_f < 0.05 \text{ m}^2/\text{s}$) for the beam ions (Ruskov *et al.*, 1995).
- Fig. 36 Ion and electron temperature profiles in a discharge heated with 23.5 MW of neutral beam heating and in another supplemented by an additional 5.5 MW of ICRF heating (Wilson *et al.*, 1995).
- Fig. 37 Measurements and prediction using the PICES and TRANSP codes of the fraction of rf power absorbed by electron and ions versus the triton beam power fraction. Modulation of the rf power together with the evolution of the electron and ion

temperature is used to infer the fraction of power absorbed by ions and electrons (Phillips *et al.*, 1995).

- Fig. 38 Mode conversion of the fast wave results in strong and highly localized electron heating at the ion-ion hybrid layer (Majeski *et al.*, 1996).
- Fig. 39 Observed radius of electron power deposition as a function of toroidal field, for constant ^3He fraction and density. The open symbols denote the observed location from electron temperature measurement and the line denotes the location of mode conversion layer (Majeski *et al.*, 1996).
- Fig. 40 The measured mode conversion current drive is compared with the predicted current drive (Majeski *et al.*, 1996).
- Fig. 41 Illustration of confined passing alpha particle orbits, confined trapped alpha on banana orbits and unconfined trapped alphas.
- Fig. 42 Fraction of alpha particles collected by a detector located near the bottom of the vessel (90°). The decrease in loss with increasing current is in good agreement with the predictions of the first orbit loss model. The data is normalized at low currents as indicated (Zweben *et al.*, 1995a).
- Fig. 43 The increase in alpha loss to the detector at the bottom of the machine resulting from ICRF waves is plotted as a function of toroidal field. The shaded range of toroidal field denotes where marginally passing alpha particles can be in Doppler-shifted resonance with the waves. Loss proceeds by conversion of these marginally passing orbits to lost banana orbits as the alphas are heated.
- Fig. 44 Measurements of the confined alpha particle spectrum following neutral beam heating of a D-T plasma. The TRANSP calculations which are normalized at one point are in good agreement with the observed slowing down spectrum (Petrov *et al.*, 1995; Medley *et al.*, 1996a).
- Fig. 45 Measured alpha-CHERS spectra at $r/a=0.3$ in a non-sawtooth TFTR D-T supershot are in good agreement with predictions based on TRANSP calculation of the alpha density (McKee *et al.*, 1995b).
- Fig. 46 Pellet charge exchange measurements of the confined alpha particles prior to and after the sawtooth instability (in a companion discharge). The observed redistribution is in reasonable accord with the magnetic reconnection model which incorporates the effect of the helical electric field (Petrov *et al.*, 1996).
- Fig. 47 Alpha-CHERS measurements of alpha density profiles before and after a sawtooth crash are in good agreement with predictions of the Kolesnichenko *et al.*, (1992) sawtooth model (Stratton *et al.*, 1996).
- Fig. 48 The measured ripple boundary is determined from the major radius at which confined alpha particles are measured by the pellet charge exchange diagnostic. The location of the observed presence of deeply trapped alpha particles is in reasonable accord with a simple estimate of the calculated ripple boundary using the Goldston-White-Boozer formalism (Duong *et al.*, 1996a).
- Fig. 49 Measured and modeled ash profile shapes measured 1.95 s after the start of deuterium-tritium beam injection. The errors include uncertainties related to the atomic physics of charge exchange and beam attenuation, as well as photon. The thick dashed line represents the helium ash profile shape predicted under the

assumption of no radial transport of the thermalized ash. The thinner dashed line represents the predicted profile shape including the effects of radial transport and wall recycling. The shaded region is the difference in the profile shapes that are predicted with and without the central source of thermalizing alpha particles, but with transport in both cases (Synakowski *et al.*, 1995a).

- Fig. 50 The first burst of alpha particles prior at 3.9525 sec to the detector in the bottom of the vessel precedes the thermal quench of the plasma as measured by the electron temperature diagnostic and is coincident with the MHD activity responsible for the subsequent disruption (Janos *et al.*, 1996).
- Fig. 51 Alpha particle loss due to neoclassical tearing modes correlated with fluctuations in the edge magnetic field (McGuire *et al.*, 1996).
- Fig. 52 Increased alpha particle loss is correlated with the occurrence of multiple high-n modes (a) as well as single n (=6) mode (b). These modes are identified as kinetic ballooning modes (KBM) (Chang *et al.*, 1996b).
- Fig. 53 Fraction of energetic particles power lost from the plasma and the TAE mode amplitude versus the heating power in TFTR discharges. Energetic particle loss resulted from TAE instabilities driven by neutral beam injection and ICRF heating but not by alpha particles (Darrow *et al.*, 1996b).
- Fig. 54 TAE mode amplitude in D-T plasmas are higher than in companion D shots with the same ICRF heating power used to generate the energetic tail of H-minority particles (Wong *et al.*, 1996a).
- Fig. 55 Alpha-driven TAE mode in TFTR occurring ≈ 0.1 s after neutral beam injection in a D-T discharge with weak central magnetic shear. a) The evolution of β_N and β_α . b) The occurrence of magnetic fluctuations with different toroidal mode numbers is observed. c) The evolution of the frequency of the magnetic fluctuations. The frequency is consistent with the density-dependent TAE frequency, and mode timing is in reasonable agreement with the theoretical prediction based on beam ion damping (Nazikian *et al.*, 1996a).
- Fig. 56 TAE mode amplitude measurements using a magnetic pickup coil at the edge increases with fusion power as expected for alpha-driven TAE near threshold condition for instability. Modes are observed with $\beta_\alpha(0) > 0.03\%$ in weak central shear discharge with $q_0 \sim 1.1 - 1.3$ (Nazikian *et al.*, 1996a).
- Fig. 57 Correlation between ICE intensity, P_{ICE} , and total neutral emission rate for ohmic and neutral beam heating in both D and D-T discharges (Cottrell *et al.*, 1993).
- Fig. 58 Comparison of the electron temperature profile for a set of similar D-T and D discharges with comparable energy confinement times and neutral beam heating power. The measured difference in electron temperature is consistent with the predicted change due to alpha heating. The neutron profile which is a measure of the alpha particle birth profile is shown for comparison (Taylor *et al.*, 1996b).
- Fig. 59 Fast ion loss as measured by the 45° detector in the TFTR vessel indicates the loss of deuterium beam ions heated by mode converted ion Bernstein waves. The flux of particles is in accord with a simple model of fast ion heating by the mode converted wave.
- Fig. A1 The JET tritium gas collection system (JET Team, 1992).

Fig. A2 The TFTR tritium gas fuel cycle (Williams *et al.*, 1996).

Table I Comparison of JET and TFTR Engineering Parameters

	<u>JET</u>	<u>TFTR</u>
Plasma major radius, R	2.96 m	2.6m
Plasma minor radius (horizontal), a	1.25m	0.9m
Plasma elongation ratio, κ	1.68	1.0
Toroidal magnetic field (plasma center), B_t	3.45 T	5.9 T
Plasma current, I_p	7.0 MA	3.0 MA
Neutral beam power, P_b	18 MW	40 MW
ICRF power, P_{ICRF}	22 MW	11 MW

Table II Diagnostic Measurements on TFTR

Profile Data

$T_e(\mathbf{r})$

TV Thomson Scattering
ECE Heterodyne Radiometer
ECE Fourier Transform Spectrometer
ECE Grating Polychromator

$n_e(\mathbf{r})$

TV Thomson Scattering
Multichannel Far Infra-Red Interferometer

$T_i(\mathbf{r})$

Charge-Exchange Recombination Spectroscopy
X-ray Crystal Spectrometer

$q(\mathbf{r})$

Motional Stark Effect Polarimeter

Fusion Neutrons

Epithermal Neutrons
Neutron Activation Detectors
14 MeV Neutron Detectors
Collimated Neutron Spectrometer
Multichannel Neutron Collimator
Fast Neutron Scintillation Counters
Gamma Spectrometer

Alpha-particles

Lost Alpha/Triton Array
Alpha-Charge-Exchange Analyzer
Alpha -Charge-Exchange Recomb. Spectroscopy

Impurity Concentration

Visible Bremsstrahlung Array
VUV Survey Spectrometer
Multichannel Visible Spectrometer
X-ray Pulse Height Analyzer

Radiated Power

Tangential Bolometers
Bolometer Arrays
Wide-Angle Bolometers

Fluctuations/Wave Activities

Microwave Scattering
X-ray Imaging System
Ion Cyclotron Emission/RF Probes
ECE Grating Polychromator
Mirnov Coils
Neutron Fluctuation Detector

Magnetic Measurement

Plasma Current
Plasma Geometry
Diamagnetic Flux
Loop Voltage

Plasma Edge/Wall

Plasma TV
IR Camera
Filtered Diodes (H-alpha)
Filtered Diodes (C-II)
Fabry-Perot Spectrometer
Sample Exposure Probe

Table III Summary of JET Experimental Parameters Comparing a High Performance D and D-T Discharge from the Preliminary Tritium Experiment (JET Team, 1992).

Parameters	Units	#26087	#26148
Plasma Current (I_p)	MA	3.1	3.1
Toroidal Field (B_t)	T	2.8	2.8
NB Power (P_b)	MW	14.9	14.3
Central Electron Density [$n_e(0)$]	10^{19} m^{-3}	5.1	3.6
Central (D+T) density [$(n_D(0) + n_T(0))$]	10^{19} m^{-3}	4.1	2.4
Z_{eff}		1.8	2.4
$T_e(0)$	keV	10.5	9.9
$T_i(0)$	keV	18.6	18.8
Plasma Diamagnetic Energy (W_{dia})	MJ	11.6	9.1
dW_{dia}/dt	MW	6.0	4.7
$\tau_E = W_{\text{dia}}/(P_{\text{tot}} - dW_{\text{dia}}/dt)$	s	1.2	0.9
$[n_D(0) + n_T(0)] T_i(0) \tau_E$	$10^{20} \text{ m}^{-3} \text{ keV s}$	9.0	3.8
$[(n_D(0) + n_T(0)) T_i(0) \tau_E]^*$	$10^{20} \text{ m}^{-3} \text{ keV s}$	5.4	2.5
Ratio of average T to (D + T) density		0	0.11
Maximum Fusion Power	MW	0.05	1.7
β_n		2.2	1.7

Table III introduces several important parameters which will be used in this paper. The plasma purity is an important consideration for several reasons. Impurities dilute the plasma and reduce the plasma reactivity. Also radiation from impurity ions in the plasma core can be an energy loss mechanism reducing the confinement of the plasma. In present experiments, this problem has been alleviated by the choice of materials, and wall coatings and the design of divertor and limiter. Impurity radiation in the edge of the plasma can be beneficial by reducing the heat flux to the divertor or limiter. The parameter, $Z_{\text{eff}} = \sum n_i z_i^2 / n_e$, is used to characterize the plasma purity though for detailed analysis the composition of the ion species must be included.

The ratio of the plasma pressure to the toroidal field pressure, $\beta_t = p/(B_t^2/2\mu_0)$ where $\langle p \rangle$ is the volume averaged plasma kinetic pressure is customarily used to characterize the performance of a magnetic confinement system. The parameter of relevance for fusion yields which is appropriately weighted to take into account the plasma reactivity is $\beta_t^* = \langle\langle p \rangle\rangle / (B_t^2/2\mu_0)$, where $\langle\langle p \rangle\rangle$ is the root-mean-square pressure, $\langle\langle p \rangle\rangle = [\int p^2 dV / \int dV]^{0.5}$. In a tokamak with typical current profiles, the MHD stability limit was described by Troyon *et al.*, 1984 in terms of $\beta_N = \beta_t(\%) \cdot a(\text{m}) \cdot B_t(\text{T}) / I_p(\text{MA})$ and the corresponding fusion reactivity weighted parameter is $\beta_N^* = \beta_N \langle\langle p \rangle\rangle / p$.

The plasma stored energy in the above experiments was measured using a diamagnetic loop.

Table IV. Summary of TFTR Experimental Parameters Achieved in High Performance Supershot Discharges (Hawryluk *et al.*, 1995; McGuire *et al.*, 1996).

Parameters	Units	68522	76778	80539	83546
Plasma Current (I_p)	MA	2.0	2.5	2.7	2.3
Toroidal Field (B_t)	T	5.0	5.1	5.6	5.5
NB Power (P_b)	MW	30.8	33.7	39.6	17.4
Tritium NB Power	MW	0	20.0	25.5	17.4
Central Electron Density [$n_e(0)$]	10^{19} m^{-3}	9.6	8.5	10.2	8.5
Central Hydrogenic Density $n_{\text{HYD}}(0) = [n_{\text{H}}(0) + n_0(0) + n_{\text{T}}(0)]$	10^{19} m^{-3}	6.8	6.3	6.7	6.6
Z_{eff}		2.6	2.2	2.4	2.0
$T_e(0)$	keV	11.7	11.5	13	12.0
$T_i(0)$	keV	29.0	44	36	43
Plasma Energy (W_{TOT})	MJ	5.4	6.5	6.9	4.9
dW_{TOT}/dt	MW	2.1	7.5	0	3.0
$\tau_E = W_{\text{TOT}}/(P_{\text{TOT}} - dW/dt)$	s	0.19	0.24	0.18	0.34
$n_{\text{HYD}}(0) T_i(0) \tau_E$	$10^{20} \text{ m}^{-3} \text{ keVs}$	3.9	7.1	4.3	9.6
$n_{\text{HYD}}(0) T_i(0) \tau_E^*$	$10^{20} \text{ m}^{-3} \text{ keVs}$	3.6	5.5	4.2	8.0
Ratio of average T to (D+T) density		0	0.5	0.47	0.58
Maximum Fusion Power	MW	0.065	9.3	10.7	2.8
β_n		2.1	2.0	1.8	1.5
β_n^*		3.5	3.1	3.0	3.0

Table V. Summary of TFTR Experimental Parameters Achieved in High- ℓ_i and Enhanced Reverse Shear Discharges by Means of Current Profile Modification (McGuire *et al.*, 1996)

Parameters	Units	high ℓ_i 95603	ERS 88170
Plasma Current (I_p)	MA	2.0	1.6
Toroidal Field (B_t)	T	4.8	4.6
NB Power (P_b)	MW	35.5	28.1
Central Electron Density [$n_e(0)$]	10^{19} m^{-3}	6.9	9.0
Central Hydrogenic Density [$n_H(0) + n_D(0) + n_T(0)$]	10^{19} m^{-3}	6.0	7.0
Z_{eff}		1.6	2.1
$T_e(0)$	keV	8.0	8.0
$T_i(0)$	keV	45	25
Plasma Energy (W_{TOT})	MJ	5.7	3.9
dW_{TOT}/dt	MW	11.0	3.0
$\tau_E = W_{\text{TOT}}/(P_{\text{TOT}} - dW_{\text{TOT}}/dt)$	s	0.23	0.15
$n_{\text{HYD}}(0) T_i(0) \tau_E$	$10^{20} \text{ m}^{-3} \text{ keVs}$	6.2	2.6
$n_{\text{HYD}}(0) T_i(0) \tau_E^*$	$10^{20} \text{ m}^{-3} \text{ keVs}$	4.3	2.4
Ratio of average T to (D-T) density		0.42	0
Maximum Fusion Power	MW	8.7	
β_n		2.4	1.95
β_n^*		3.9	3.7

Table VI Alpha-particle parameters for JET and TFTR (Balet *et al.*, 1993 and Budny *et al.*, 1995, respectively).

	JET	TFTR	
	26148	76778	80539
$n_{\alpha}(0)/n_e(0)$	4.8×10^{-4}	1.5×10^{-3}	1.5×10^{-3}
$\beta_{\alpha}(0)$	8.0×10^{-4}	2.1×10^{-3}	2.7×10^{-3}
$V_{\alpha}/V_A(0)$	1.84	1.66	1.70

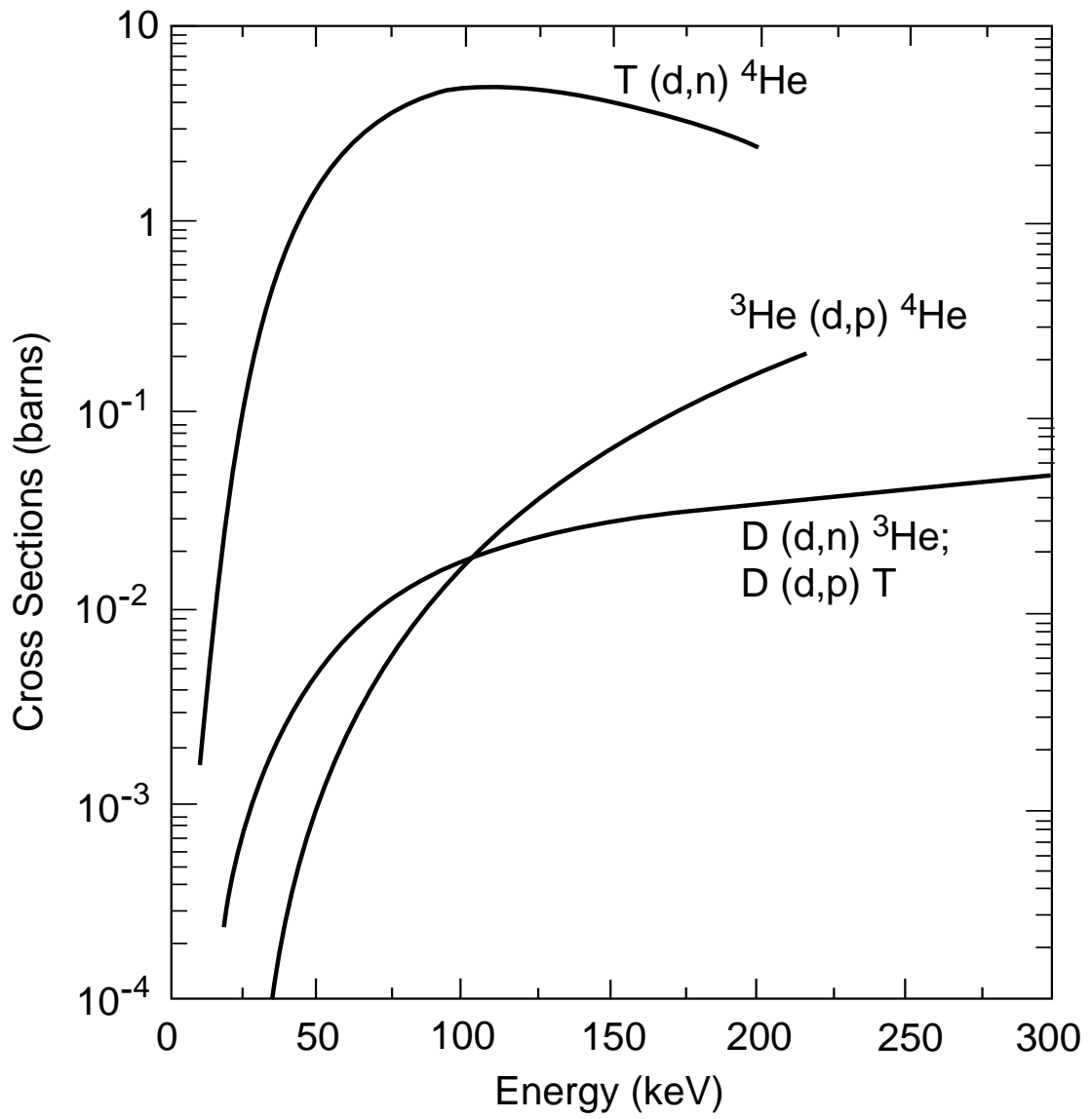


Fig. 1 Cross sections for fusion reactions of importance in magnetic fusion are plotted versus energy.

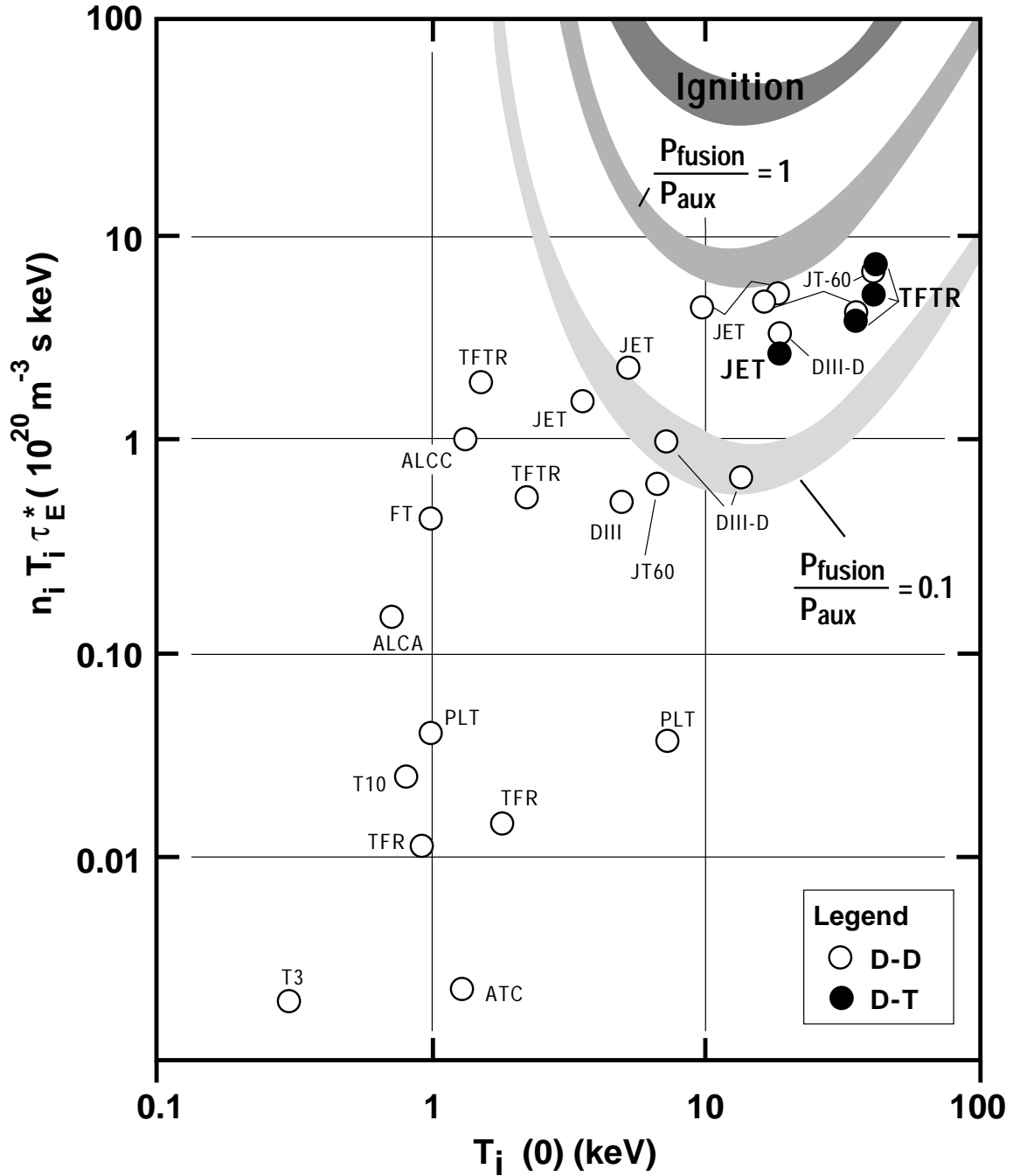


Fig. 2 The achieved product $n_{HYD} T_i(0) \tau_E^*$ where n_{HYD} is the sum of all hydrogenic densities versus $T_i(0)$ for various tokamak devices. In present devices, P_{breh} is small compared with P_{aux} and ignored. For comparison, an estimate of the criteria for $P_{fus}/P_{aux} = 1$ and ignition in which the alpha heating sustains the plasma is given.

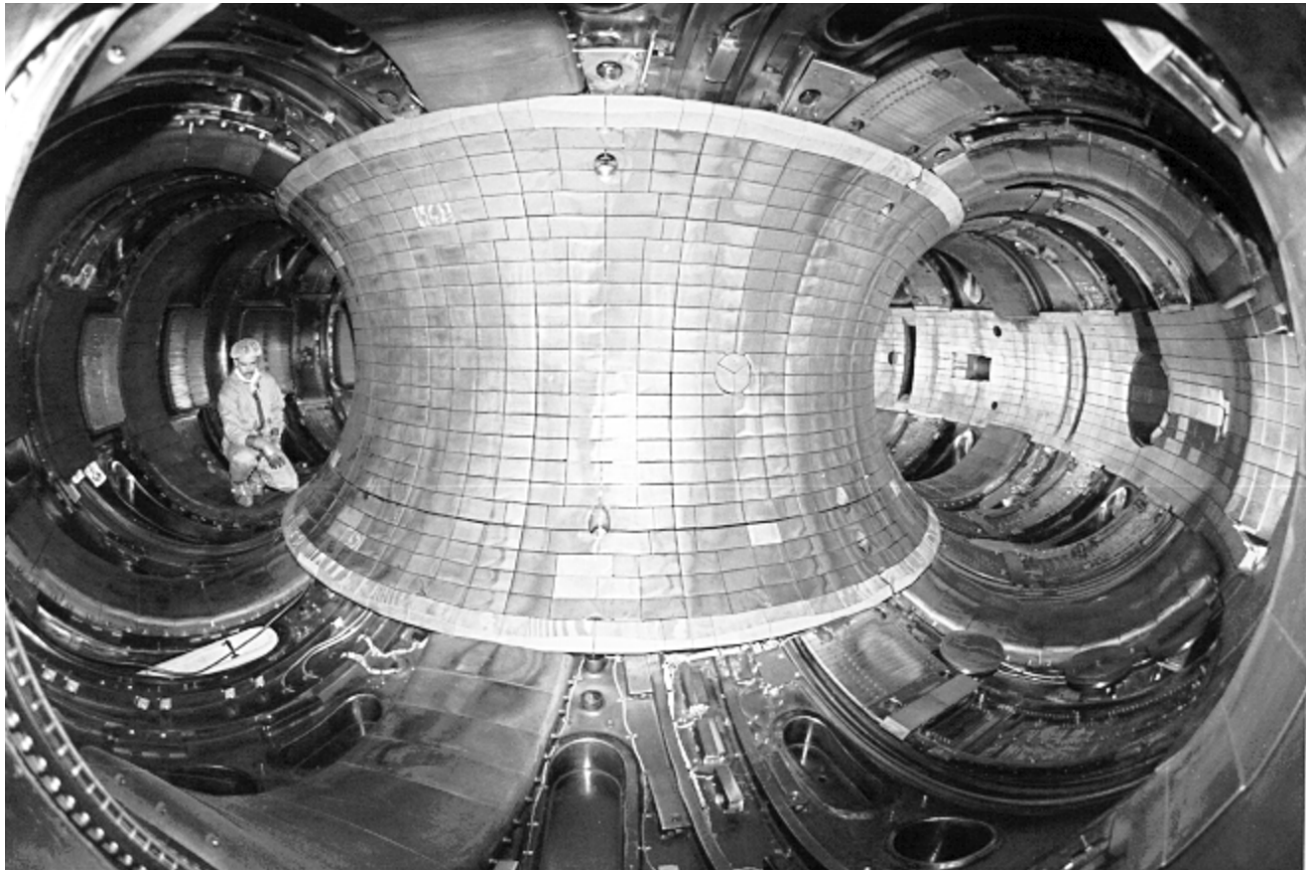


Fig. 3 The interior of the TFTR vacuum vessel is shown. The carbon-composite and graphite tiles on the inner wall limits the plasma and protects the vacuum vessel wall.

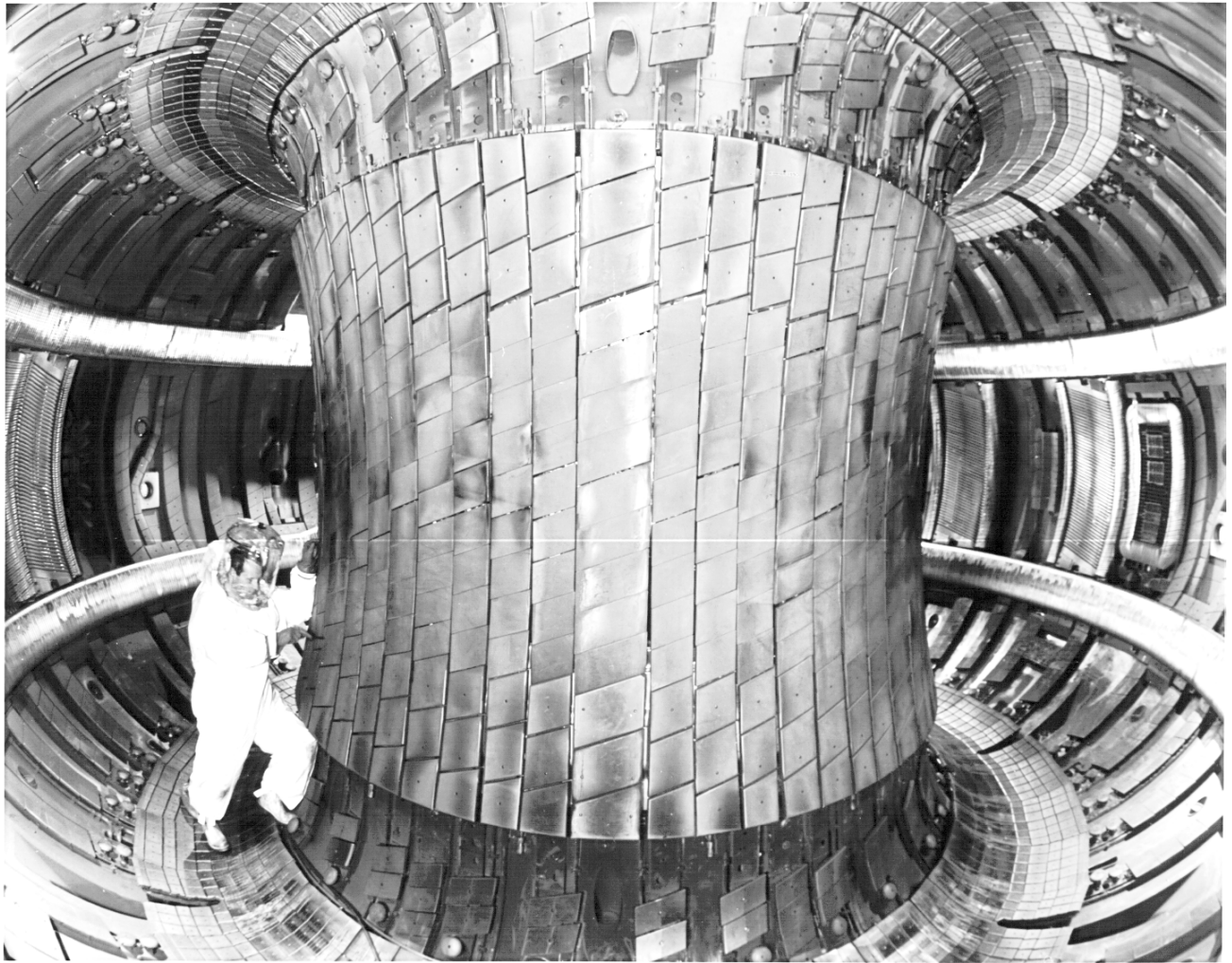


Fig. 4 Interior of the JET vacuum vessel (JET Team, 1992).

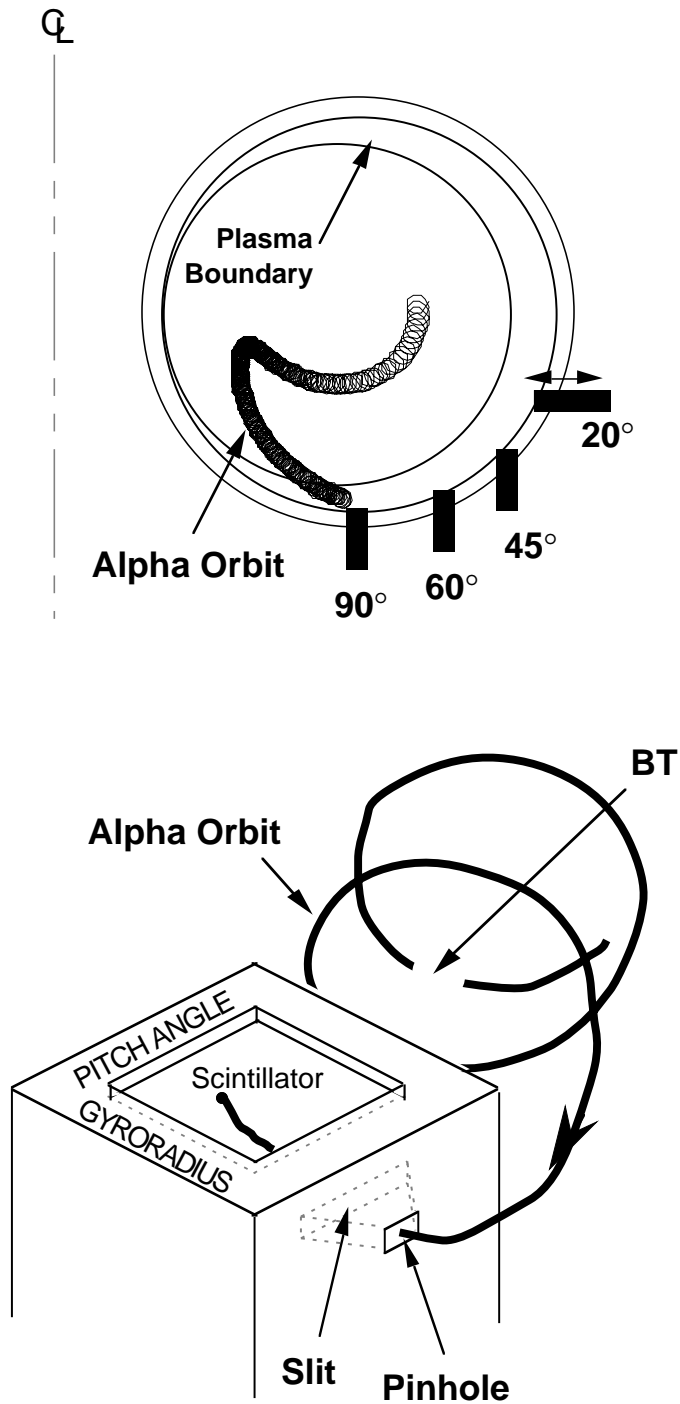


Fig. 5 Four lost alpha detectors are located behind the limiter shadow. Schematic diagram of the TFTR lost alpha detector. The escaping alphas enter a pair of apertures that disperse them in pitch angle and gyroradius (Darrow *et al.*, 1996a).

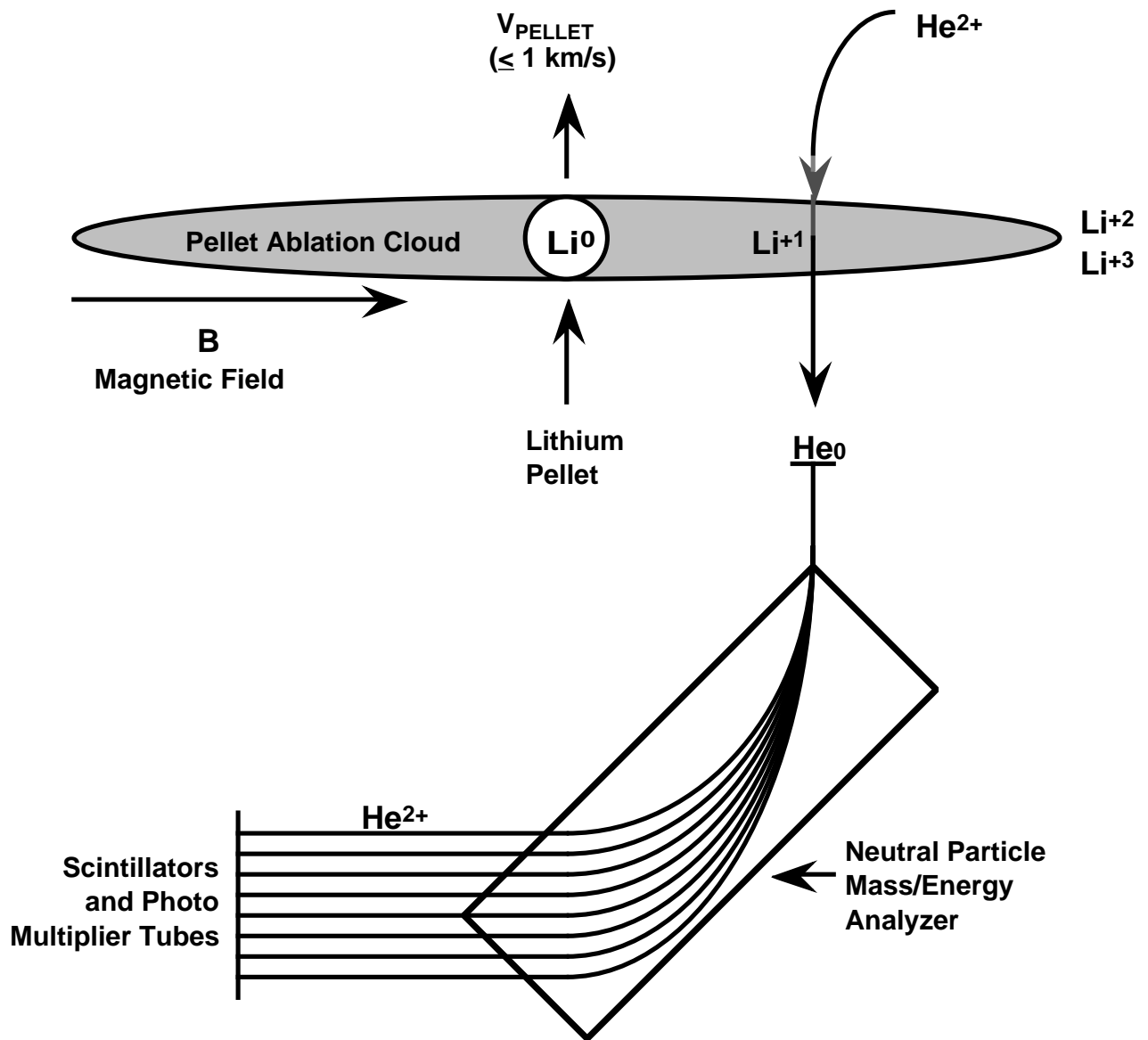


Fig. 6 Illustration of the pellet charge exchange diagnostic to measure confined alpha particles (Medley *et al.*, 1996b).

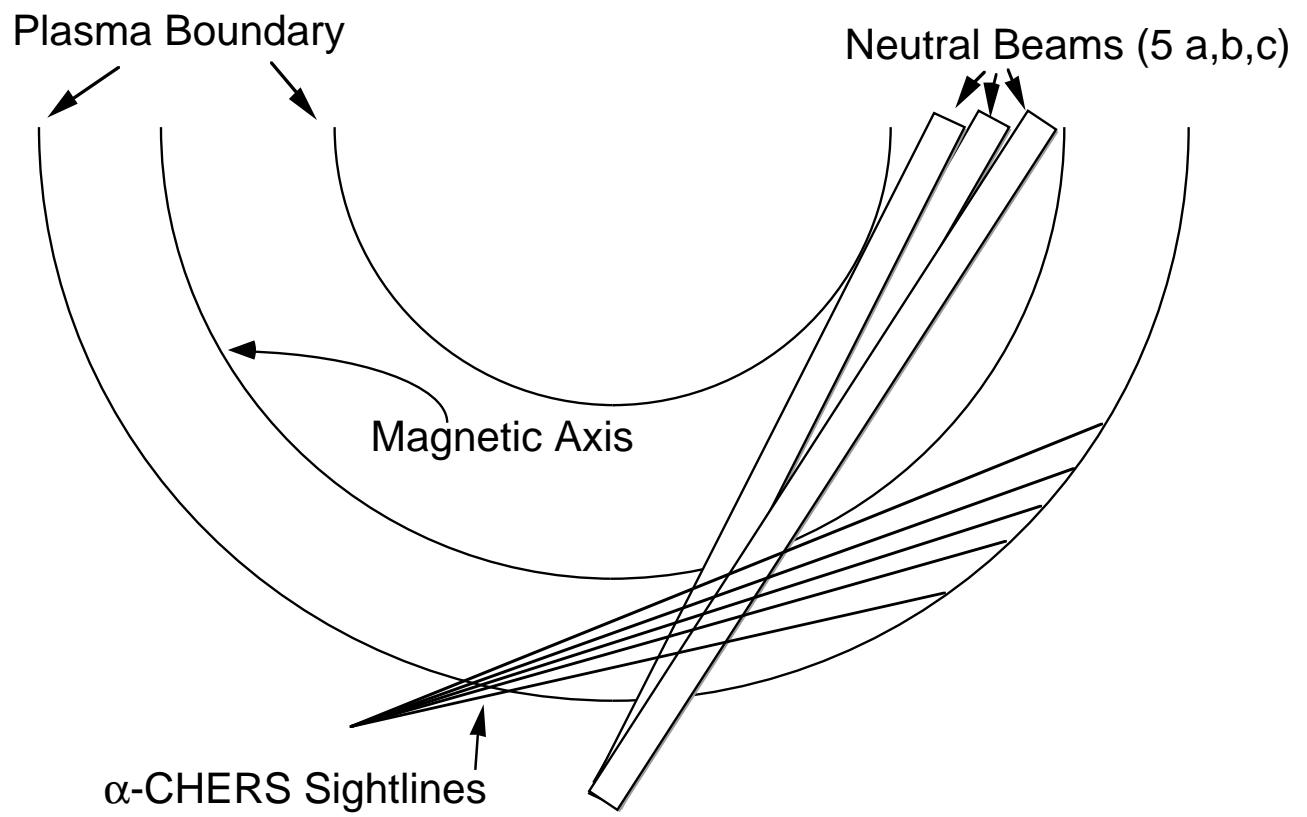


Fig. 7 Alpha-CHERS sightlines and beam viewing geometry (McKee *et al.*, 1995a, 1996).

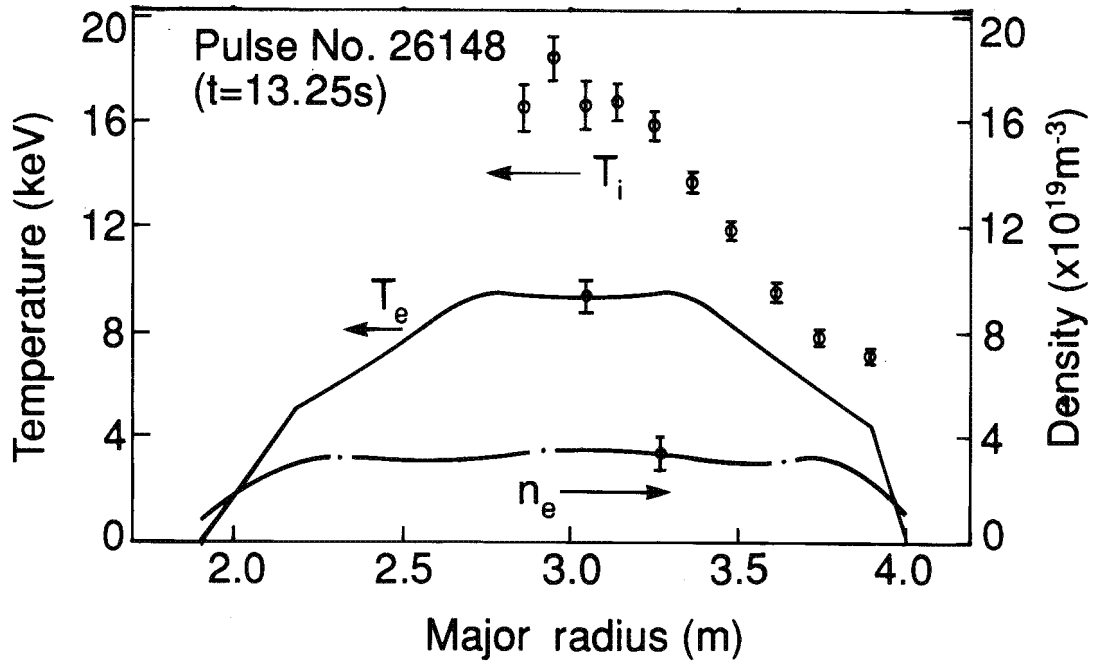


Fig. 8 Radial profiles of the ion and electron temperature and electron density for JET pulse number 26148 (JET Team, 1992).

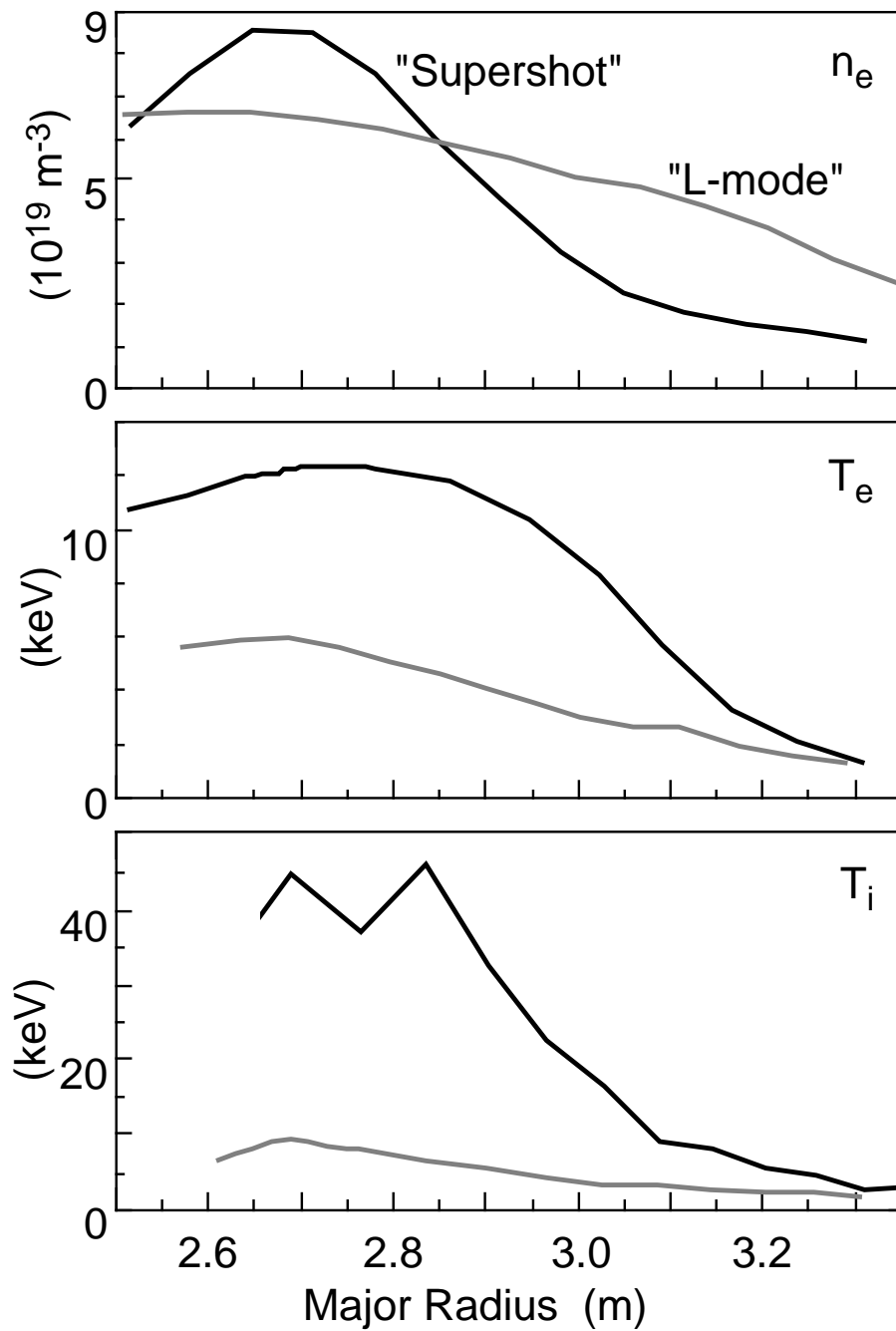


Fig. 9 Radial profiles of the ion and electron temperature and electron densities for TFTR pulse number 83546, a high performance supershot, is contrasted with a comparable L-mode discharge with similar plasma current and heating power.

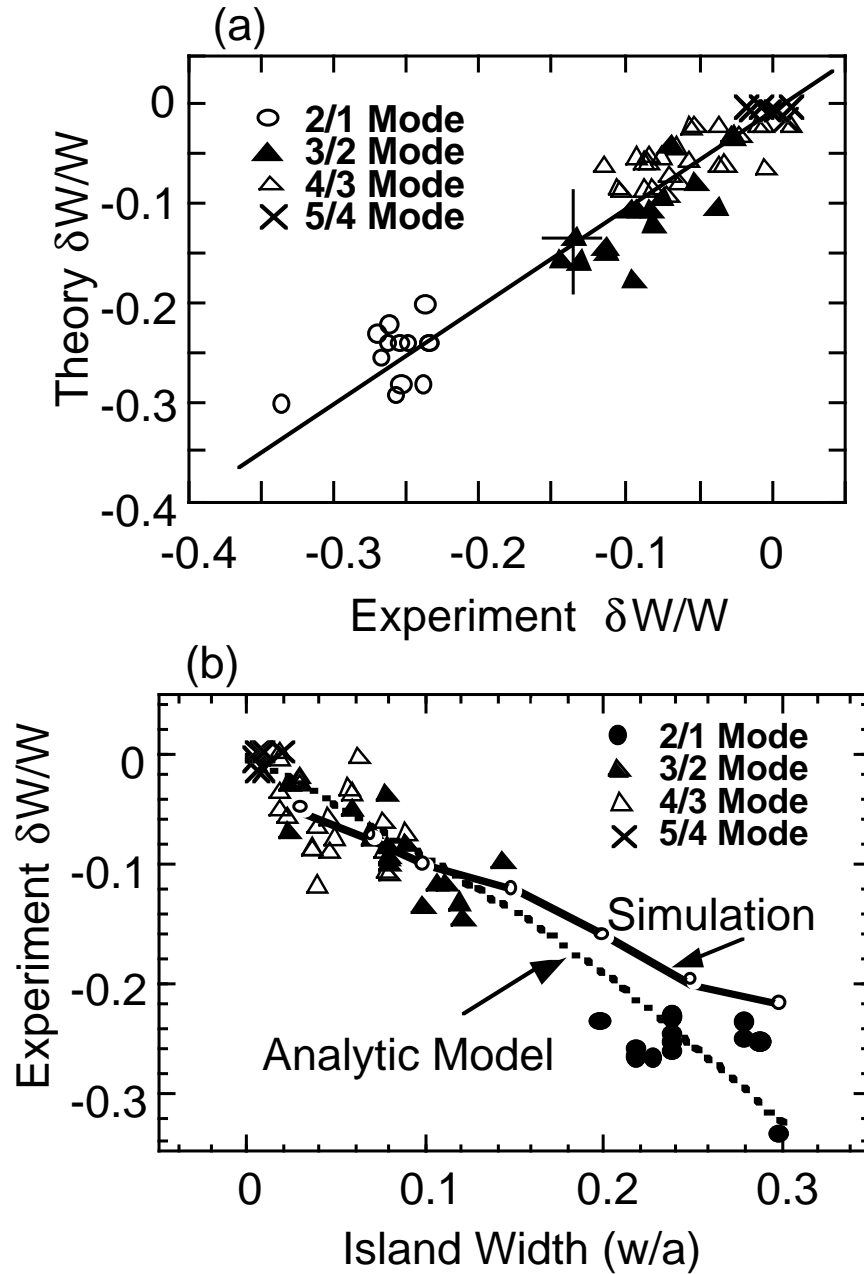


Fig. 10 (a) Comparison of stored energy deterioration ($\delta W/W$) theory and experiment due to neoclassical tearing modes. (b) The energy deterioration is proportional to the island width as predicted by the theory and simulation (Chang *et al.*, 1994).

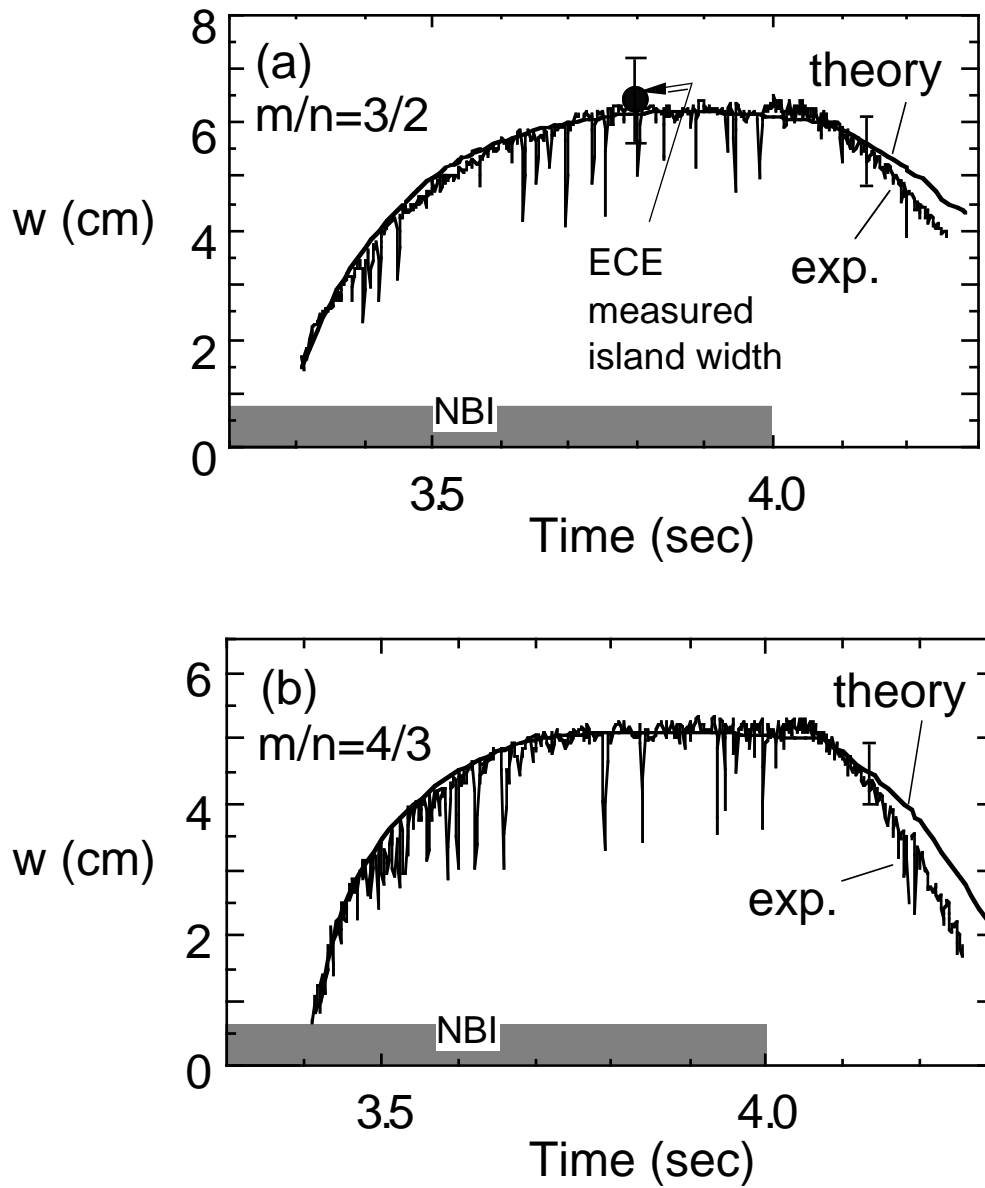


Fig. 11 Comparison of the measured magnetic island evolution with the nonlinear neoclassical p-driven tearing mode theory for (a) the $m/n=3/2$ mode case and (b) the $4/3$ mode case (Chang *et al.*, 1994).

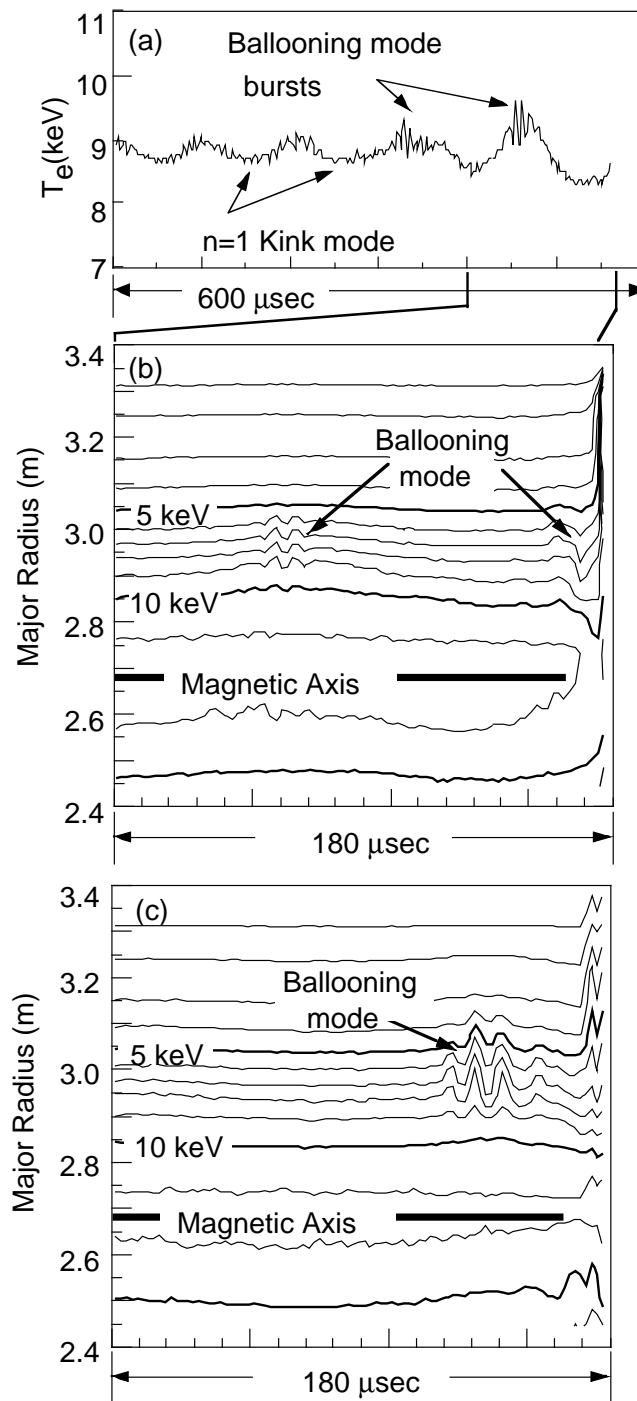


Fig. 12 a) Electron cyclotron emission measurements of the evolution of the electron temperature prior to a disruption. An $n = 1$ kink mode is observed to precede the destabilization of a ballooning mode (Fredrickson *et al.*, 1995a, 1996c).

b) Contours of the electron temperature evolution at one toroidal location. The ballooning mode is observed on the outer midplane.
 c) Contours of the electron temperature evolution toroidally separated by 126° from the previous set of measurements.

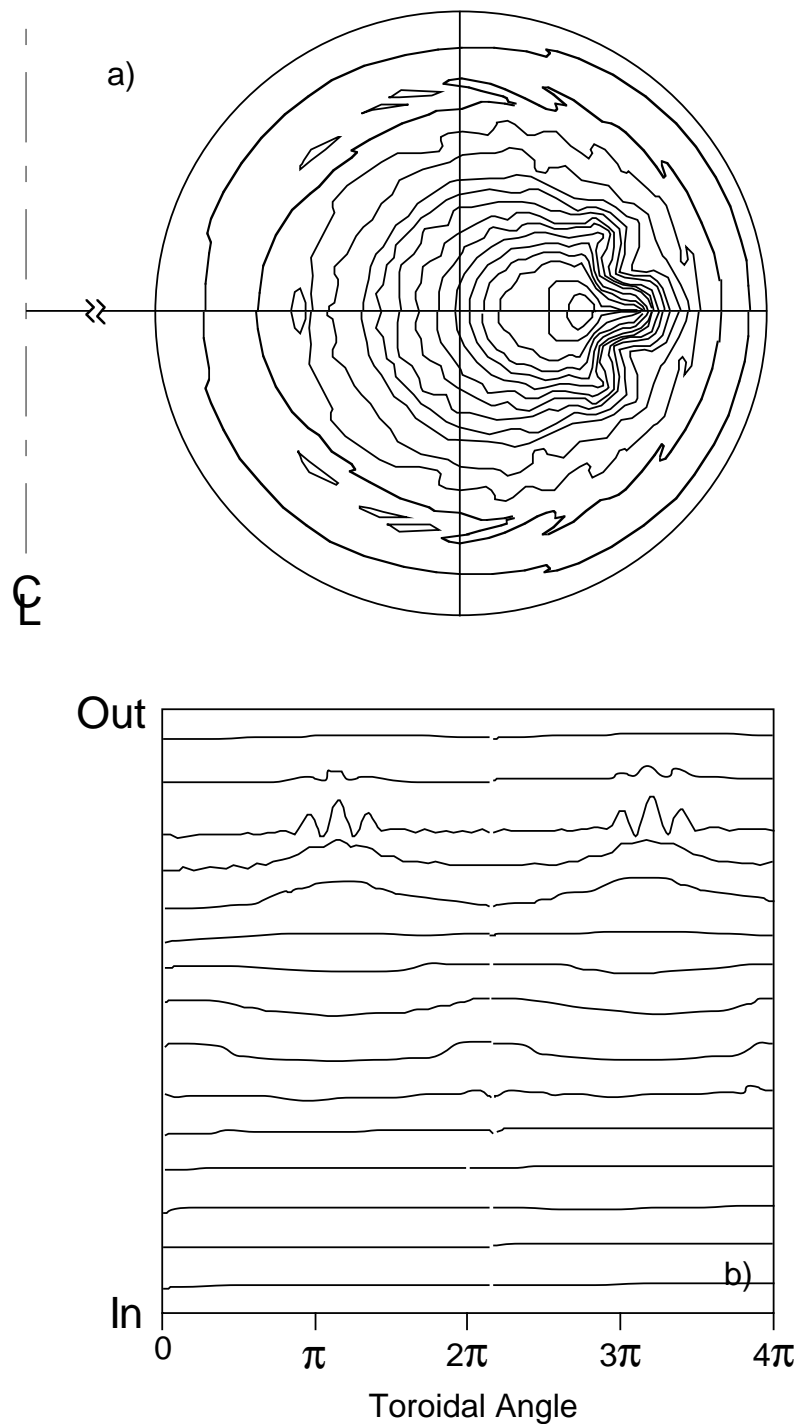


Fig. 13 a) Three dimensional nonlinear simulation of equi-pressure contours of the MHD instability.

b) Simulations of the electron cyclotron emission measurements of the electron temperature reproduce the observation of the ballooning mode shown in Fig. 12 being destabilized by a low-n kink mode with the largest displacement on the outboard side of the plasmas (Park *et al.*, 1995). Since the plasma rotates toroidally, the calculations versus toroidal angle are related to the measurements versus time.

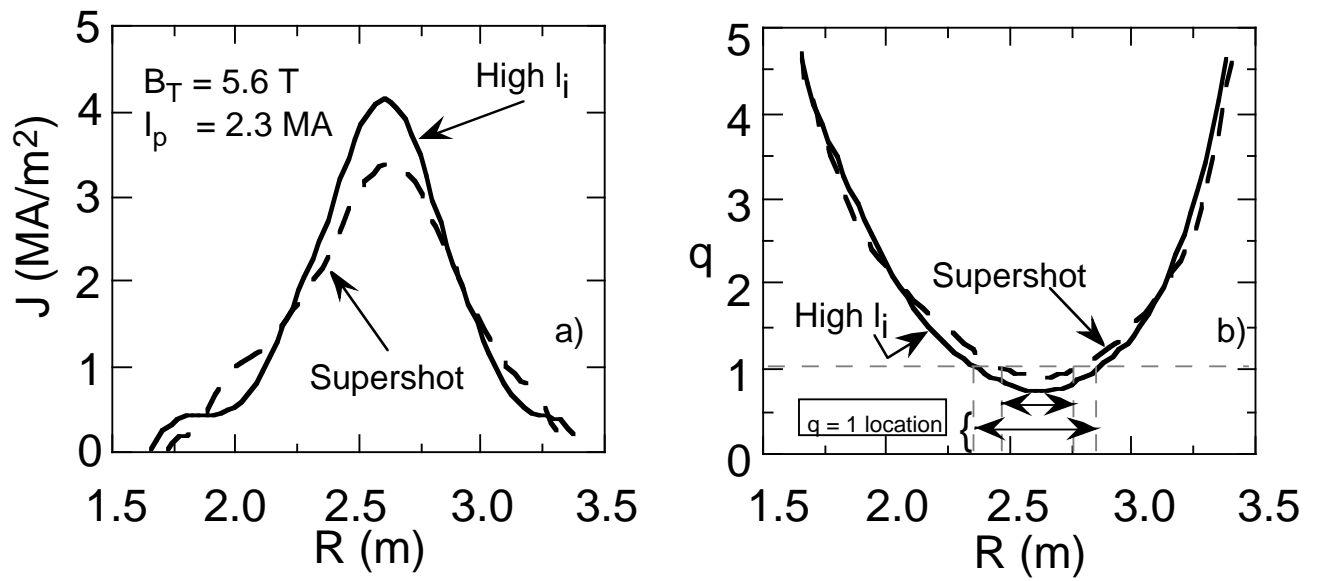


Fig. 14 Motional Stark Effect measurements of the $j(r)$ and $q(r)$ profiles in a high I_i discharge are contrasted with a supershot discharge (Sabbagh *et al.*, 1996).

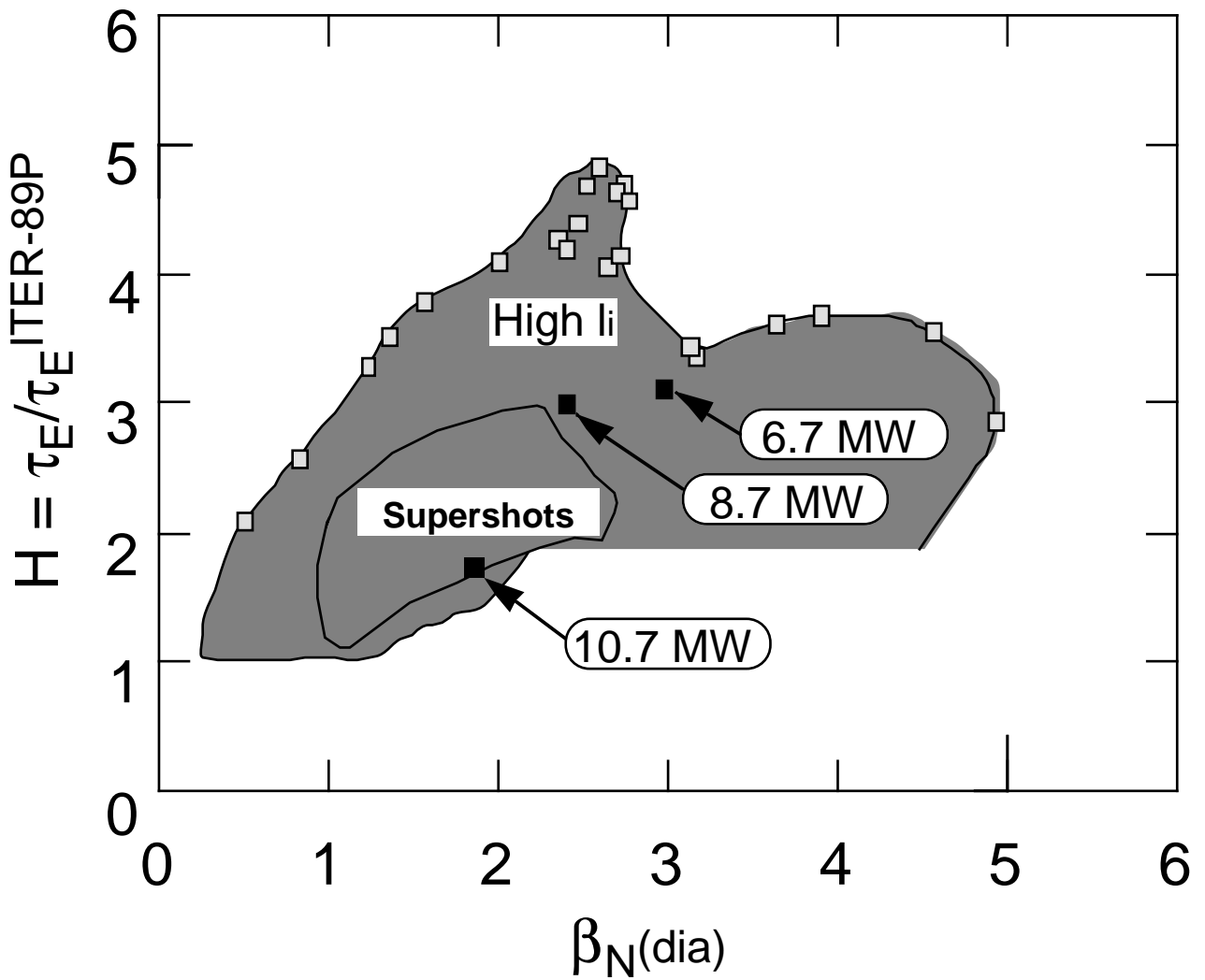


Fig. 15 Operating range of high ℓ discharges in terms of the enhancement in energy confinement time, $H = \tau_E / \tau_E^{ITER-89P}$ and β_N is compared with the operating range of supershot discharges (Sabbagh *et al.*, 1994b, 1996).

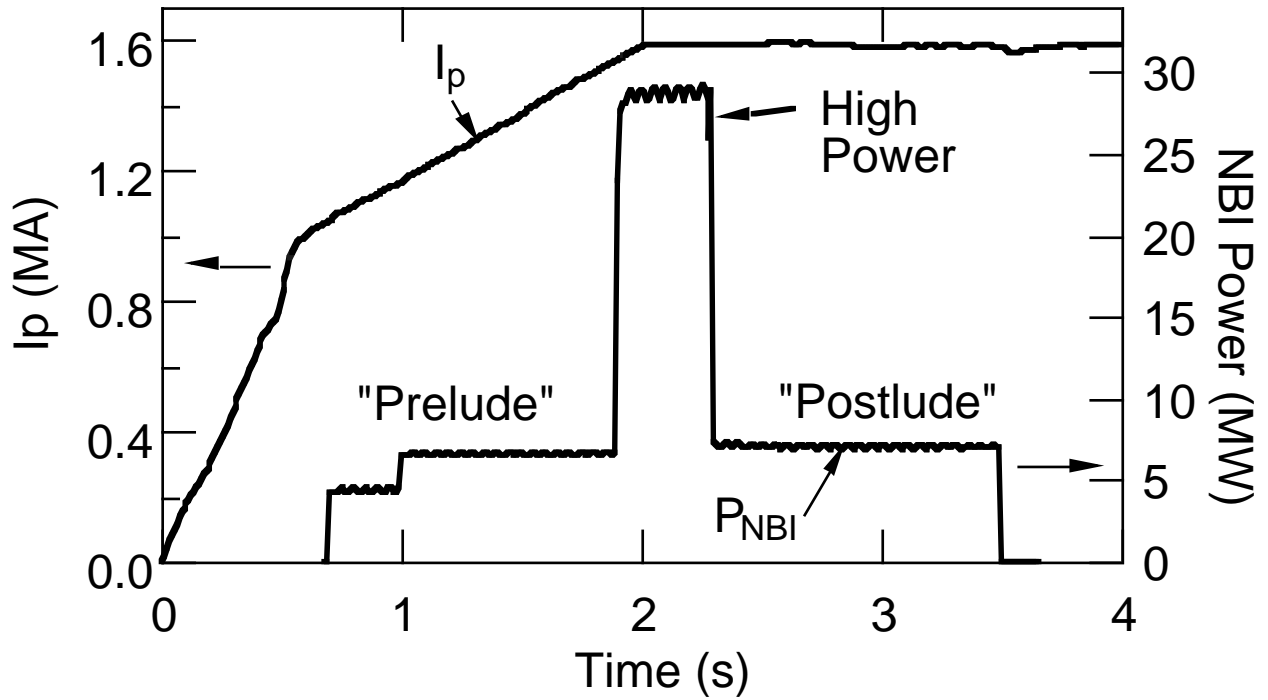


Fig. 16 Hollow current profiles are achieved by rapidly ramping the plasma current and heating the plasma in the “prelude” phase prior to the “high power” heating phase. Subsequently, the power is decreased in the “postlude” phase to study the evolution of the plasma transport (Levinton *et al.*, 1996).

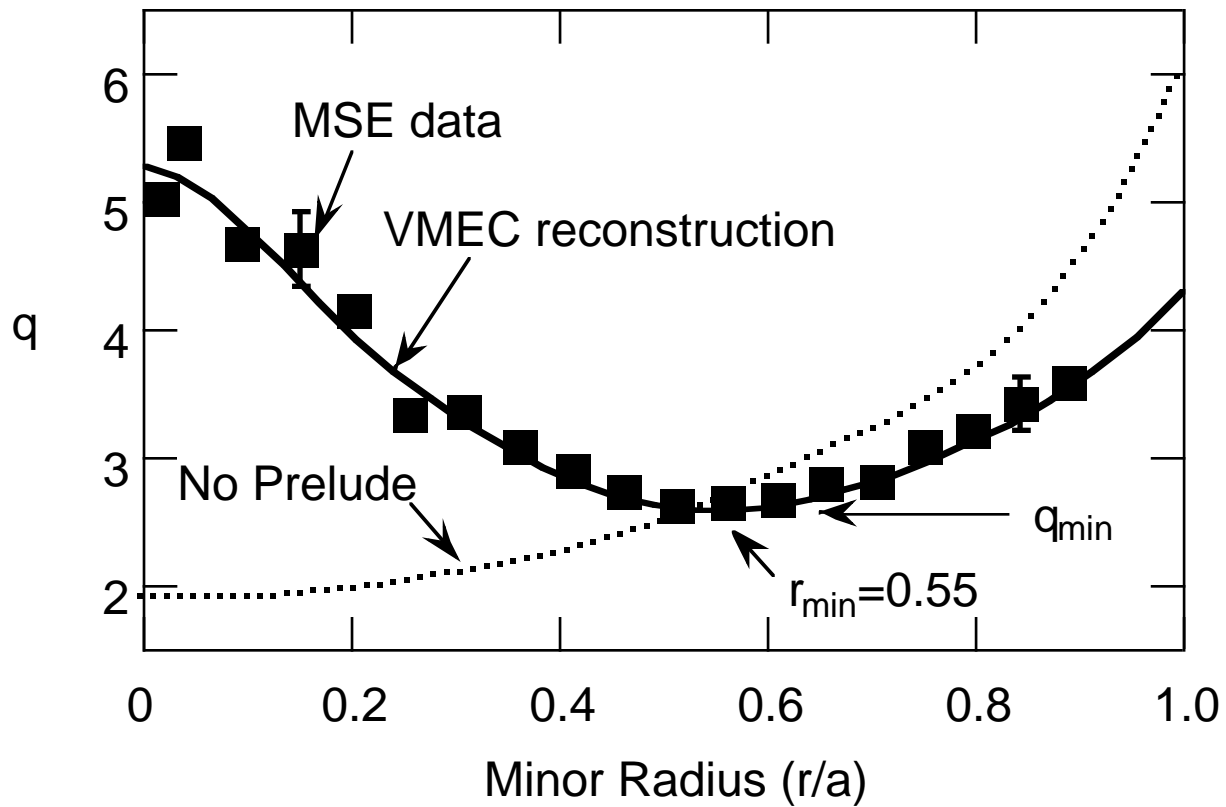


Fig. 17 Motional Stark Effect measurements of the safety factor, q , which illustrate the effect of applying heating power during the “prelude” phase. The magnetic equilibrium reconstruction analysis is shown for comparison. The normalized minor radius of the minimum of the safety factor is denoted r_{\min} and the corresponding value of the safety factor is denoted q_{\min} (Levinton *et al.*, 1996).

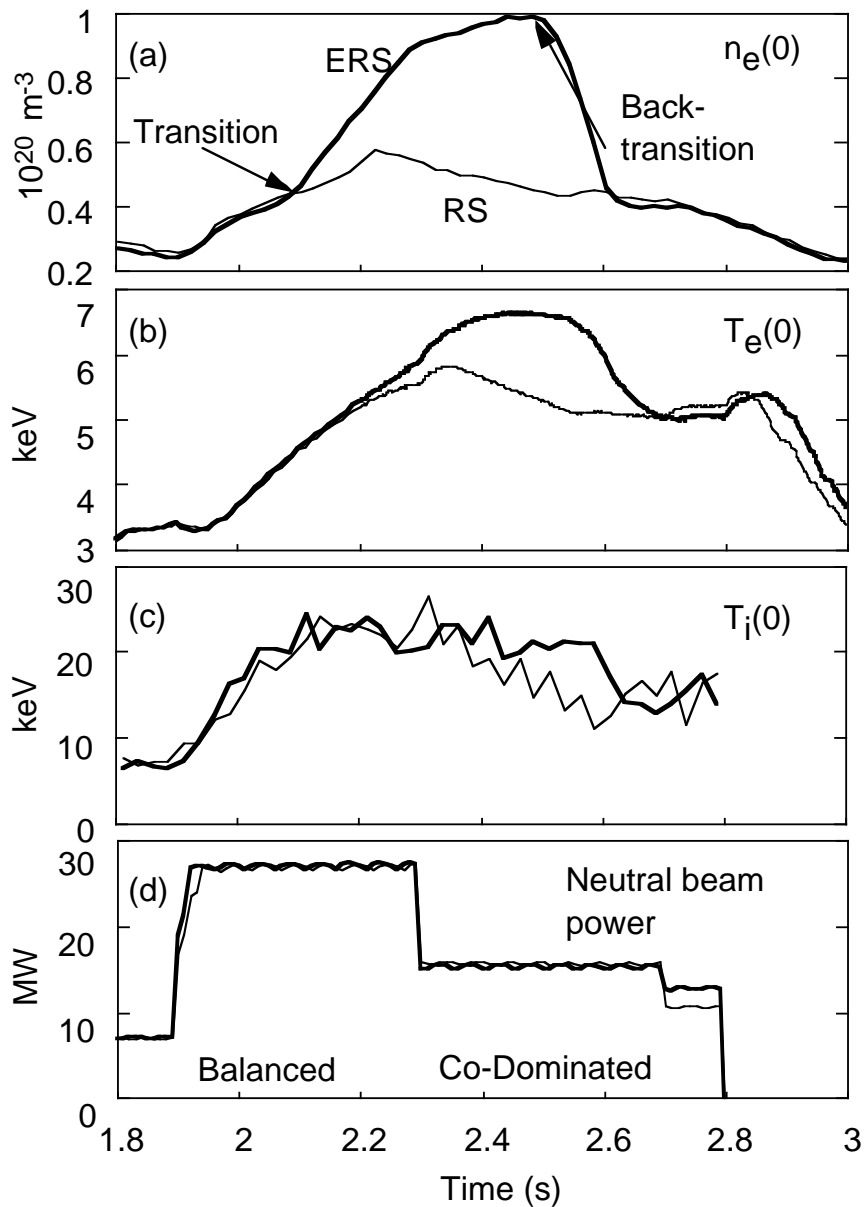


Fig. 18 Comparison of the evolution of two reverse shear discharges near the threshold power for a transition. Shown is the (a) central electron density, (b) the central electron temperature, (c) the central ion temperature, and (d) the total neutral beam power waveform. In the enhanced reverse shear discharge, the development of an internal transport barrier and reduced core transport results in a large increase in the central density and core pressure. In this ERS plasma, the loss of good core confinement in the 14 MW “postlude” period of injection is correlated with a reduction in the radial electric field magnitude \mathbf{ExB} shearing rate γ_s , induced by opposing contributions from co-rotation and the plasma pressure (Synakowski *et al.*, 1996a). After the back transition, the plasma confinement properties return to those in the reverse-shear discharge without the transport barrier.

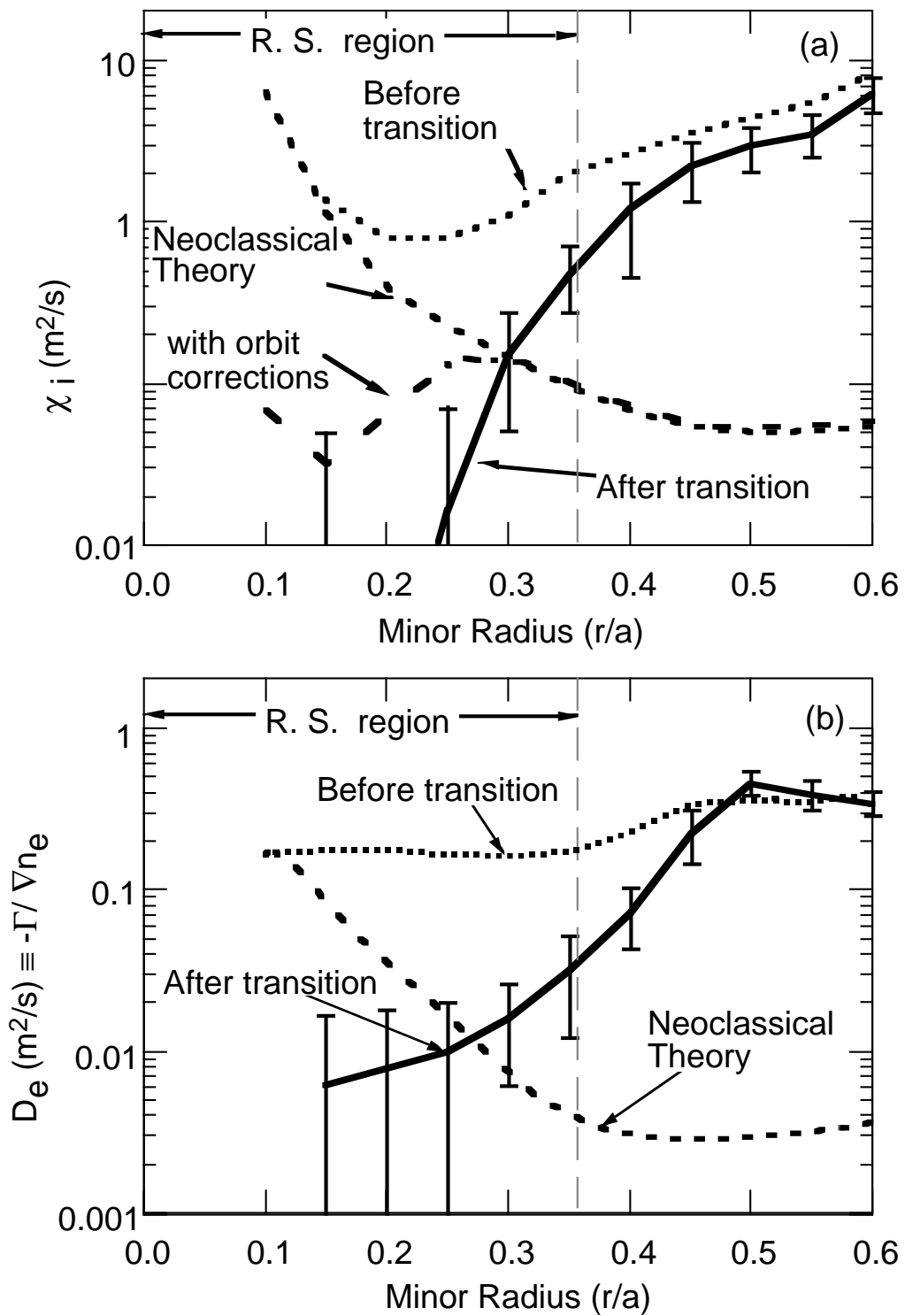


Fig. 19 The inferred ion thermal diffusivity (a) and particle diffusivity (b) is observed to decrease dramatically in the enhanced reversed shear discharges (Levinton *et al.*, 1995). For comparison, the standard calculation of neoclassical ion heat conductivity is shown as well as the recent calculations by Lin *et al.* (1996).

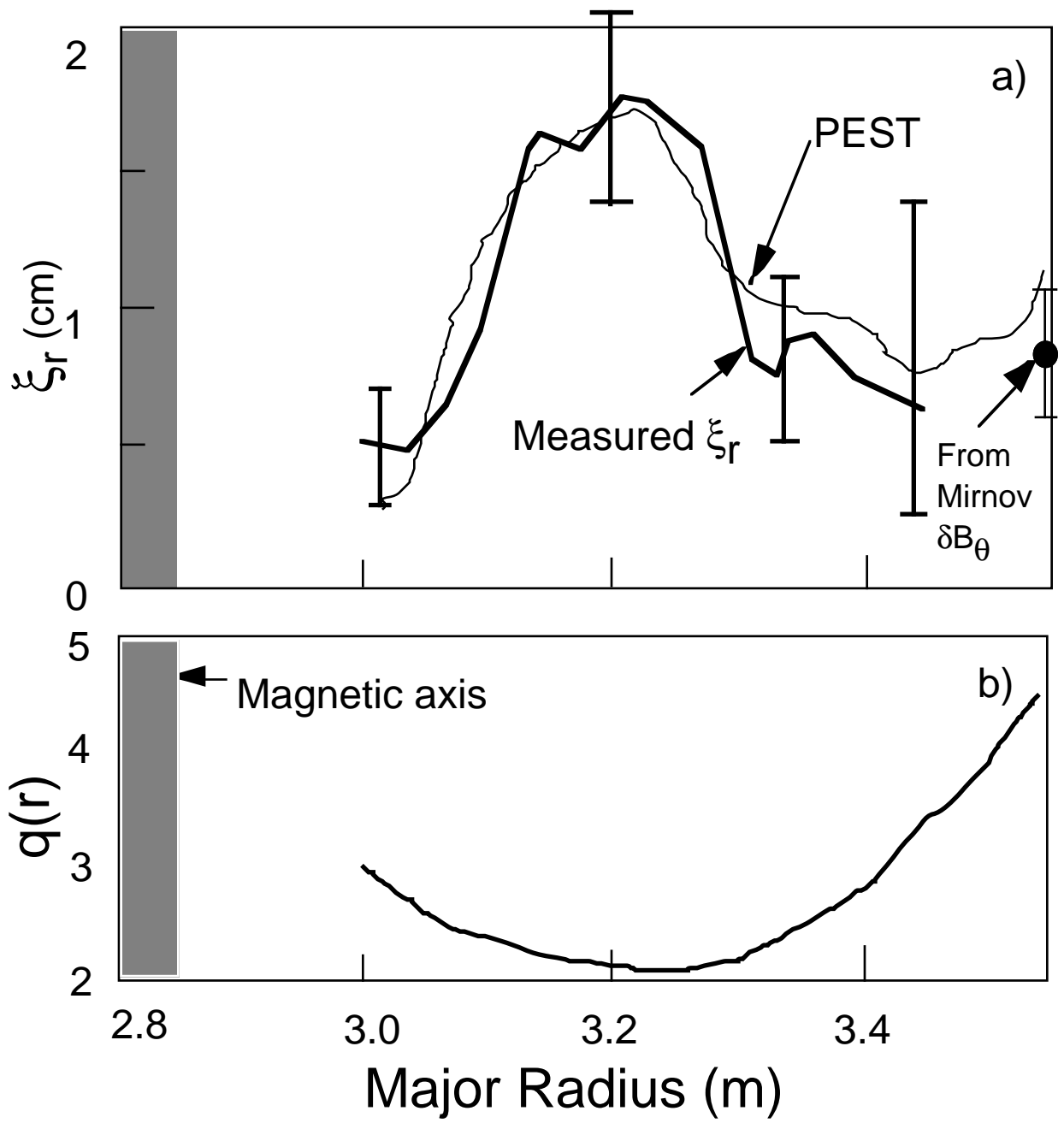


Fig. 20 a) ECE measurements of the displacement of the magnetic surfaces are in good agreement with the predictions of ideal MHD theory for reverse shear TFTR discharges (Manickam *et al.*, 1996). b) The corresponding q -profile.

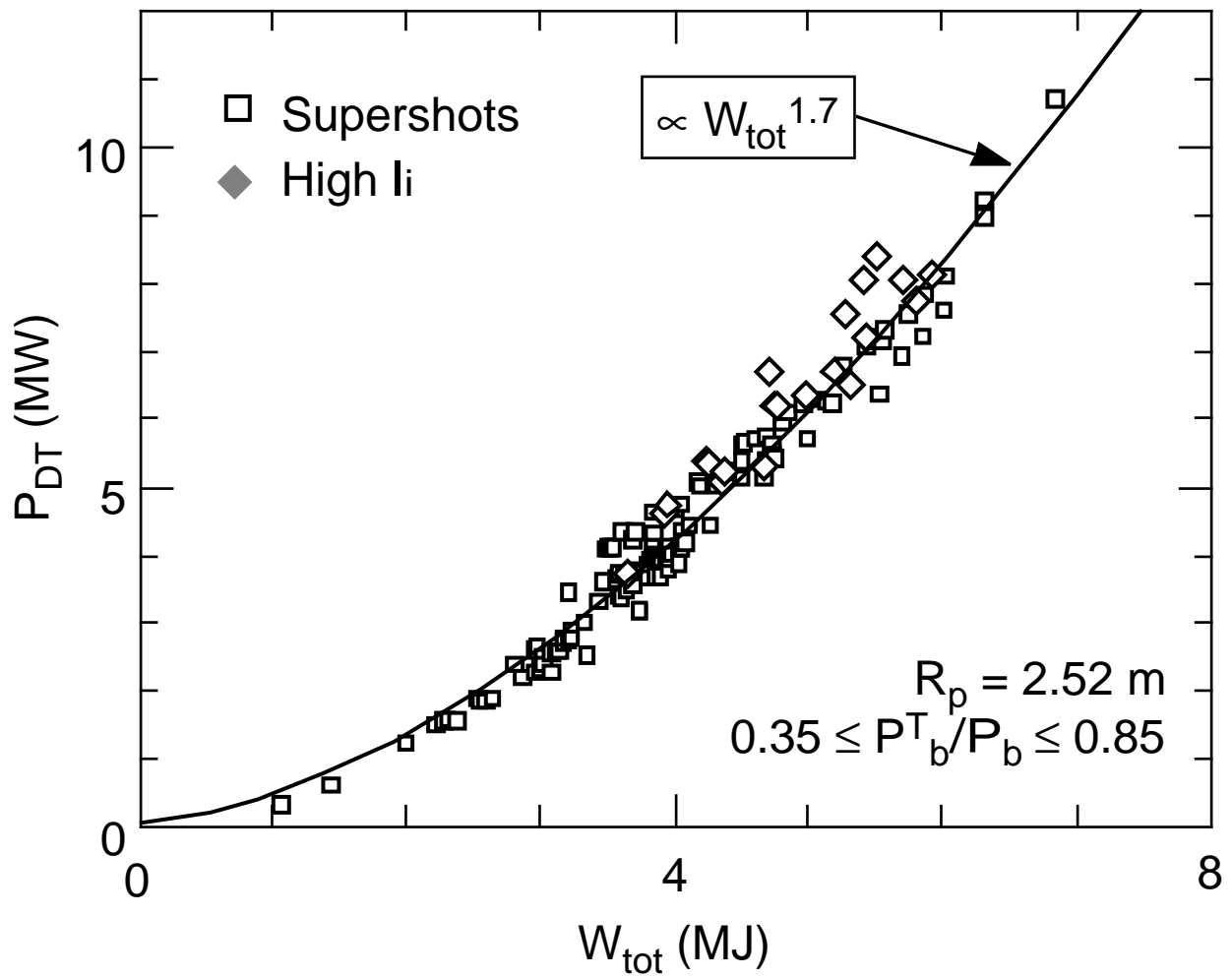


Fig. 21 Dependence of the peak D-T fusion power (averaged over a 40ms interval) on total plasma energy in high-current (≥ 2.0 MA) supershots [squares] and high- ℓ_i plasmas at 2.0 - 2.3 MA produced by cross-section expansion of low- q ($q_a \approx 2.5$) discharges [diamonds]. All plasmas have approximately the same volume ($\sim 38\text{m}^3$) and a nearly optimal mixture of D and T in the reactive region produced by neutral beam injection (Bell *et al.*, 1996).

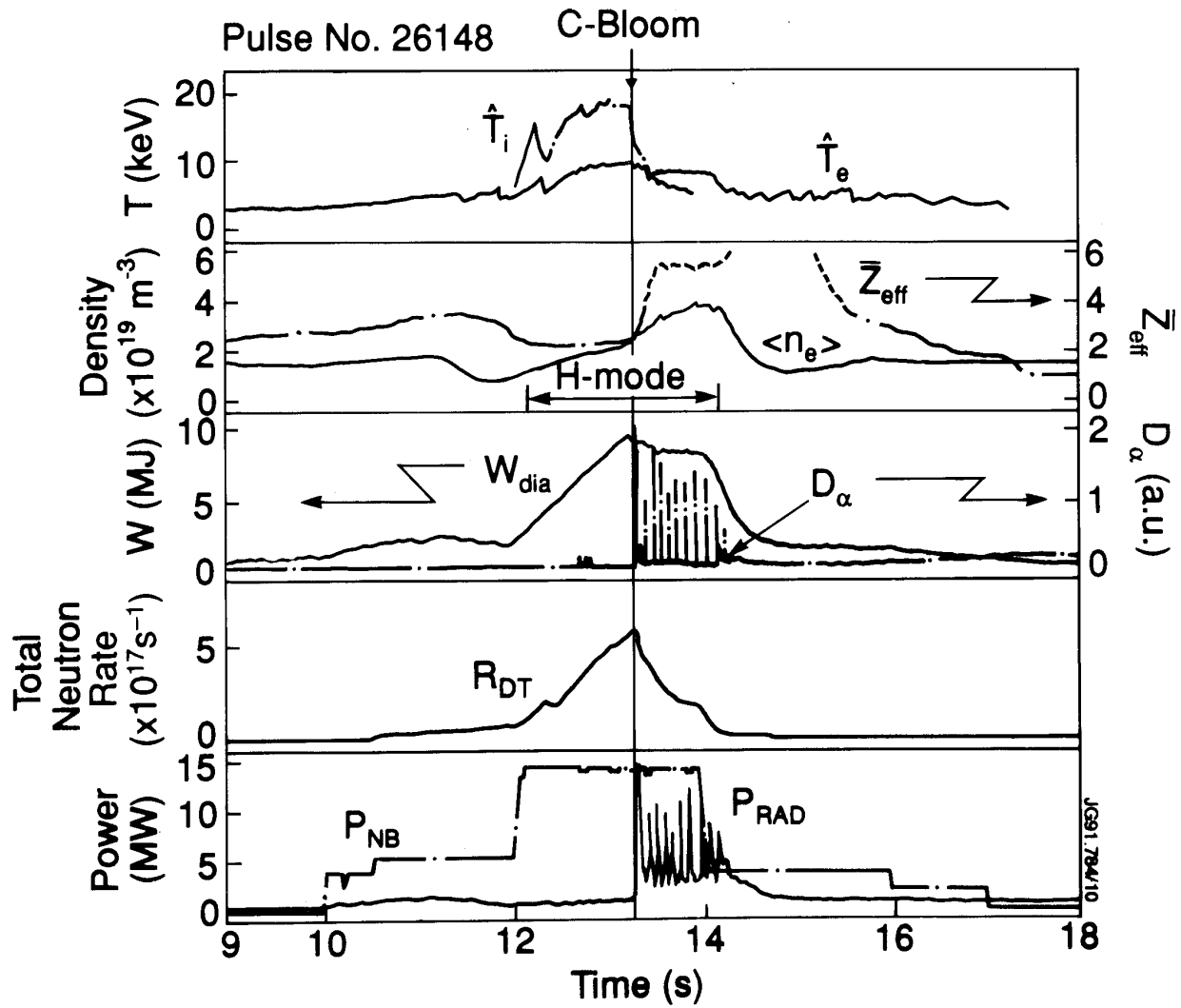


Fig. 22 Time dependence of the central electron and ion temperatures, the volume averaged electron density, the line average, Z_{eff} , the plasma diamagnetic energy, the D_α emission, the total neutron rate, and the neutral beam and radiated power for pulse No. 26148 (JET Team, 1992).

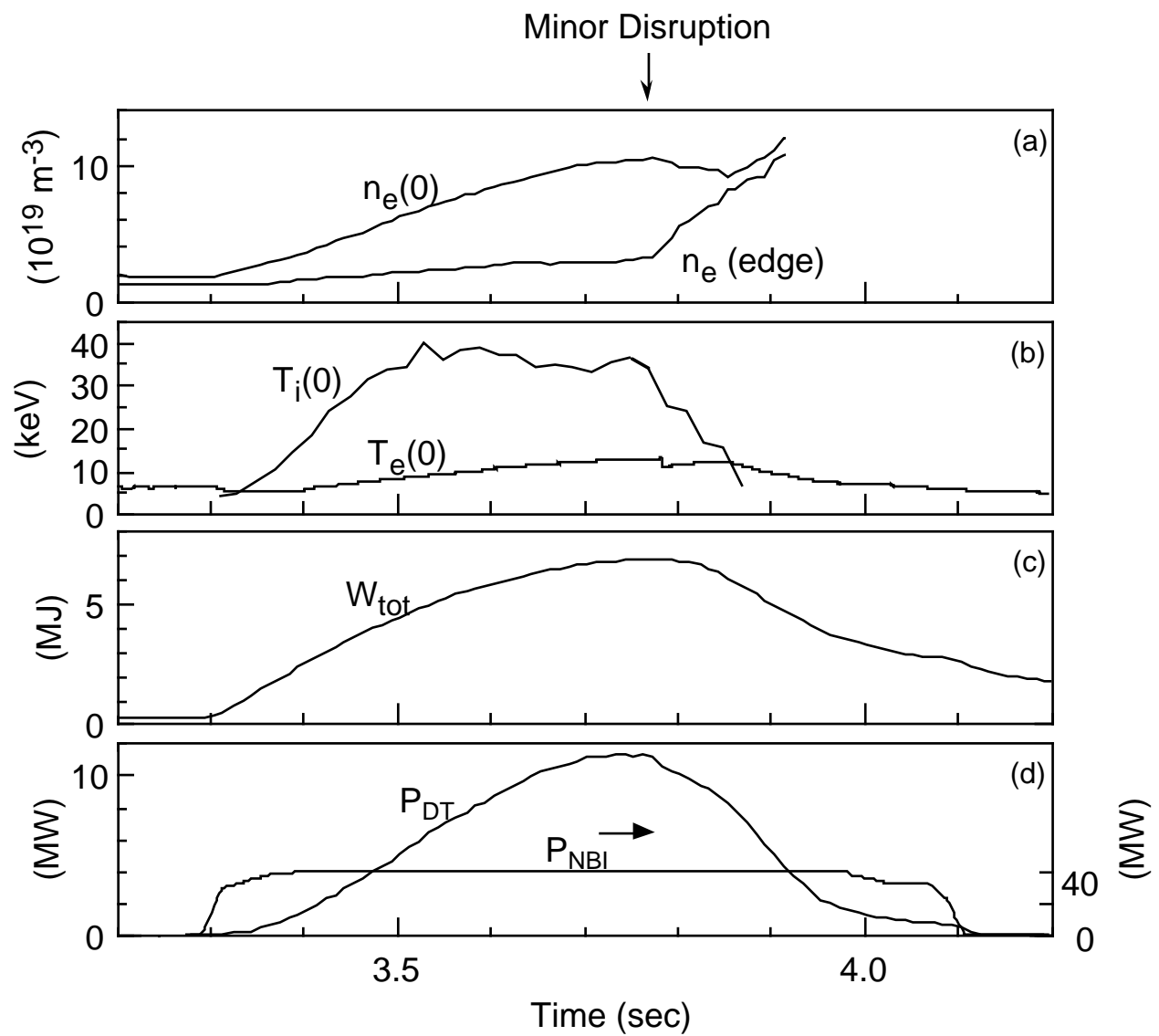


Fig. 23 Evolution of the central electron density, ion temperature, electron temperature, stored energy and fusion power for TFTR shot No. 80539.

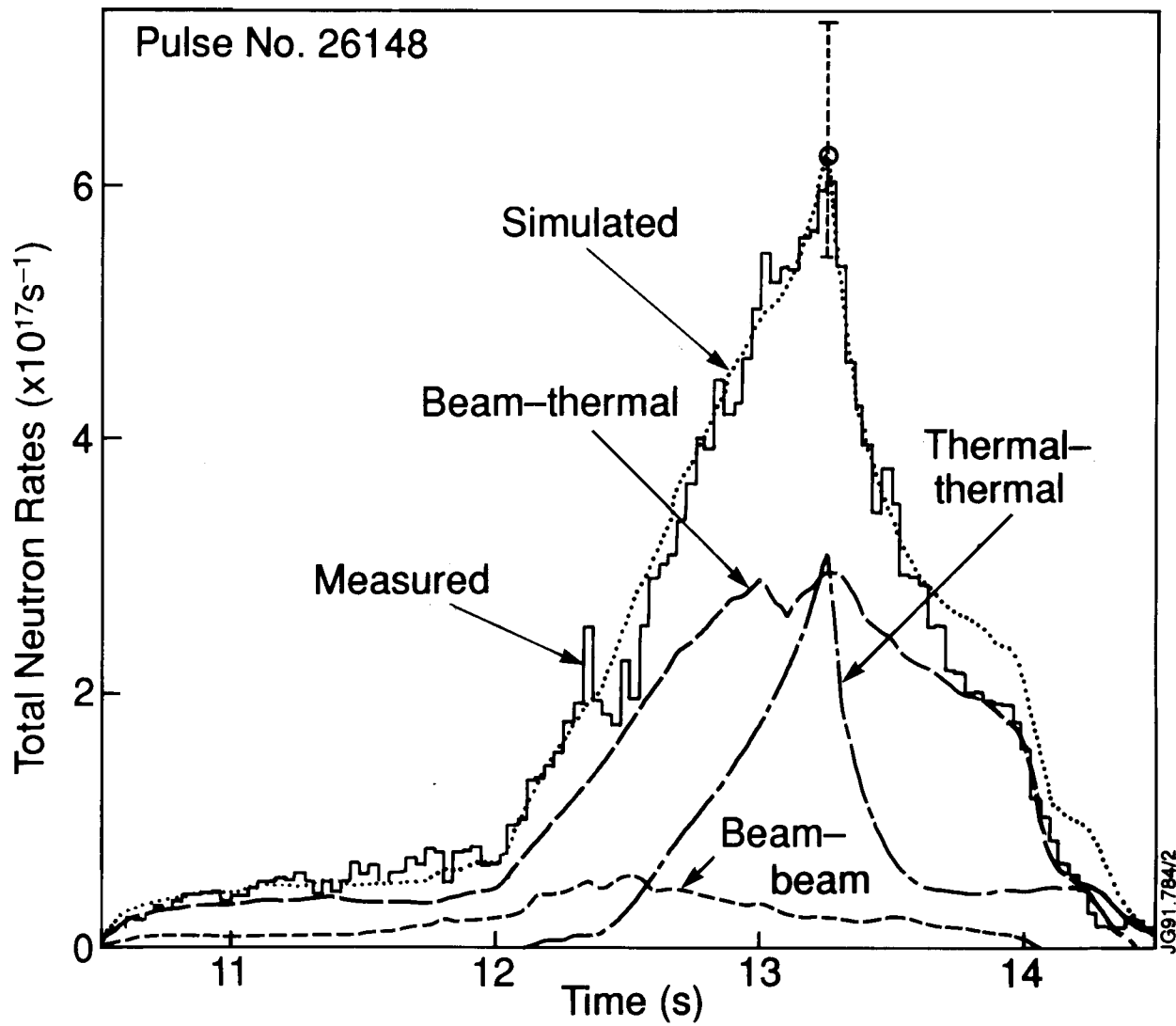


Fig. 24 Neutron source strength measurements and TRANSP simulation of the total neutron rate on JET pulse No. 26148 (JET Team., 1992).

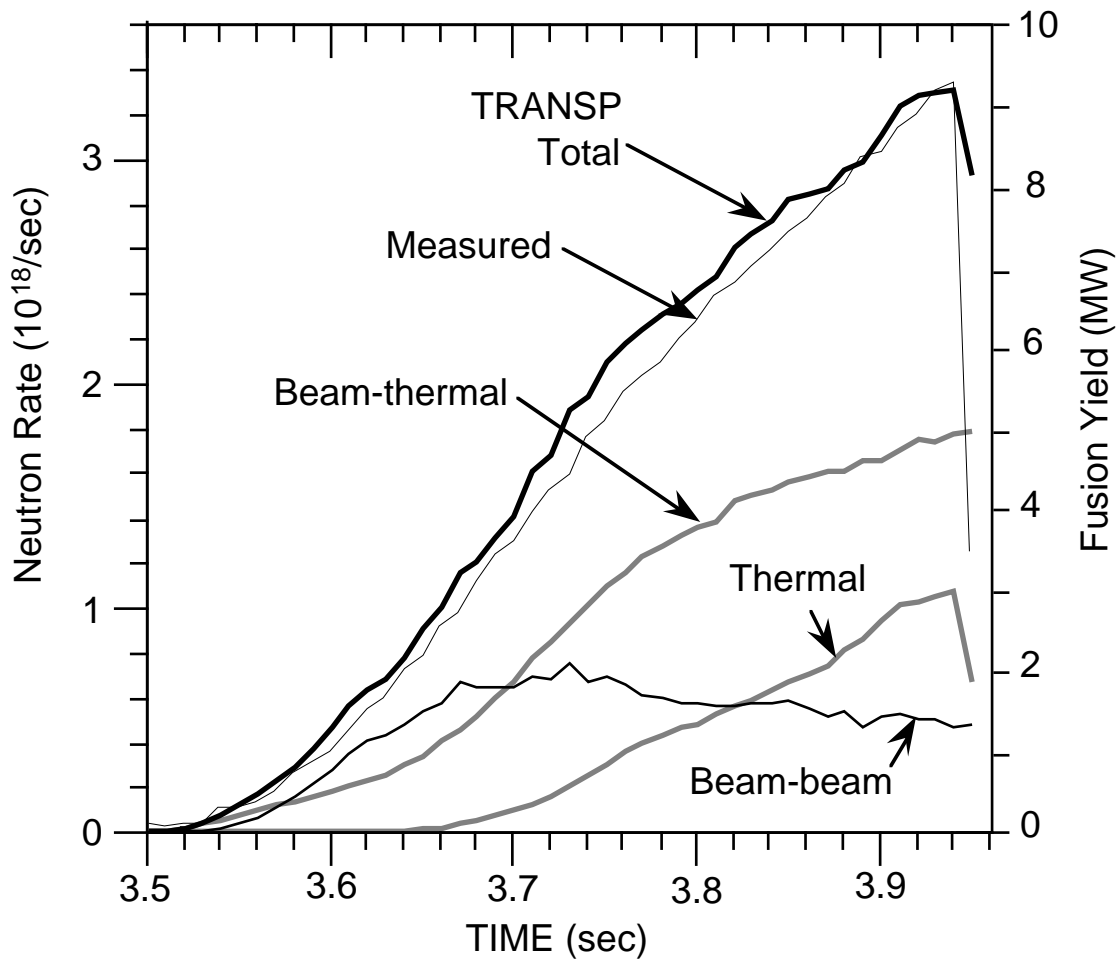


Fig. 25 Neutron source strength measurement and TRANSP simulation of the total neutron rate for TFTR pulse No. 76778 with $P_b = 33.9$ MW (Budny *et al.*, 1995).

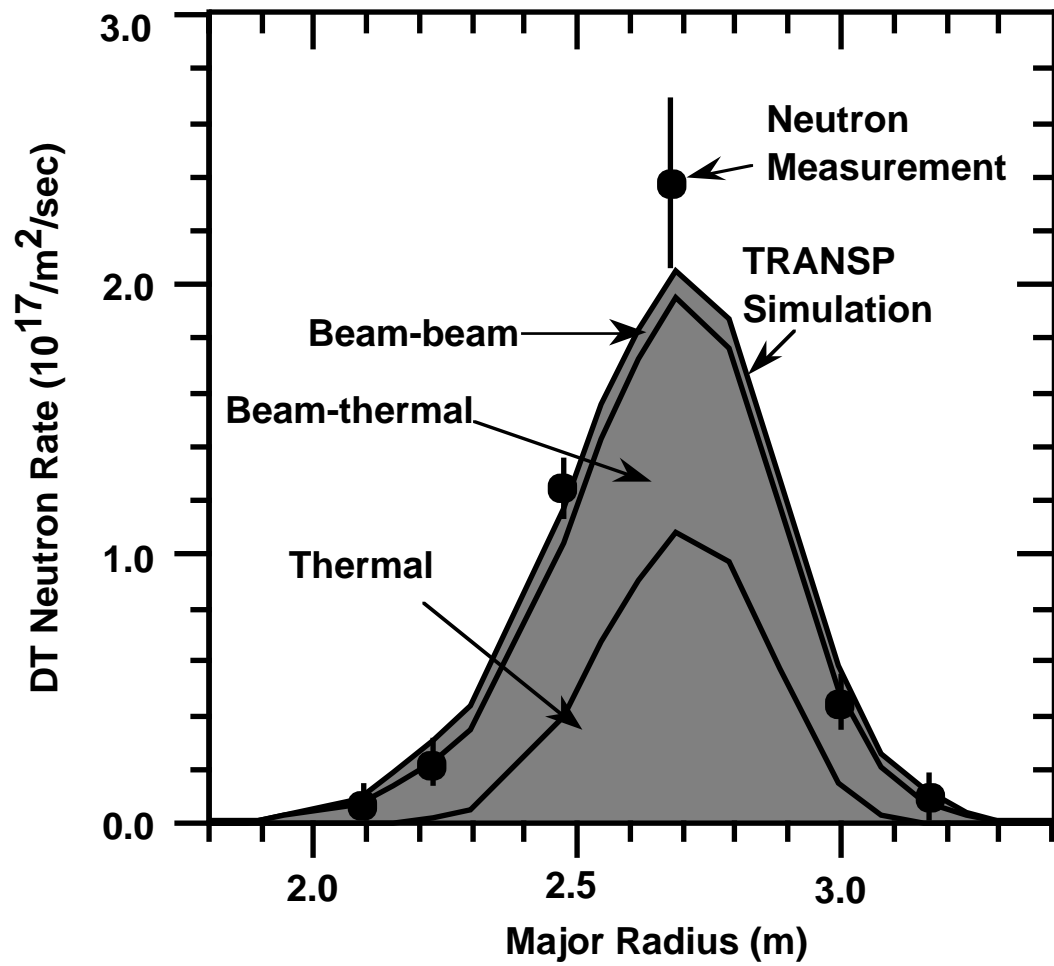


Fig. 26 Neutron emission profile as measured by the neutron collimator are compared with a TRANSP simulation. The contributions from thermal-thermal, beam-thermal and beam-beam reactions are shown (Budny *et al.*, 1995).

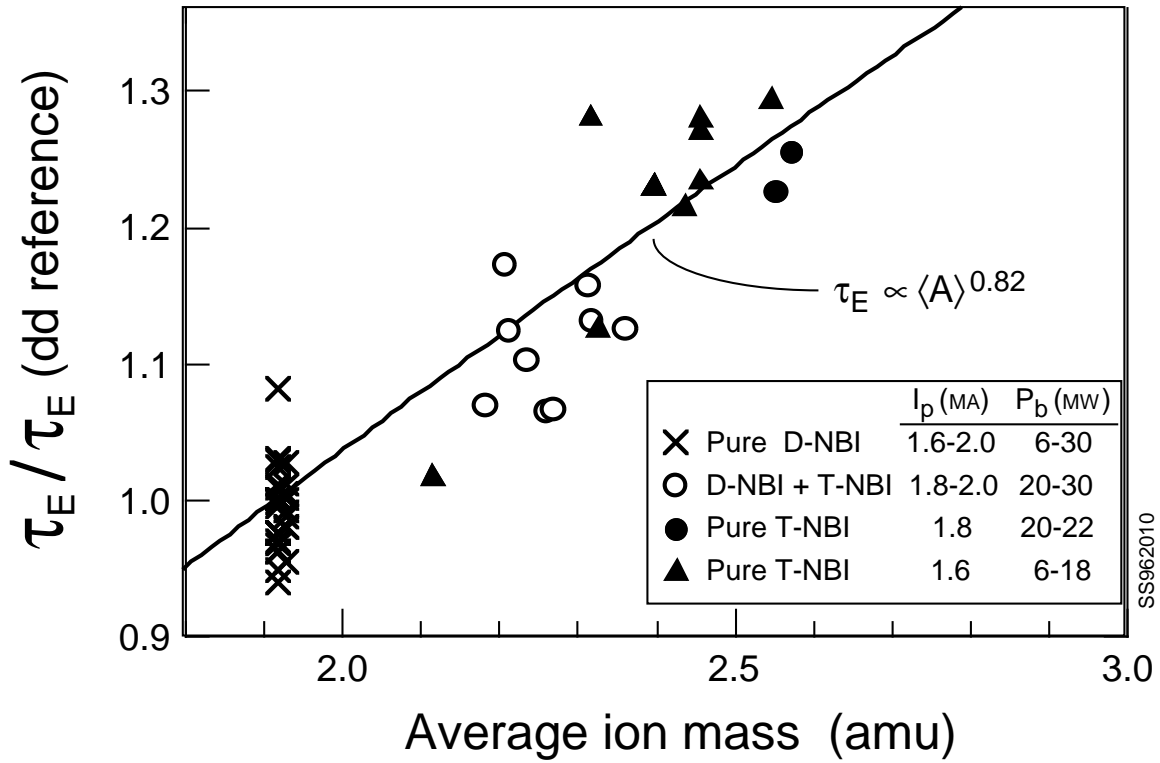


Fig. 27 The ratio of the energy confinement in a D-T discharge is compared with that in a companion D-discharge versus the average hydrogenic ion mass, $\langle A \rangle = \sum n_i A_i / \sum n_i$, where n_i is the hydrogenic density (Scott *et al.*, 1995, 1996a).

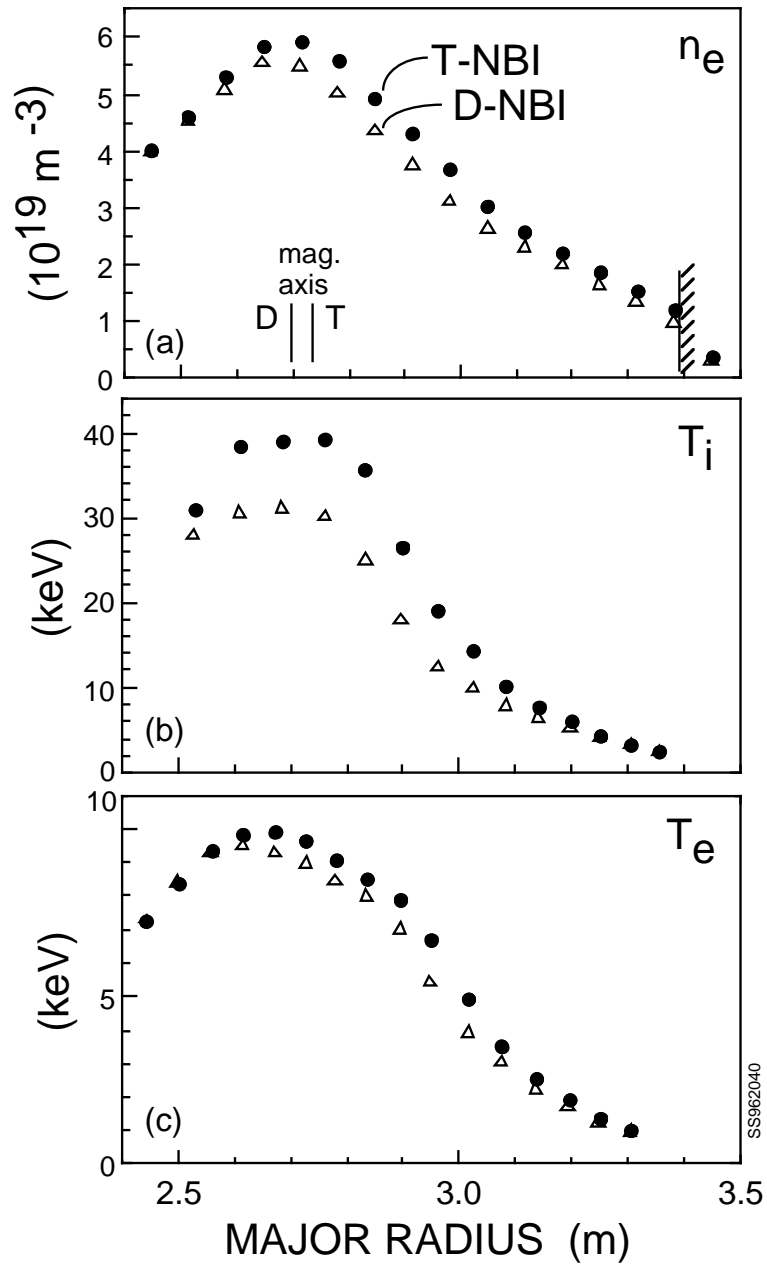


Fig. 28 Comparison of electron density, ion and electron temperature profiles for a D and a companion D-T discharge (Scott *et al.*, 1996a).

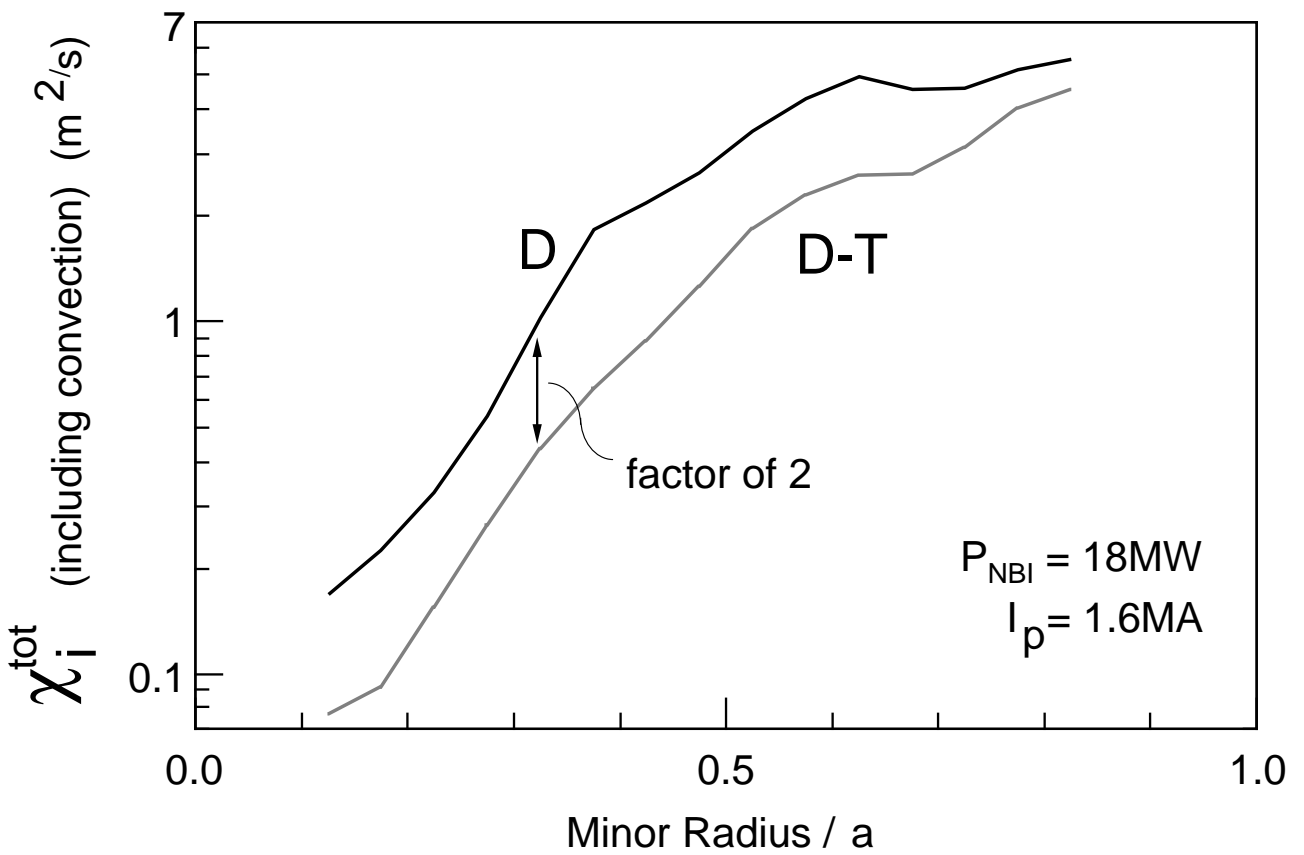


Fig. 29 Comparison of the ion thermal diffusivity in a D-T plasma heated by tritium beam with a companion D discharge. The thermal mix of the background ions is approximately a 50:50 D-T mix. (Scott *et al.*, 1996a).

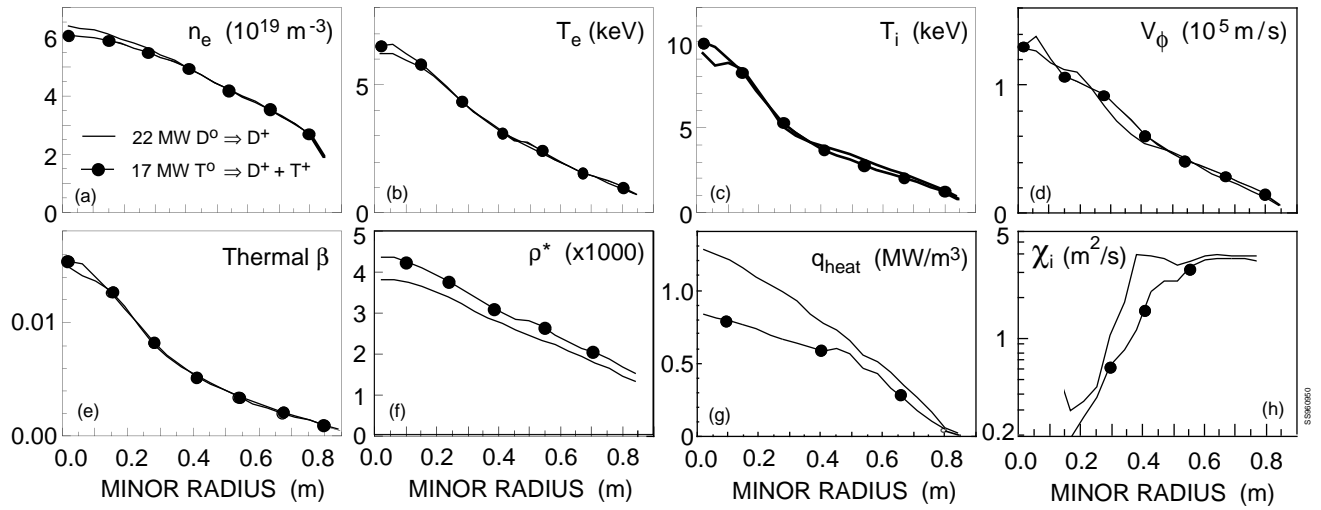


Fig. 30 Kinetic profiles in D and D-T L-mode 'isotope ρ^* -scaling' plasmas matched in density, temperature, β , v^* , B_t , I_p , Z_{eff} , and v_{*e} . Contrary to gyroBohm expectations, the D plasma with smaller ρ^* requires $\sim 30\%$ more heating power to sustain the temperature (Scott *et al.*, 1996b).

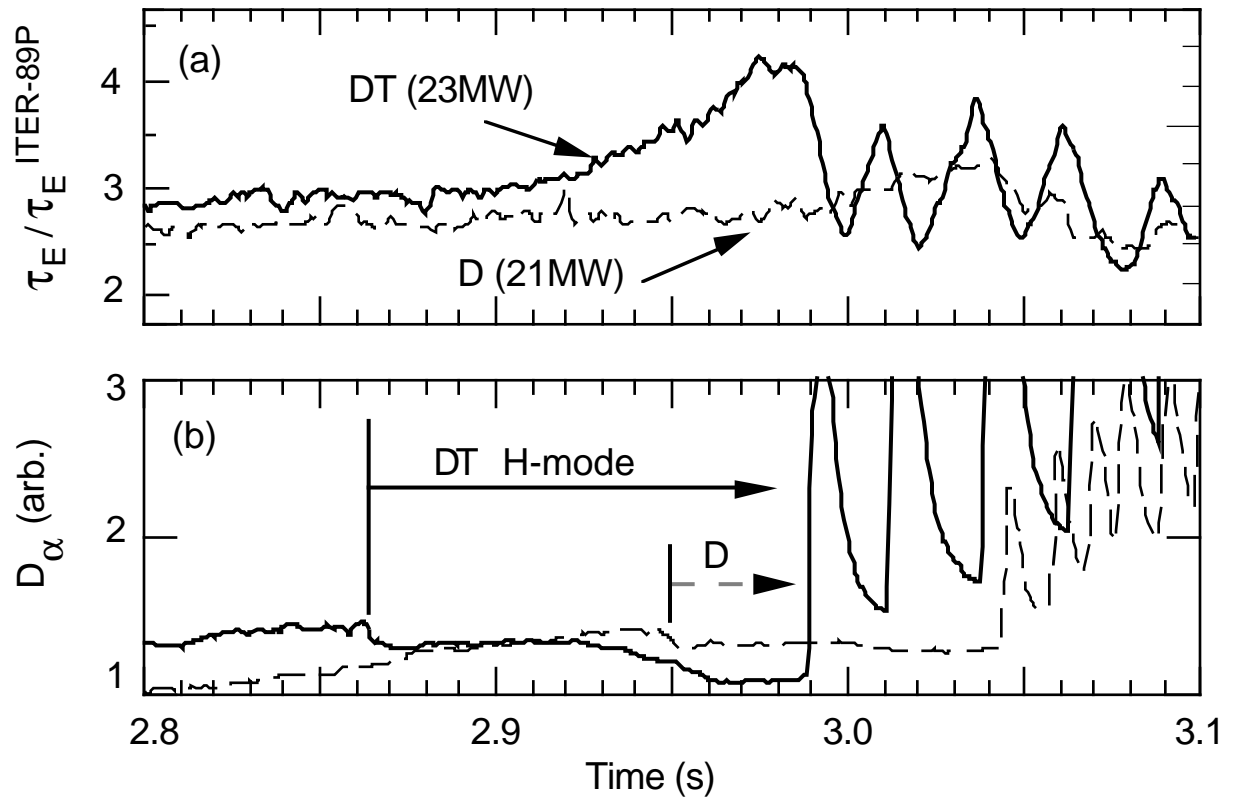


Fig. 31 Evolution of a) $\tau_E / \tau_E^{ITER-89P}$ and b) D_α for a D-T discharge and a companion D discharge on TFTR (Bush *et al.*, 1995).

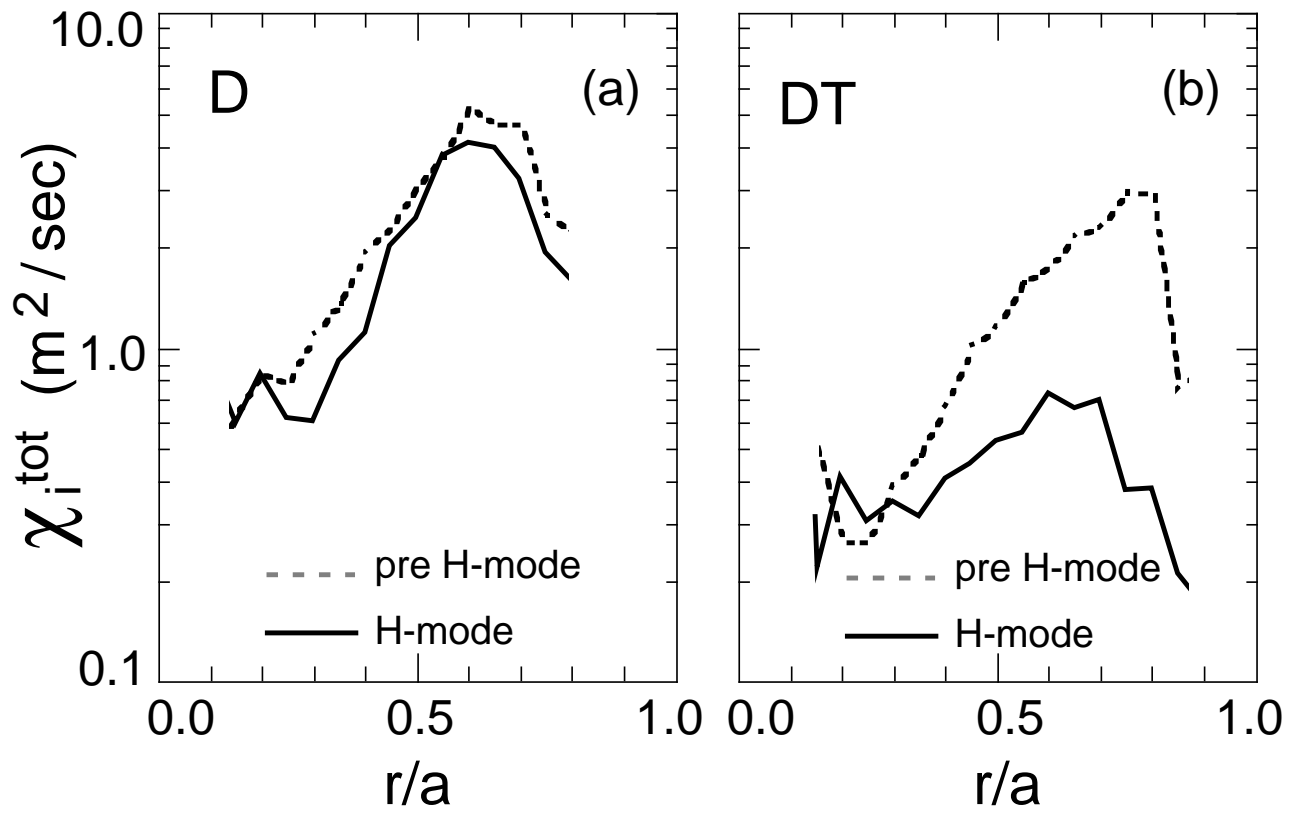


Fig. 32 Comparison of the effect of H-mode transition in a D and D-T limiter discharge on TFTR (Bush *et al.*, 1995).

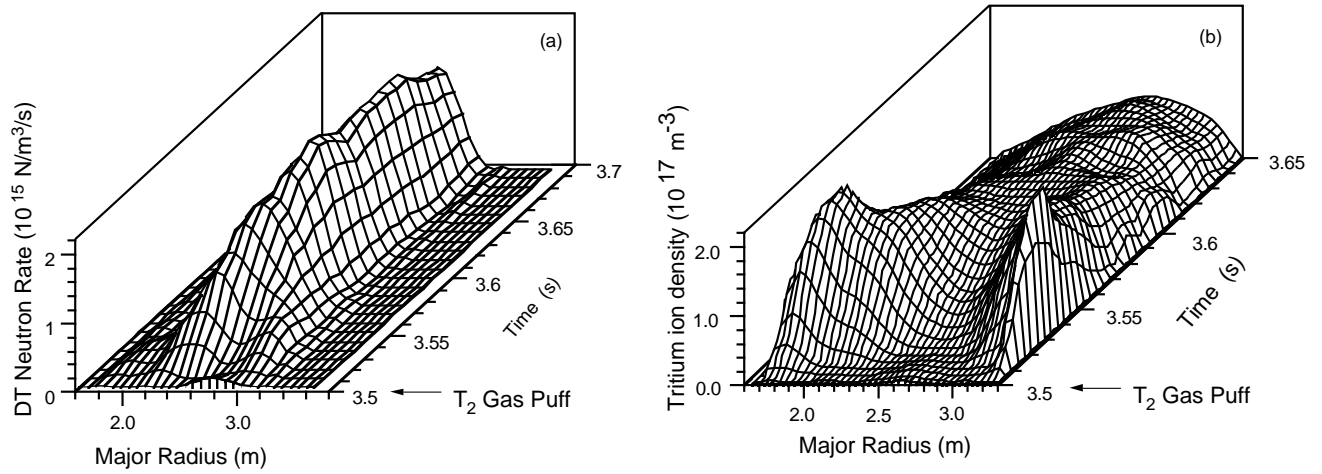


Fig. 33 Evolution of a) D-T neutron emissivity and b) the inferred tritium density profiles following a small tritium gas puff into a supershot discharge on TFTR (Johnson *et al.*, 1994; Efthimion *et al.*, 1995a).

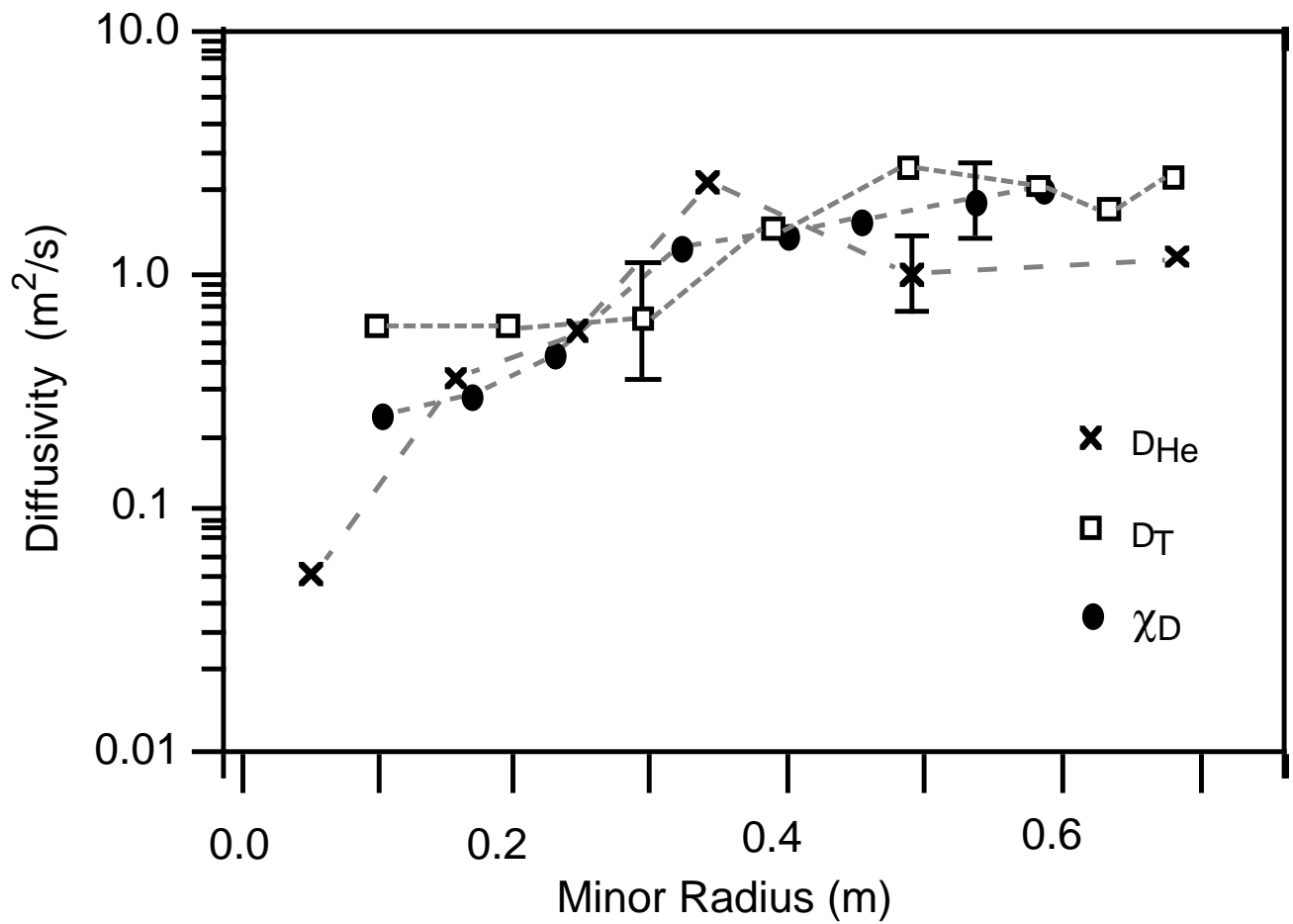


Fig. 34 The tritium particle diffusivity following a small tritium gas puff is comparable with the electron particle diffusivity as well as the He diffusivity (Efthimion *et al.*, 1995a).

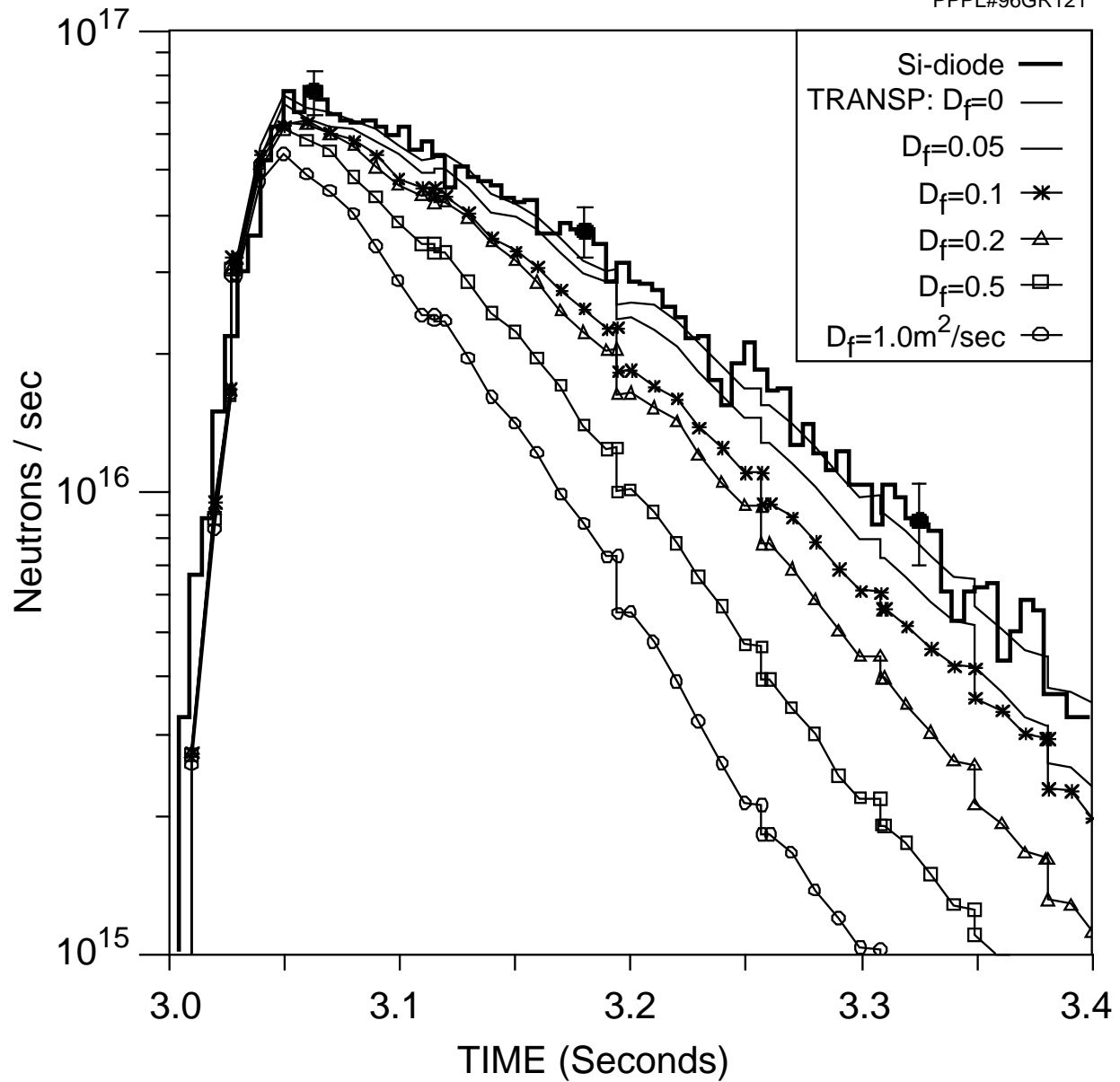


Fig. 35 The measured neutron source strength of 14 MeV neutrons by a Si diode detector due to a short pulse of high power neutral beam injection is in good agreement with simulations which assume a small radial diffusivity ($D_f < 0.05 m^2/s$) for the beam ions (Ruskov *et al.*, 1995).

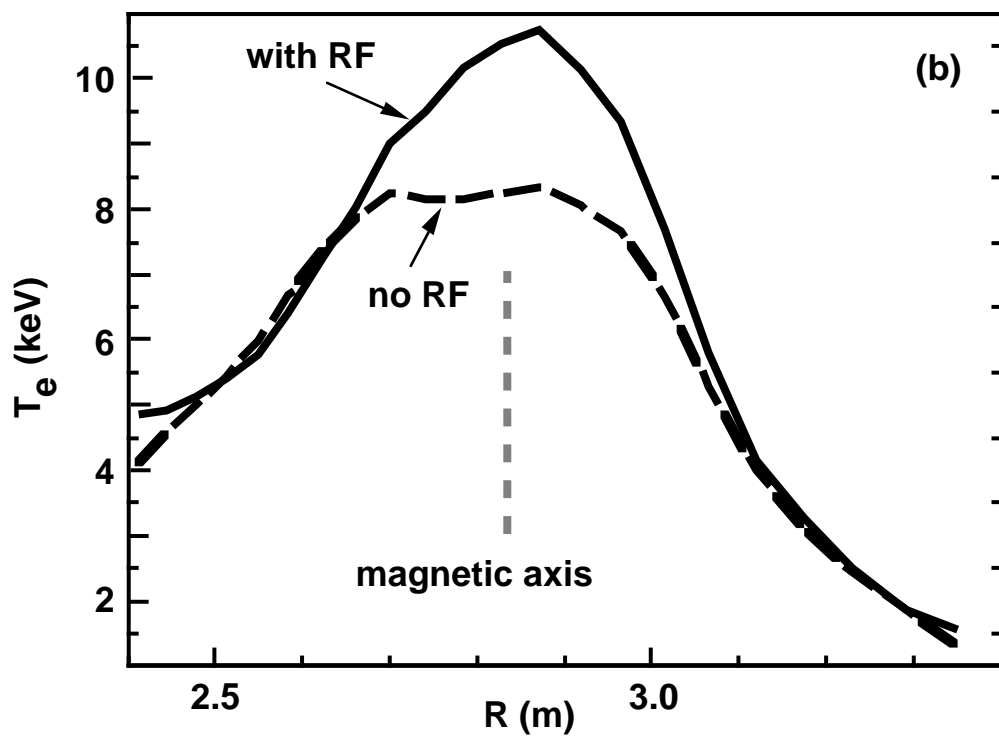
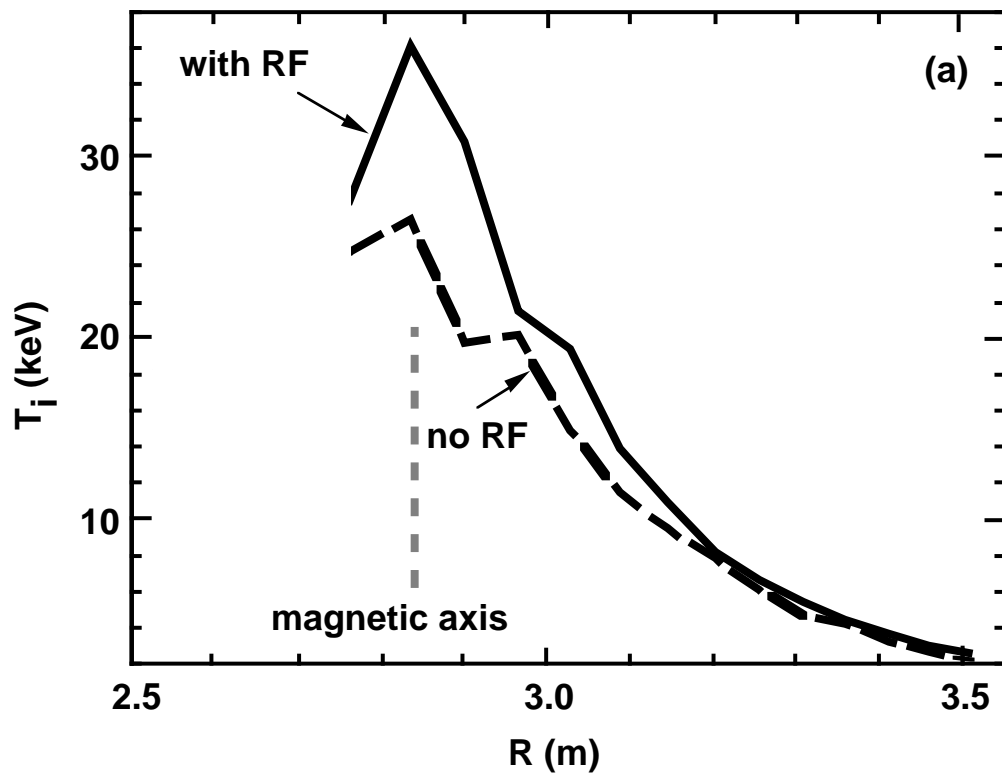


Fig. 36 Ion and electron temperature profiles in a discharge heated with 23.5 MW of neutral beam heating and in another supplemented by an additional 5.5 MW of ICRF heating (Wilson *et al.*, 1995).

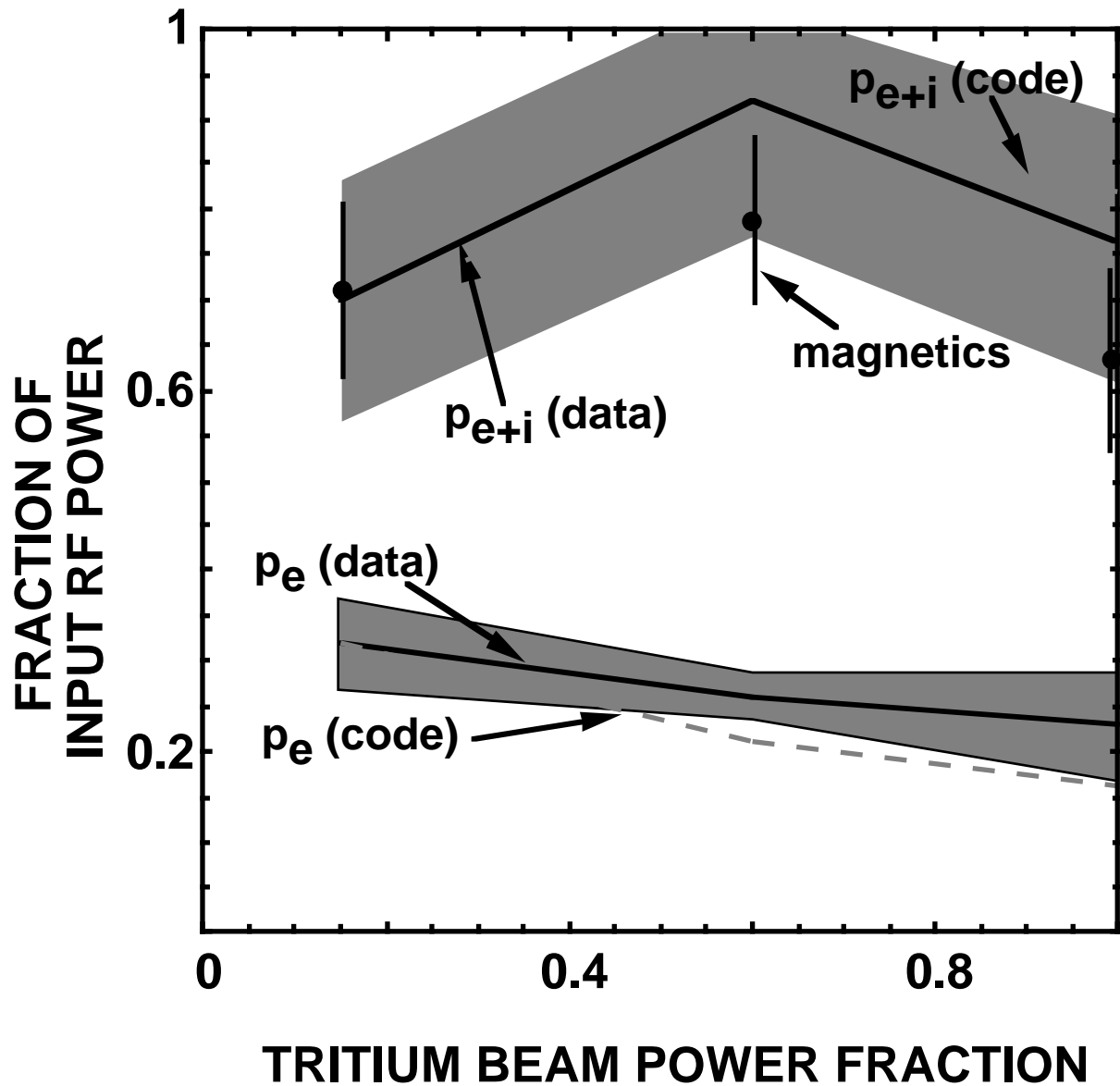


Fig. 37 Measurements and prediction using the PICES and TRANSP codes of the fraction of rf power absorbed by electron and ions versus the tritium beam power fraction. Modulation of the rf power together with the evolution of the electron and ion temperature is used to infer the fraction of power absorbed by ions and electrons (Phillips *et al.*, 1995).

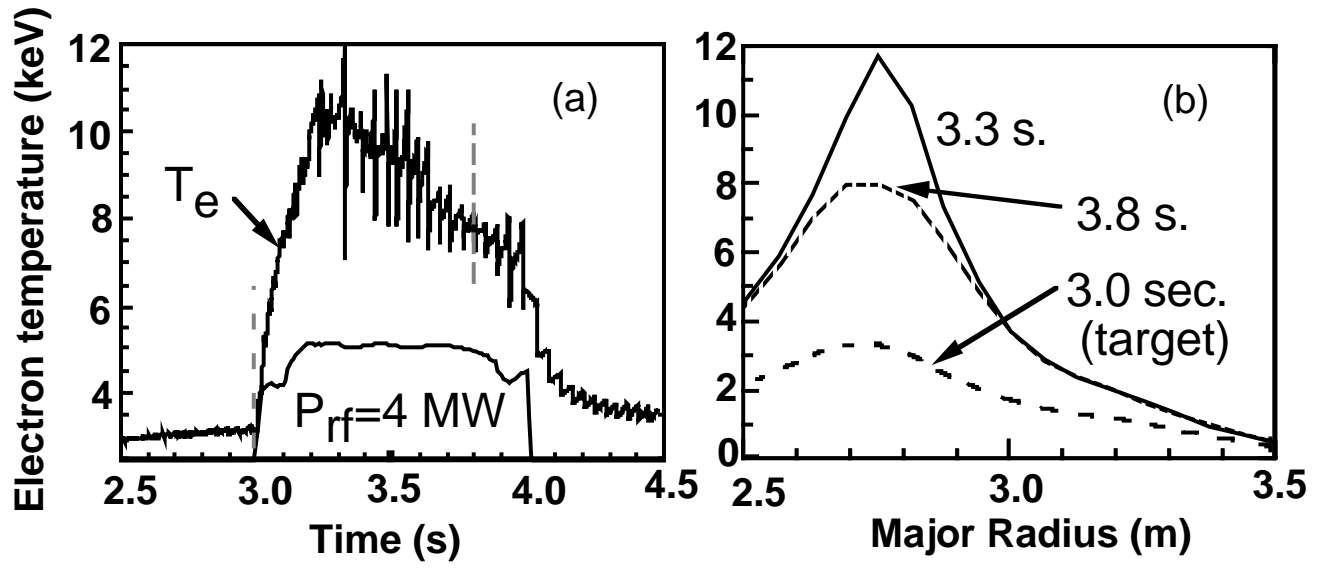


Fig. 38 Mode conversion of the fast wave results in strong and highly localized electron heating at the ion-ion hybrid layer (Majeski *et al.*, 1996).

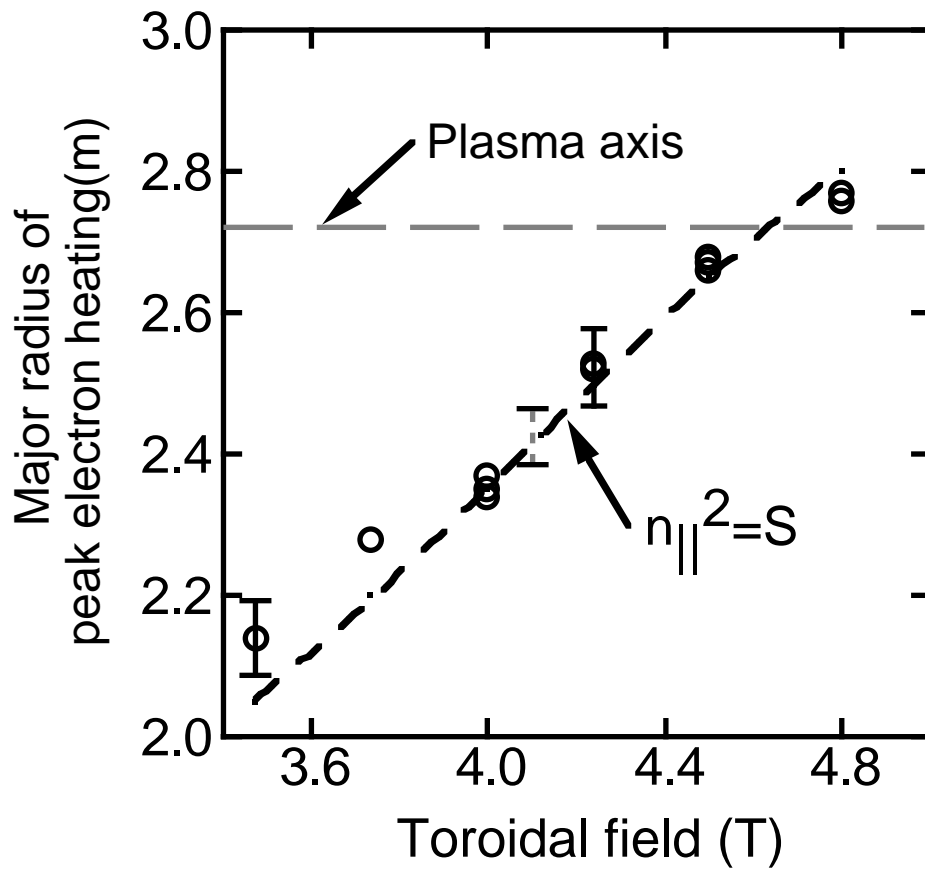


Fig. 39 Observed radius of electron power deposition as a function of toroidal field, for constant ^3He fraction and density. The open symbols denote the observed location from electron temperature measurement and the line denotes the location of mode conversion layer (Majeski *et al.*, 1996).

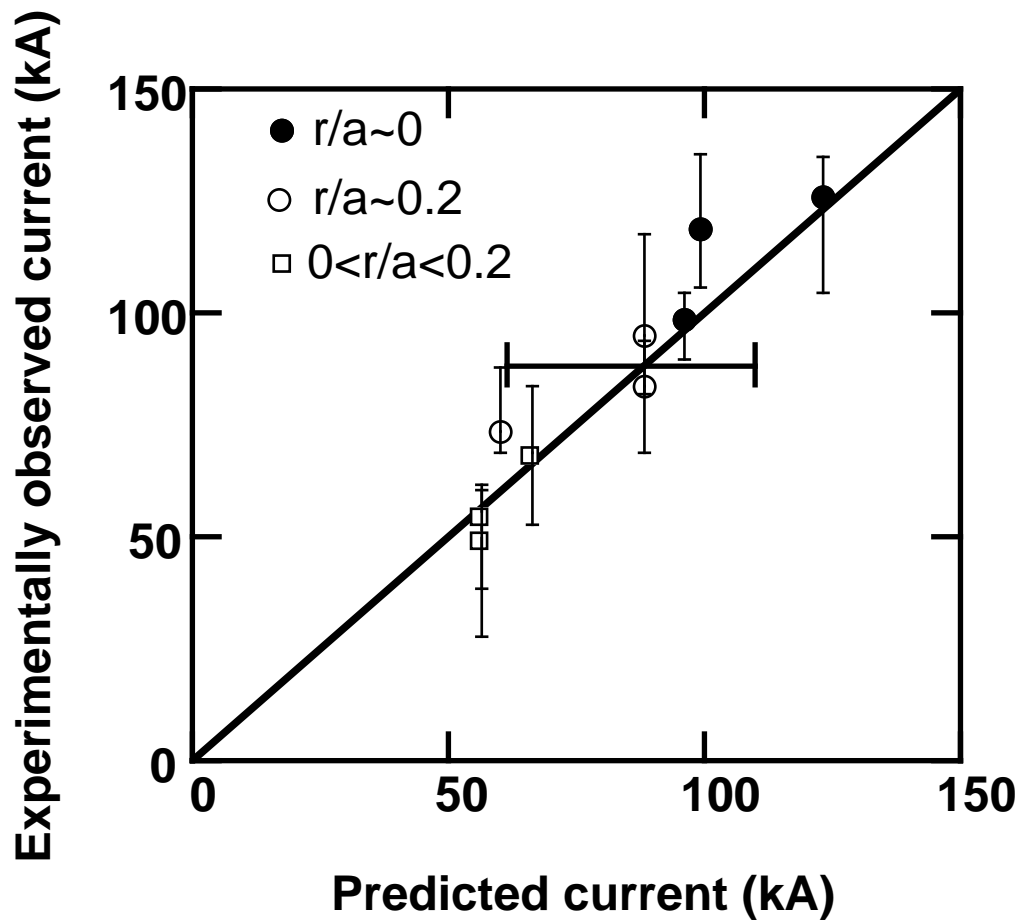


Fig. 40 The measured mode conversion current drive is compared with the predicted current drive (Majeski *et al.*, 1996).

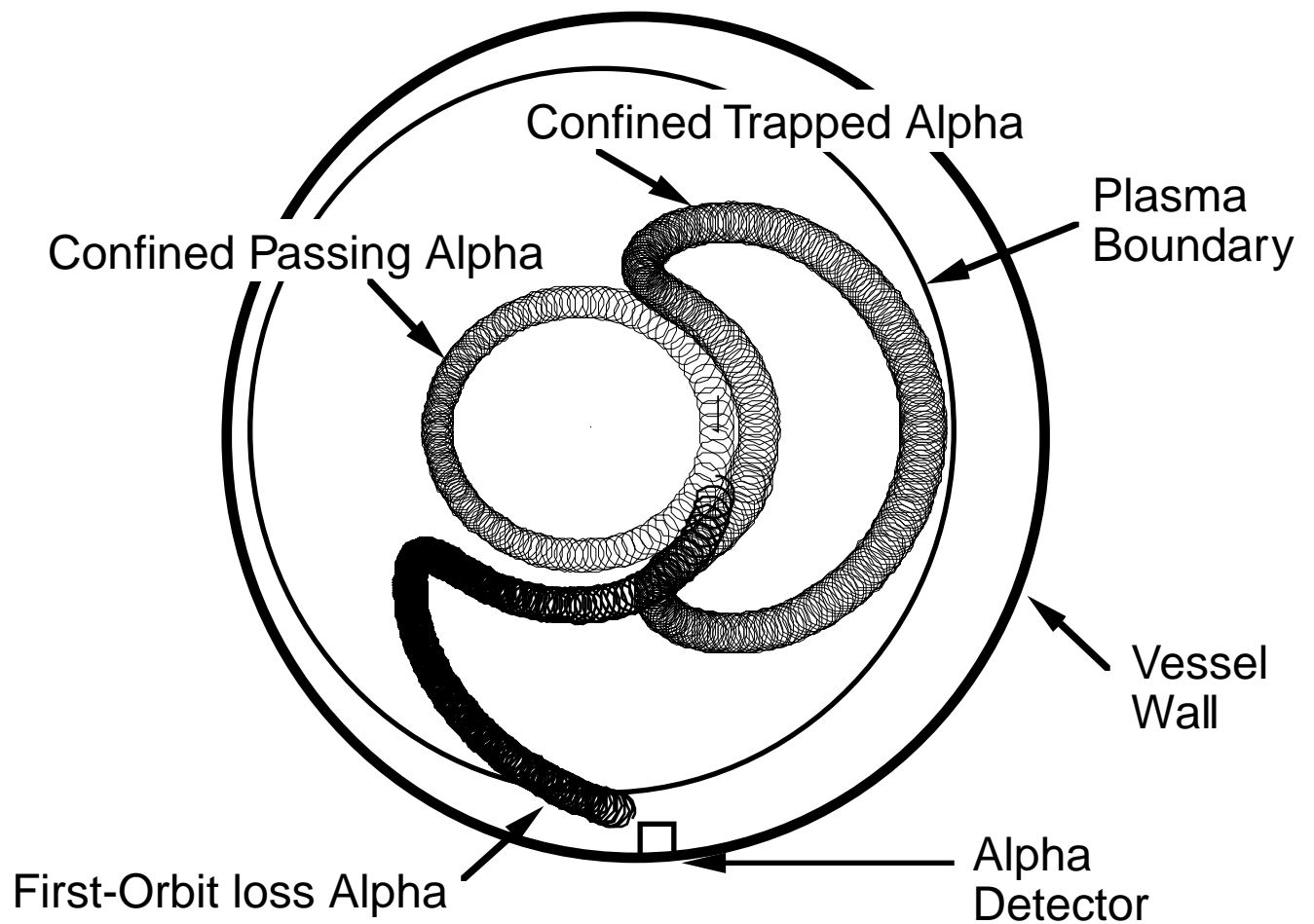


Fig. 41 Illustration of confined passing alpha particle orbits, confined trapped alpha on banana orbits and unconfined trapped alphas.

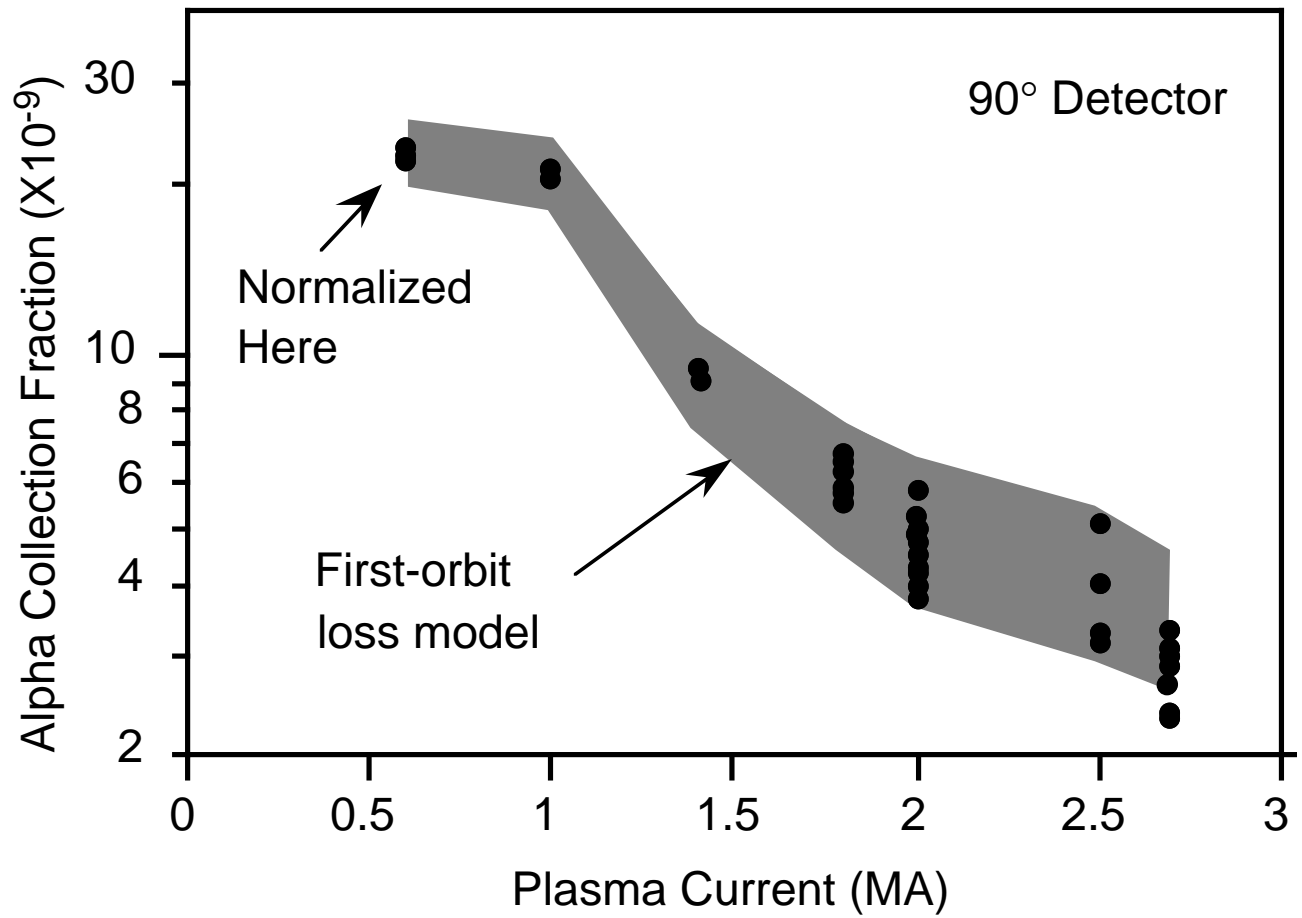


Fig. 42 Fraction of alpha particles collected by a detector located near the bottom of the vessel (90°). The decrease in loss with increasing current is in good agreement with the predictions of the first orbit loss model. The data is normalized at low currents as indicated (Zweben *et al.*, 1995a).

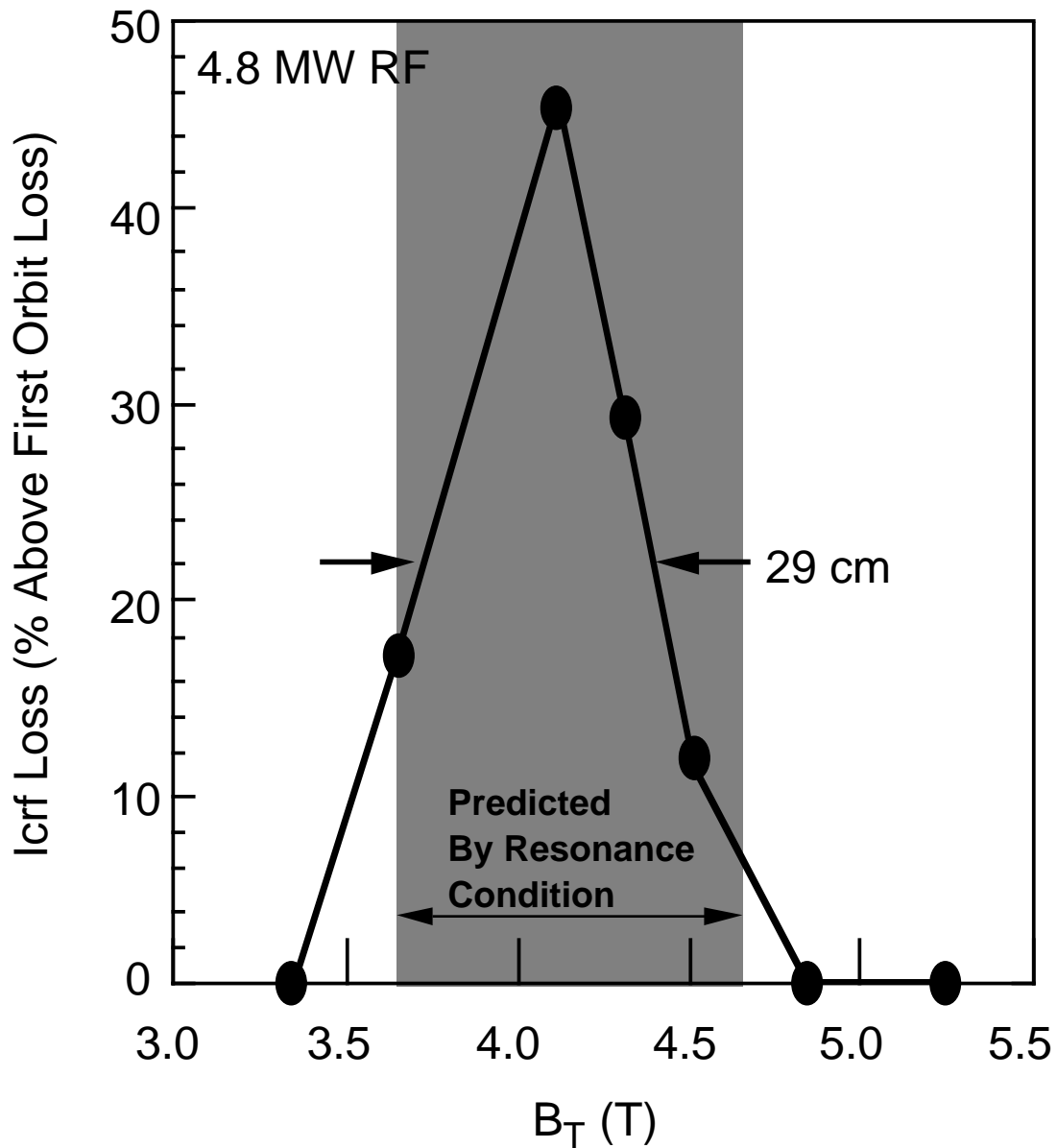


Fig. 43 The increase in alpha loss to the detector at the bottom of the machine resulting from ICRF waves is plotted as a function of toroidal field. The shaded range of toroidal field denotes where marginally passing alpha particles can be in Doppler-shifted resonance with the waves. Loss proceeds by conversion of these marginally passing orbits to lost banana orbits as the alphas are heated.

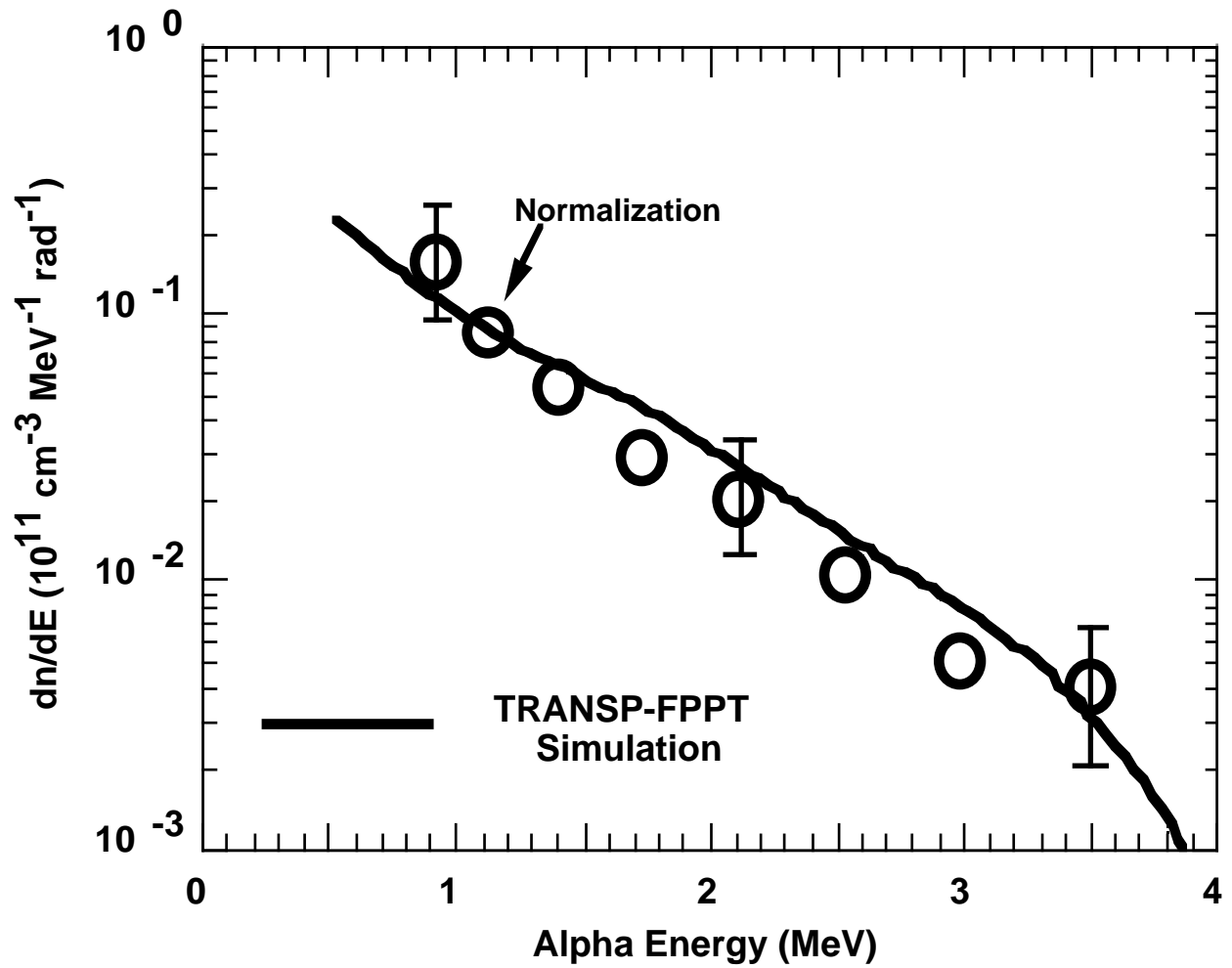


Fig. 44 Measurements of the confined alpha particle spectrum following neutral beam heating of a D-T plasma. The TRANSP calculations which are normalized at one point are in good agreement with the observed slowing down spectrum (Petrov *et al.*, 1995; Medley *et al.*, 1996a).

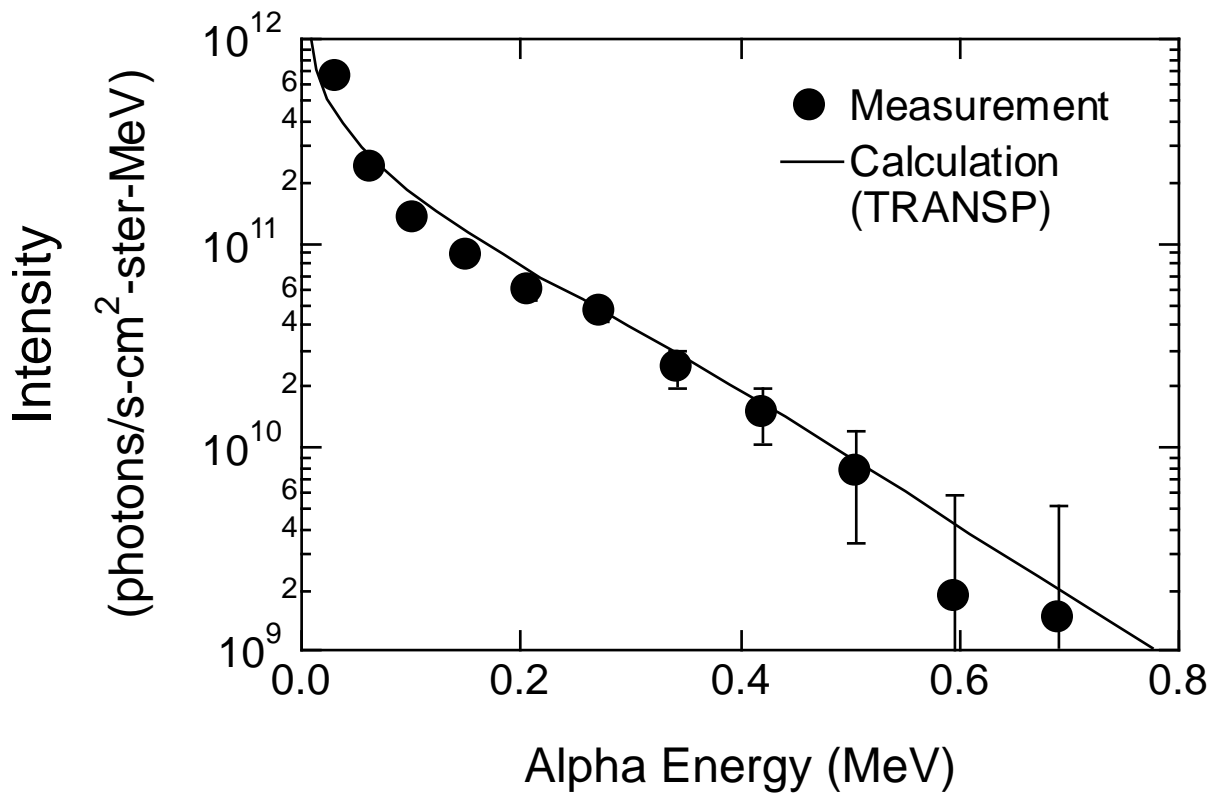


Fig. 45 Measured alpha-CHERS spectra at $r/a=0.3$ in a non-sawtooth TFTR D-T supershot are in good agreement with predictions based on TRANSP calculation of the alpha density (McKee *et al.*, 1995b).

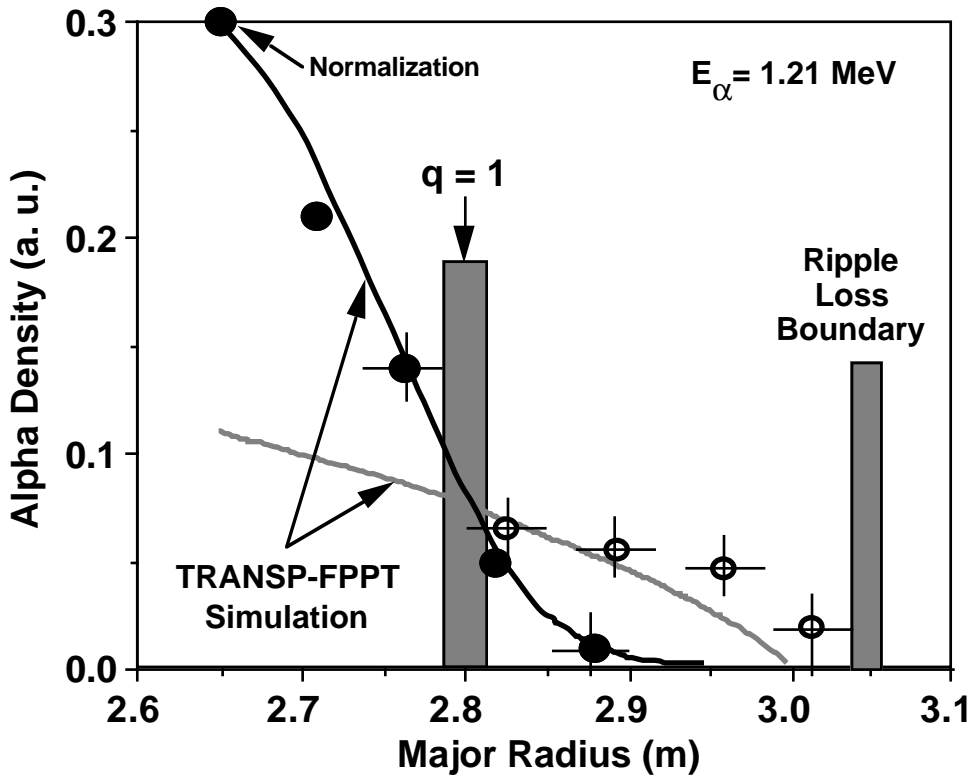


Fig. 46 Pellet charge exchange measurements of the confined alpha particles prior to and after the sawtooth instability (in a companion discharge). The observed redistribution is in reasonable accord with the magnetic reconnection model which incorporates the effect of the helical electric field (Petrov *et al.*, 1996).

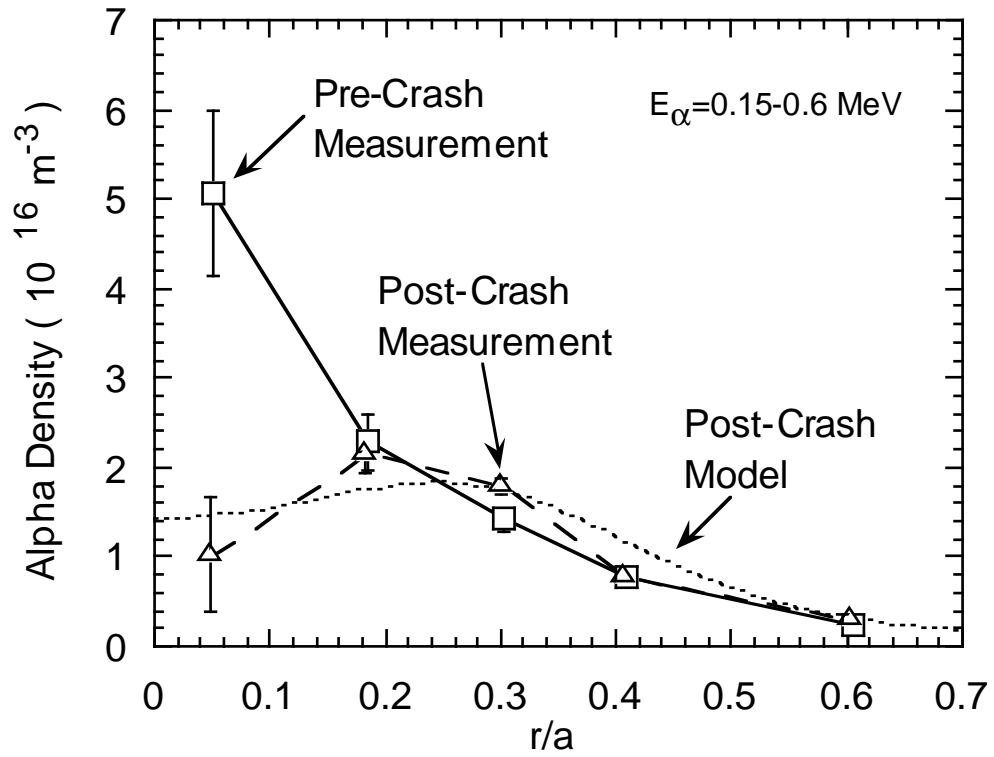


Fig. 47 Alpha-CHERS measurements of alpha density profiles before and after a sawtooth crash are in good agreement with predictions of the Kolesnichenko *et al.*, (1992) sawtooth model (Stratton *et al.*, 1996).

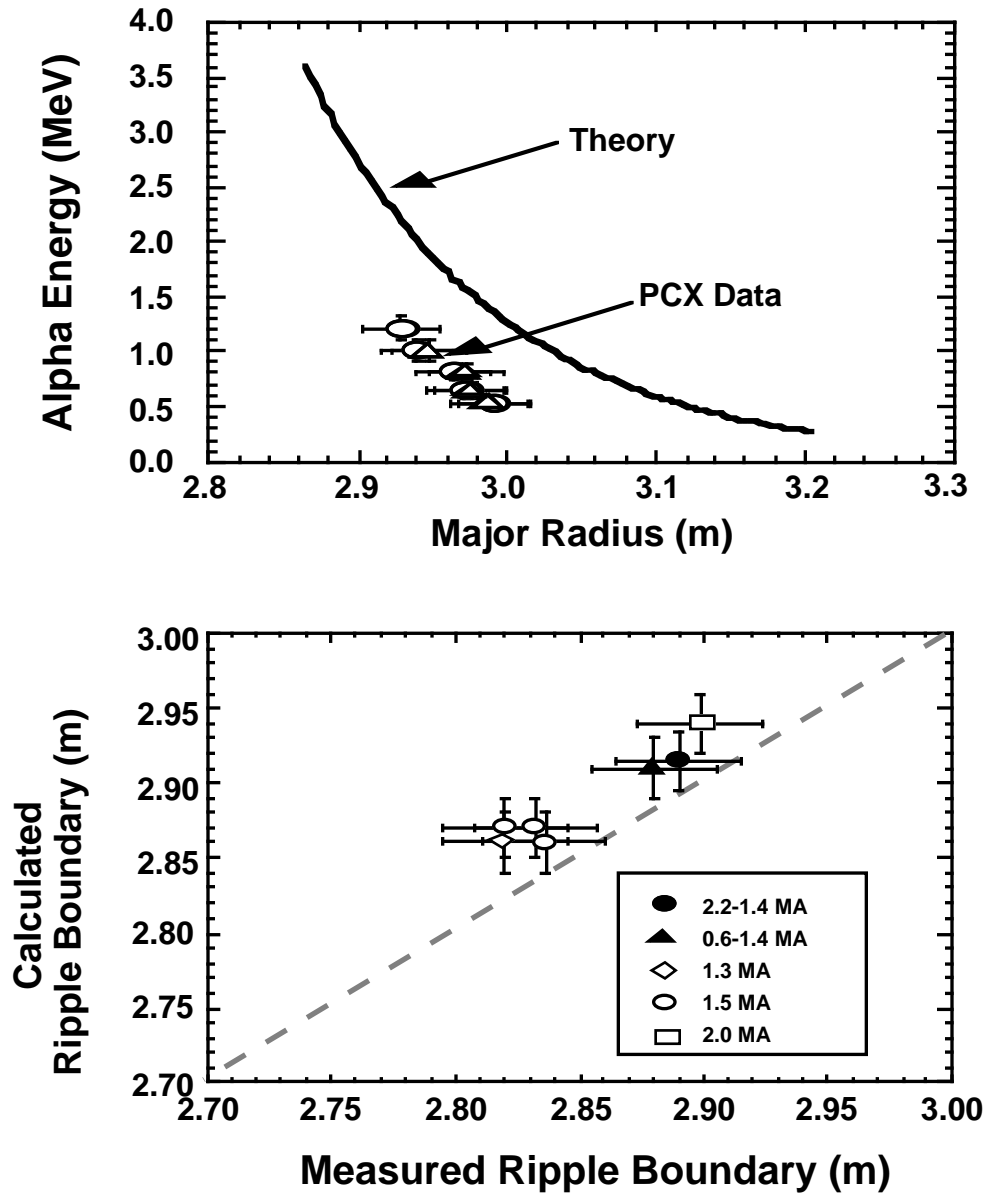


Fig. 48 The measured ripple boundary is determined from the major radius at which confined alpha particles are measured by the pellet charge exchange diagnostic. The location of the observed presence of deeply trapped alpha particles is in reasonable accord with a simple estimate of the calculated ripple boundary using the Goldston-White-Boozer formalism (Duong *et al.*, 1996a).

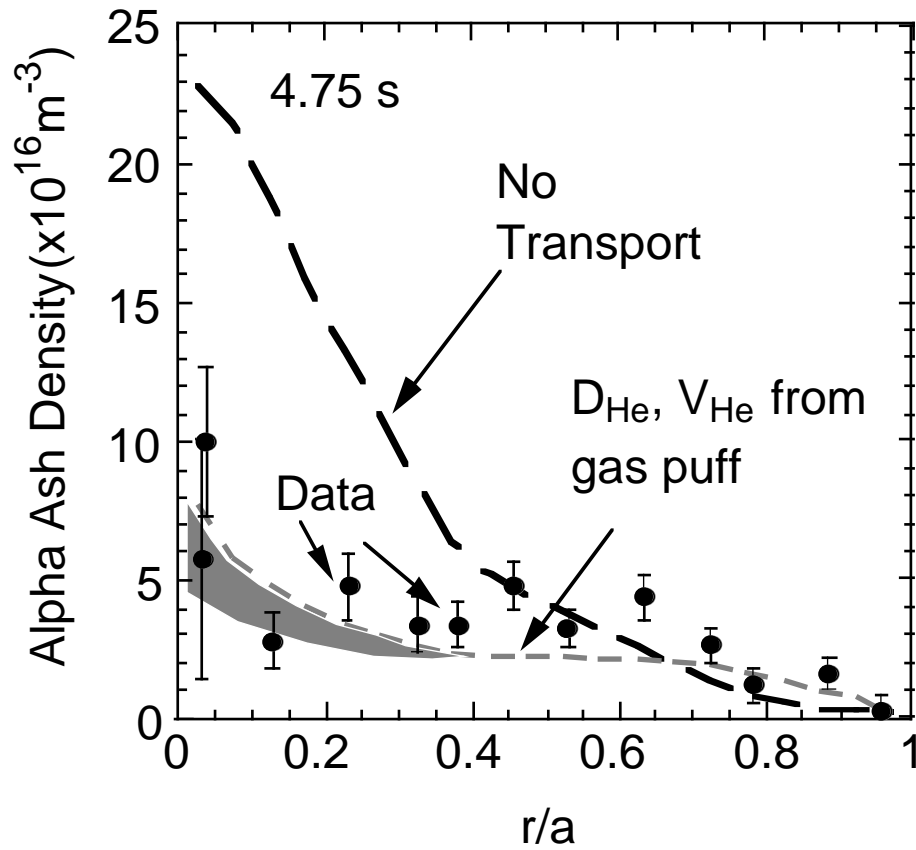


Fig. 49 Measured and modeled ash profile shapes measured 1.95 s after the start of deuterium-tritium beam injection. The errors include uncertainties related to the atomic physics of charge exchange and beam attenuation, as well as photon. The thick dashed line represents the helium ash profile shape predicted under the assumption of no radial transport of the thermalized ash. The thinner dashed line represents the predicted profile shape including the effects of radial transport and wall recycling. The shaded region is the difference in the profile shapes that are predicted with and without the central source of thermalizing alpha particles, but with transport in both cases (Synakowski *et al.*, 1995a).

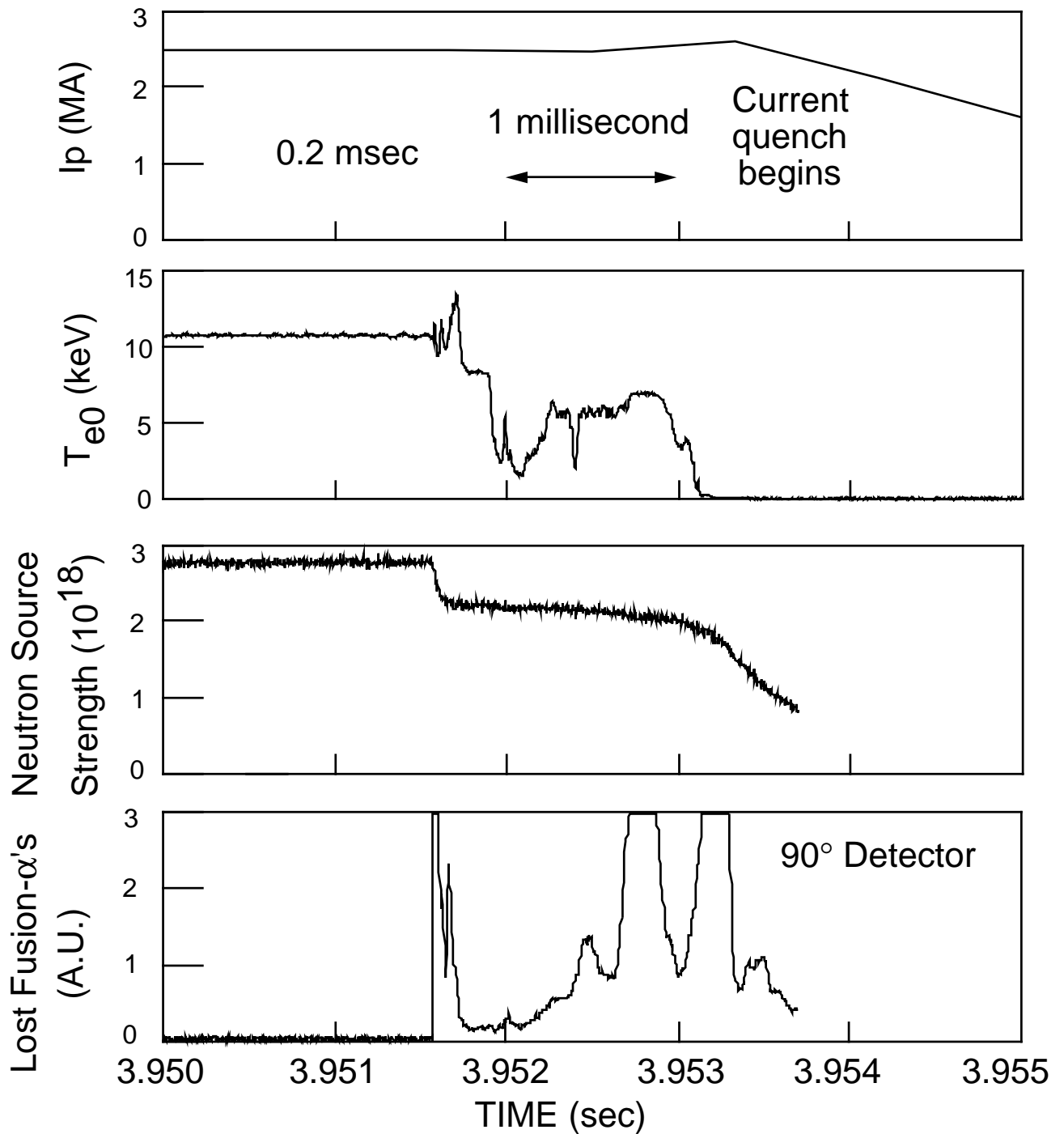


Fig. 50 The first burst of alpha particles prior at 3.9525 sec to the detector in the bottom of the vessel precedes the thermal quench of the plasma as measured by the electron temperature diagnostic and is coincident with the MHD activity responsible for the subsequent disruption (Janos *et al.*, 1996).

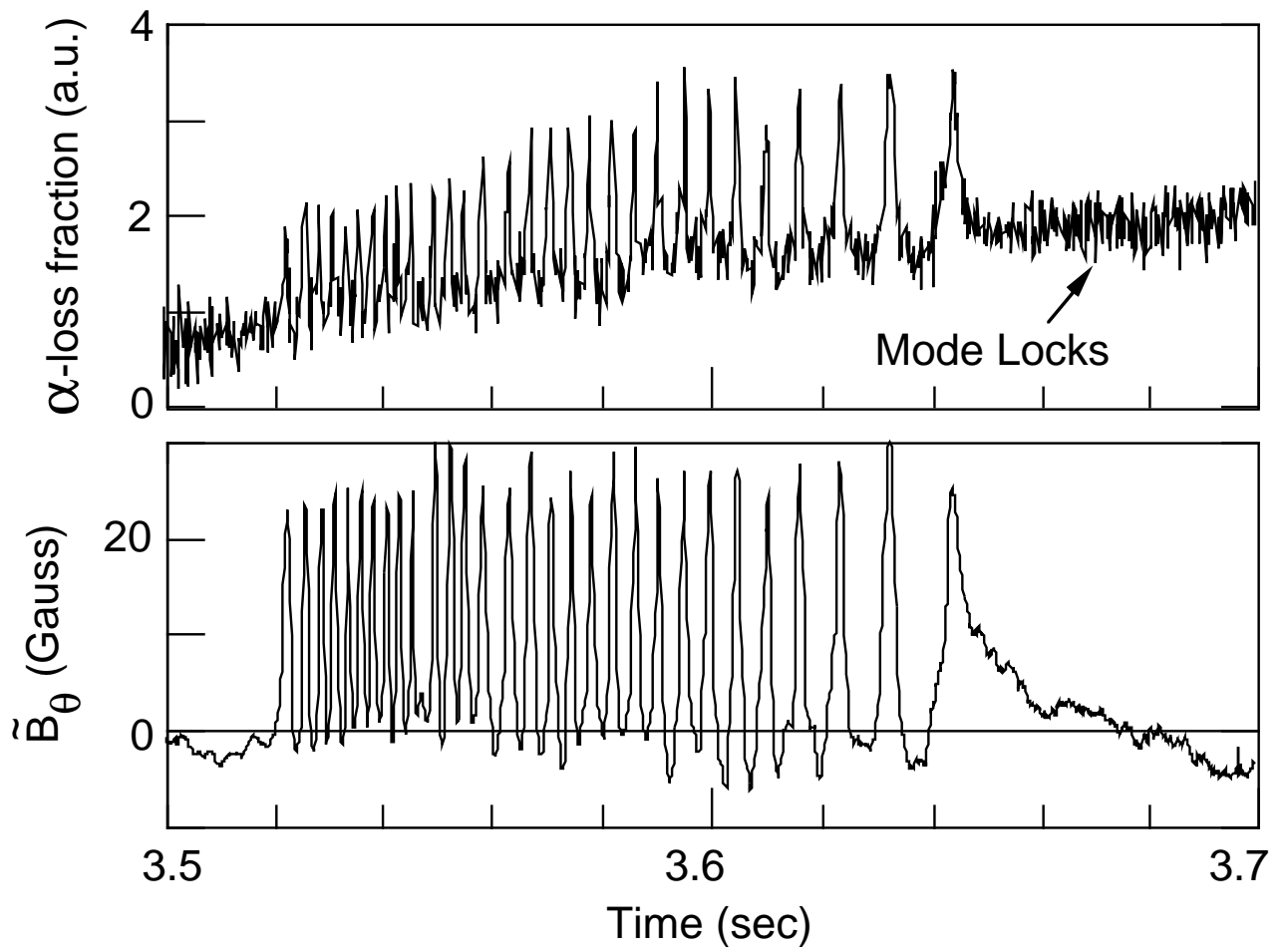


Fig. 51 Alpha particle loss due to neoclassical tearing modes correlated with fluctuations in the edge magnetic field (McGuire *et al.*, 1996).

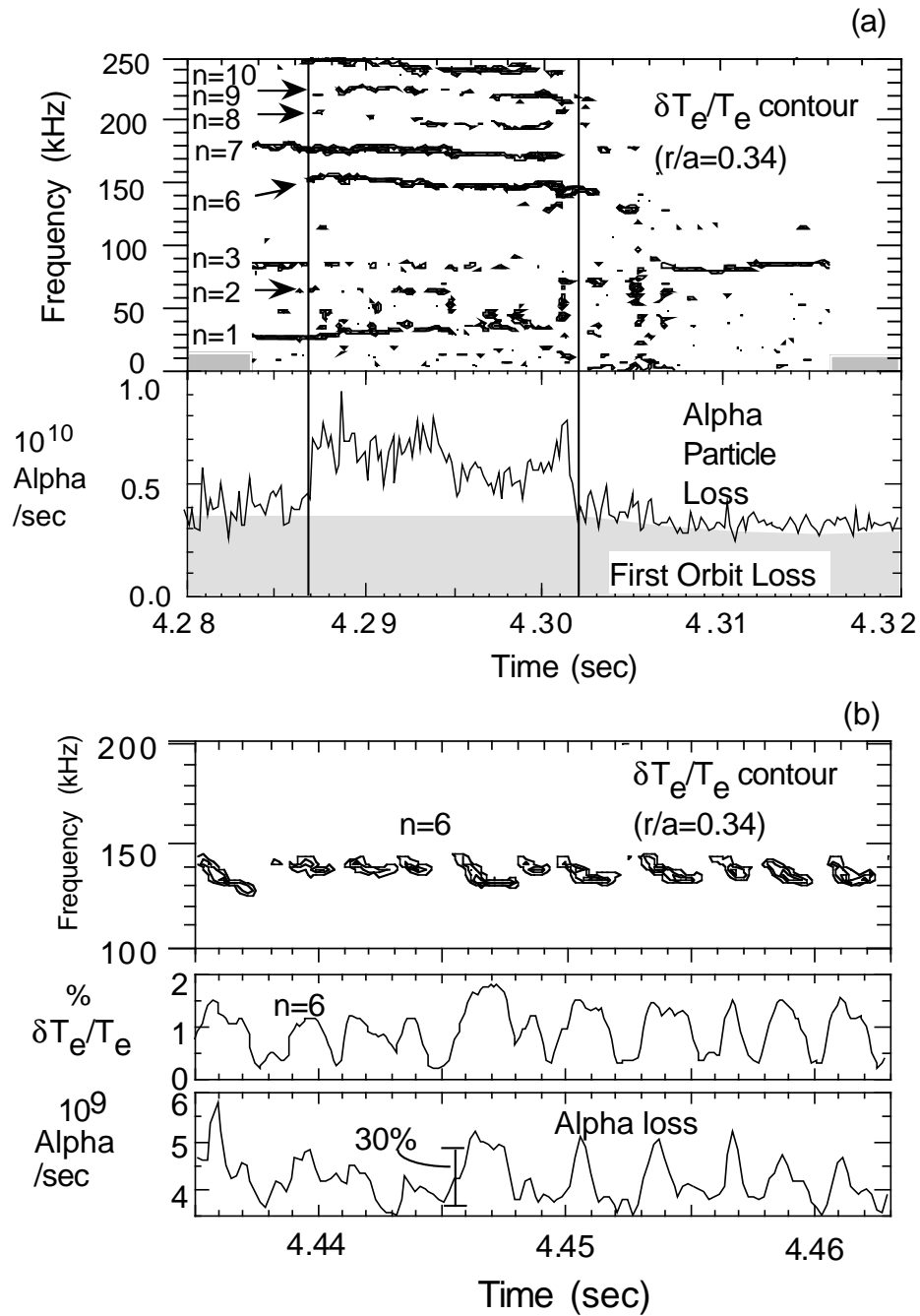


Fig. 52 Increased alpha particle loss is correlated with the occurrence of multiple high-n modes (a) as well as single n (=6) mode (b). These modes are identified as kinetic ballooning modes (KBMs) (Chang *et al.*, 1996b).

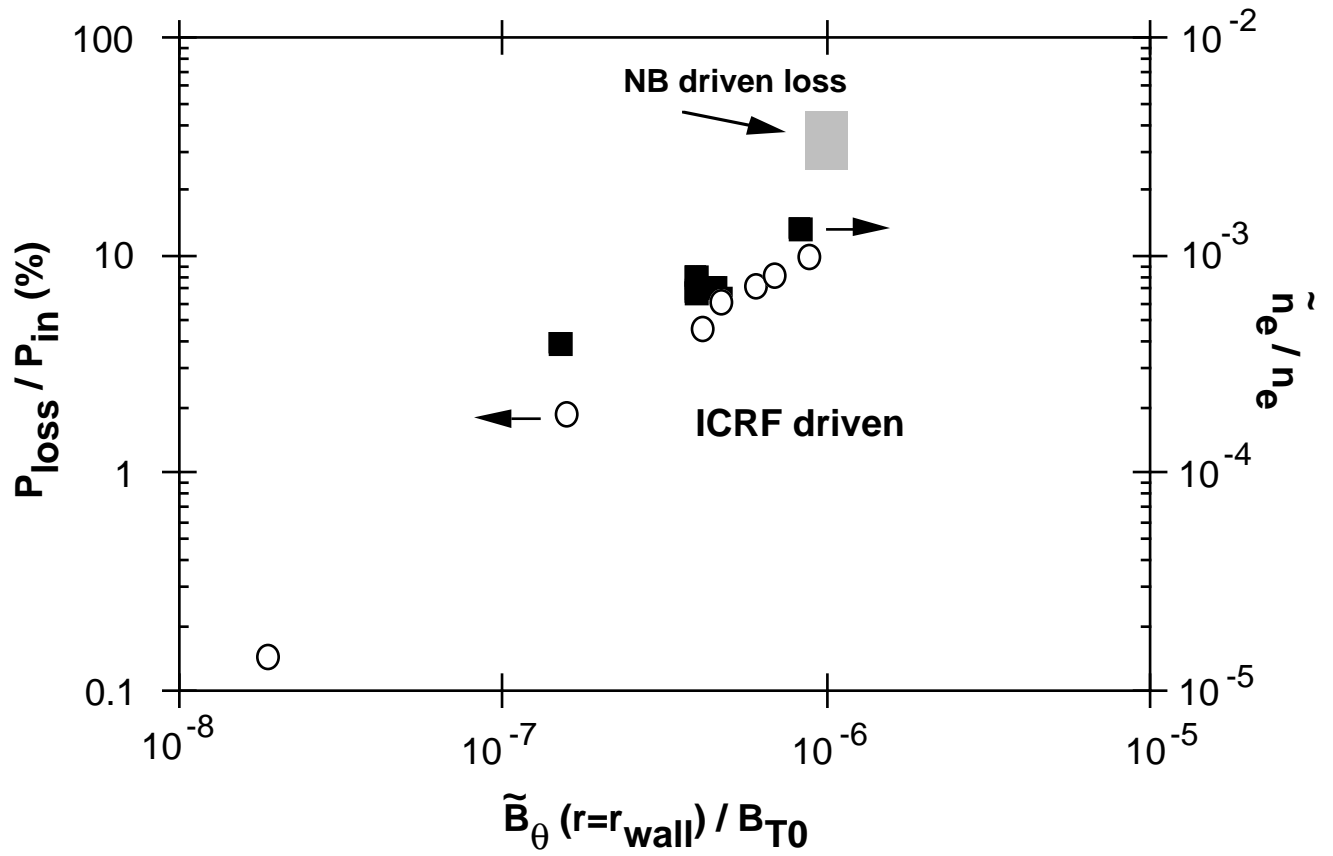


Fig. 53 Fraction of energetic particles power lost from the plasma and the TAE mode amplitude versus the heating power in TFTR discharges. Energetic particle loss resulted from TAE instabilities driven by neutral beam injection and ICRF heating but not by alpha particles (Darrow *et al.*, 1996b).

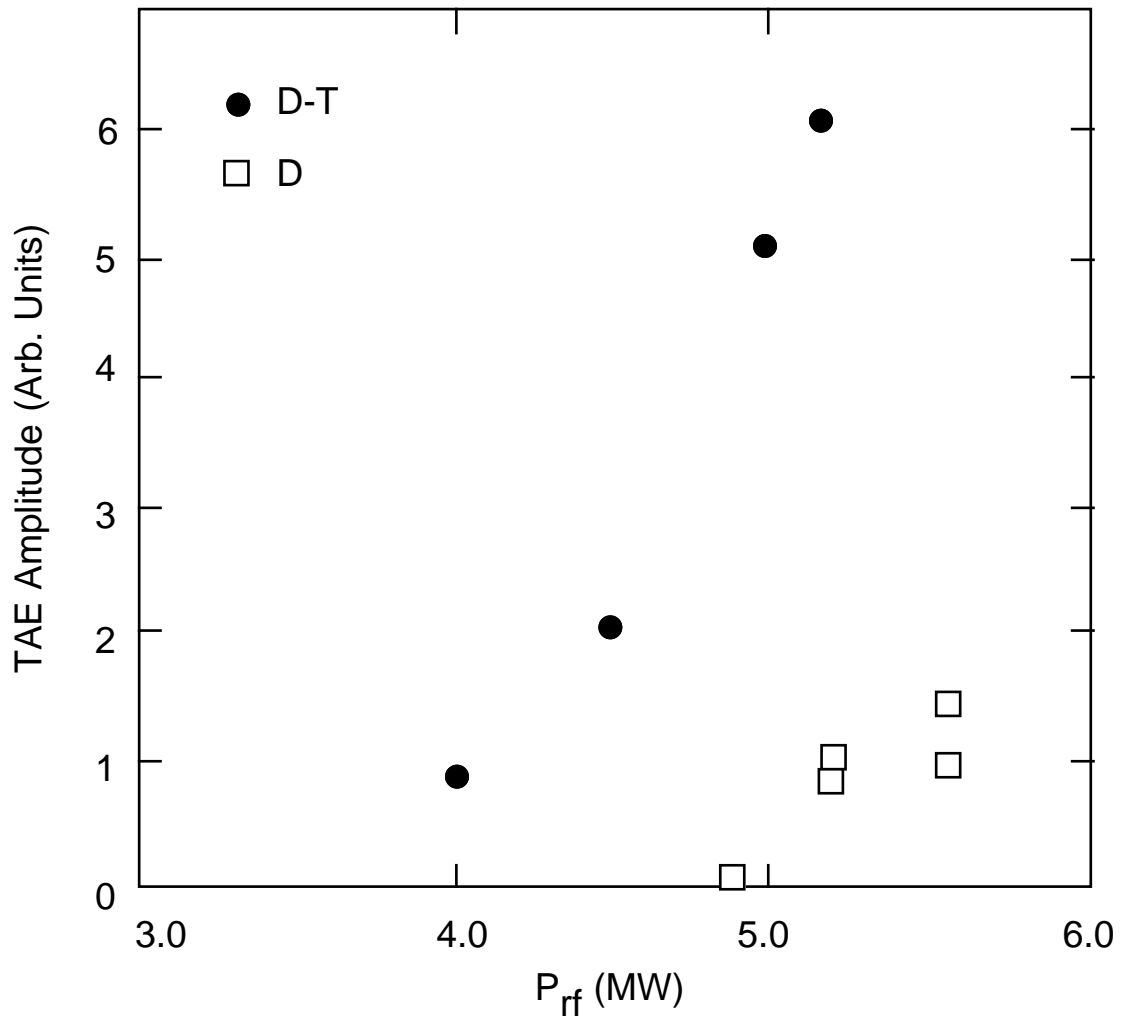


Fig. 54 TAE mode amplitude in D-T plasmas are higher than in companion D shots with the same ICRF heating power used to generate the energetic tail of H-minority particles (Wong *et al.*, 1996a).

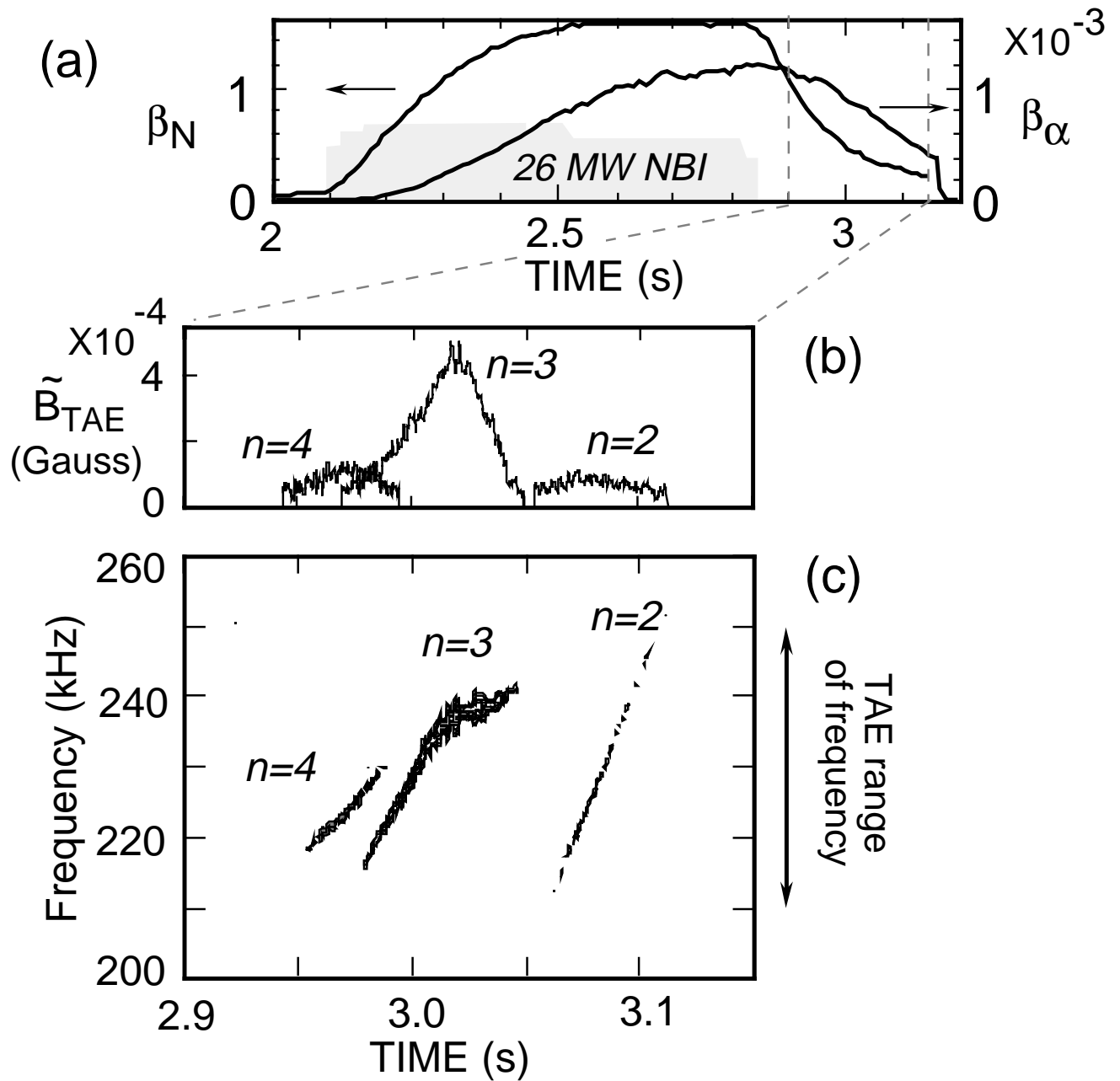


Fig. 55 Alpha-driven TAE mode in TFTR occurring ≈ 0.1 s after neutral beam injection in a D-T discharge with weak central magnetic shear. a) The evolution of β_N and β_α . b) The occurrence of magnetic fluctuations with different toroidal mode numbers is observed. c) The evolution of the frequency of the magnetic fluctuations. The frequency is consistent with the density-dependent TAE frequency, and mode timing is in reasonable agreement with the theoretical prediction based on beam ion damping (Nazikian *et al.*, 1996a).

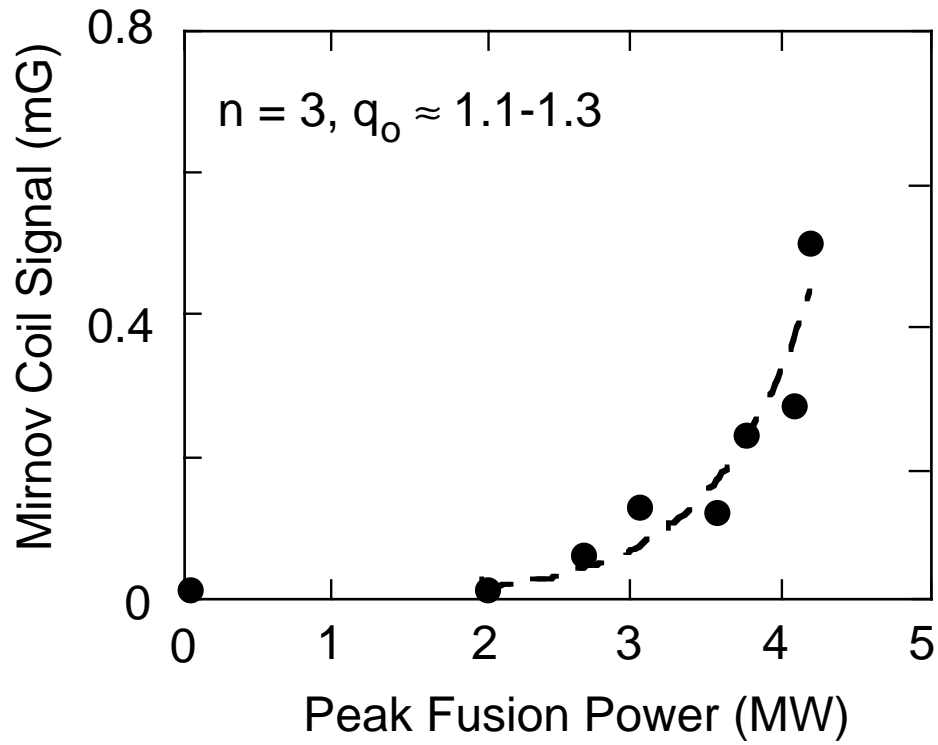


Fig. 56 TAE mode amplitude measurements using a magnetic pickup coil at the edge increases with fusion power as expected for alpha-driven TAE near threshold condition for instability. Modes are observed with $\beta_{\alpha}(0) > 0.03\%$ in weak central shear discharge with $q_0 \sim 1.1 - 1.3$ (Nazikian *et al.*, 1996a).

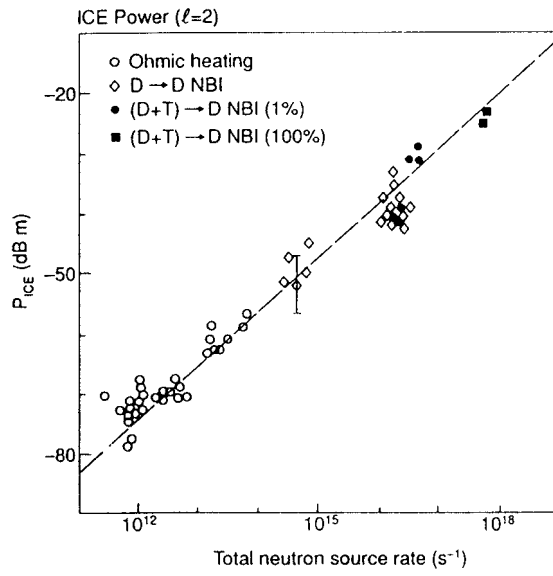


Fig. 57 Correlation between ICE intensity, P_{ICE} , and total neutral emission rate for ohmic and neutral beam heating in both D and D-T discharges (Cottrell *et al.*, 1993).

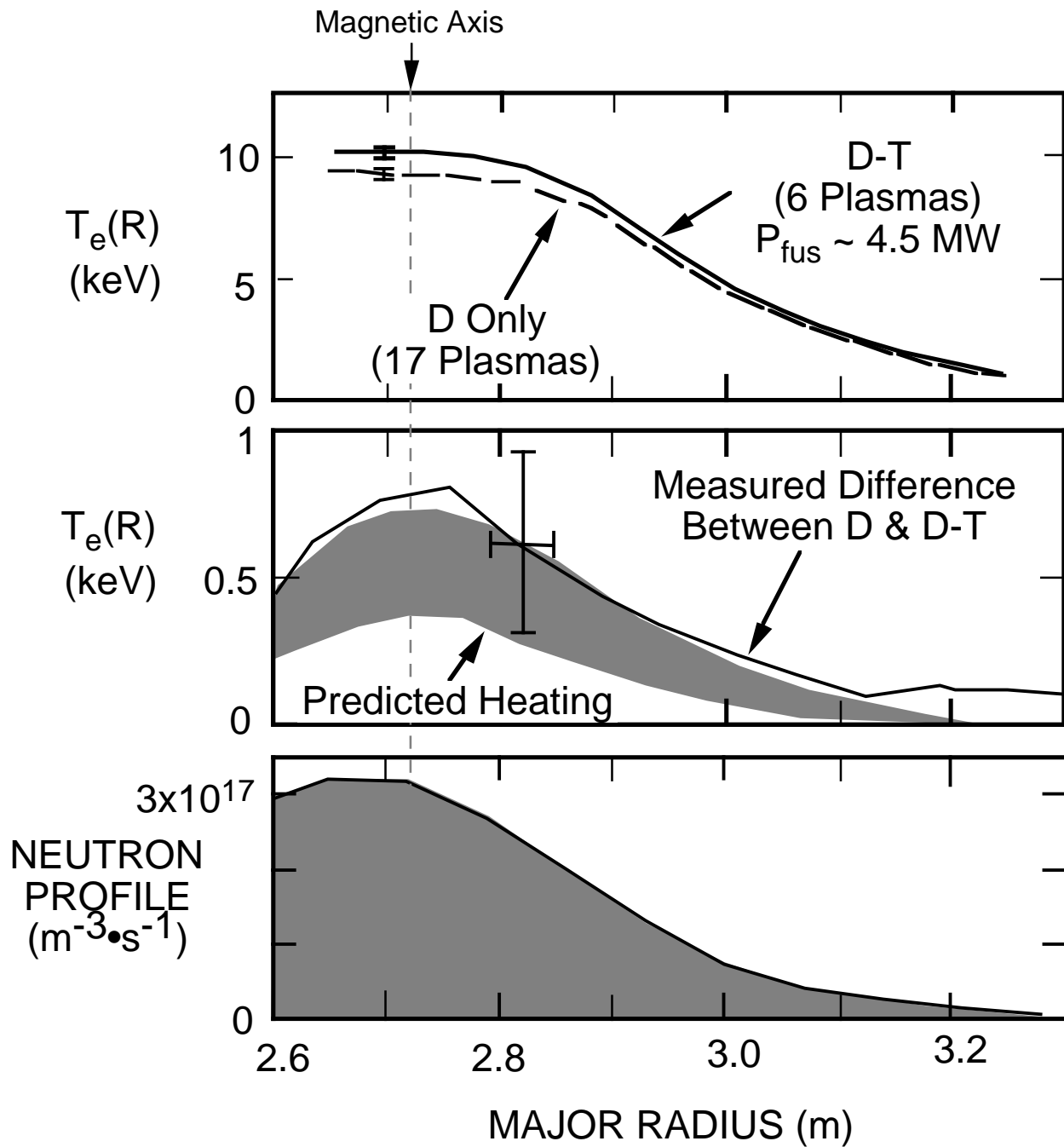


Fig. 58 Comparison of the electron temperature profile for a set of similar D-T and D discharges with comparable energy confinement times and neutral beam heating power. The measured difference in electron temperature is consistent with the predicted change due to alpha heating. The neutron profile which is a measure of the alpha particle birth profile is shown for comparison (Taylor *et al.*, 1996b).

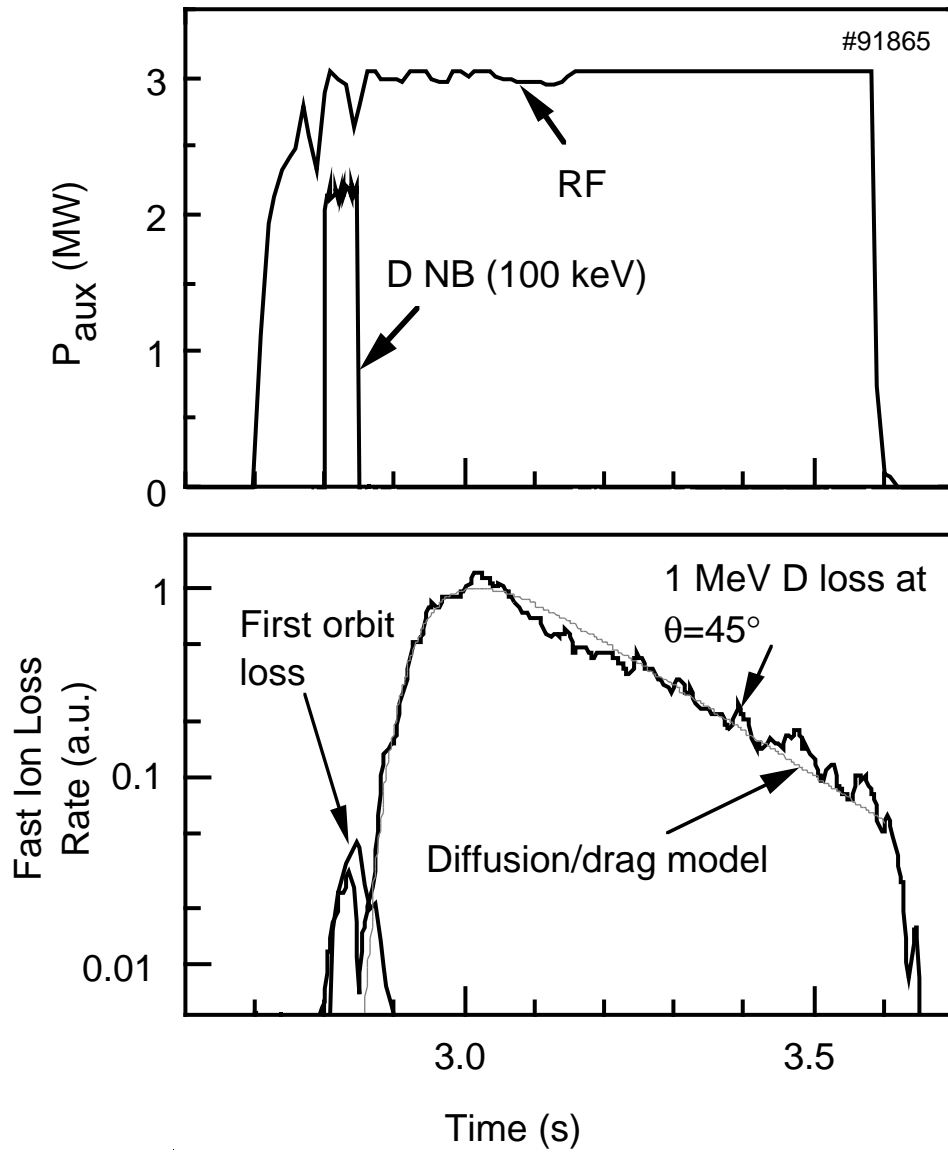


Fig. 59 Fast ion loss as measured by the 45° detector in the TFTR vessel indicates the loss of deuterium beam ions heated by mode converted ion Bernstein waves. The flux of particles is in accord with a simple model of fast ion heating by the mode converted wave.

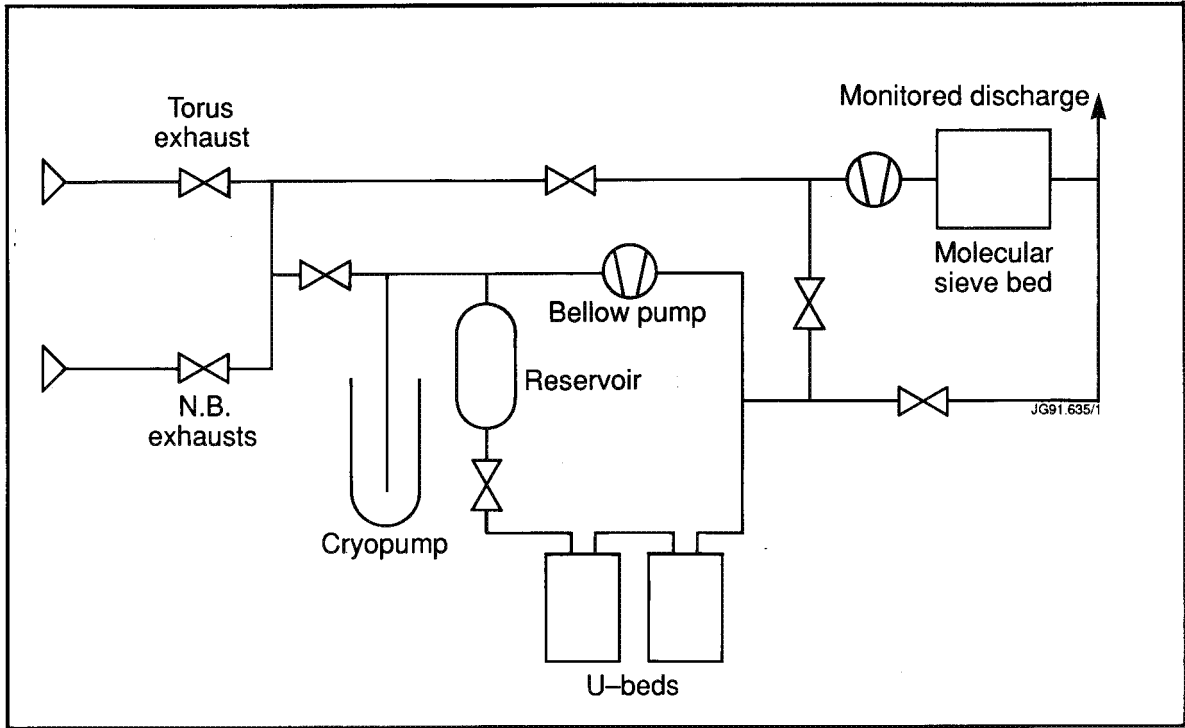


Fig. A1 The JET tritium gas collection system (JET Team, 1992).

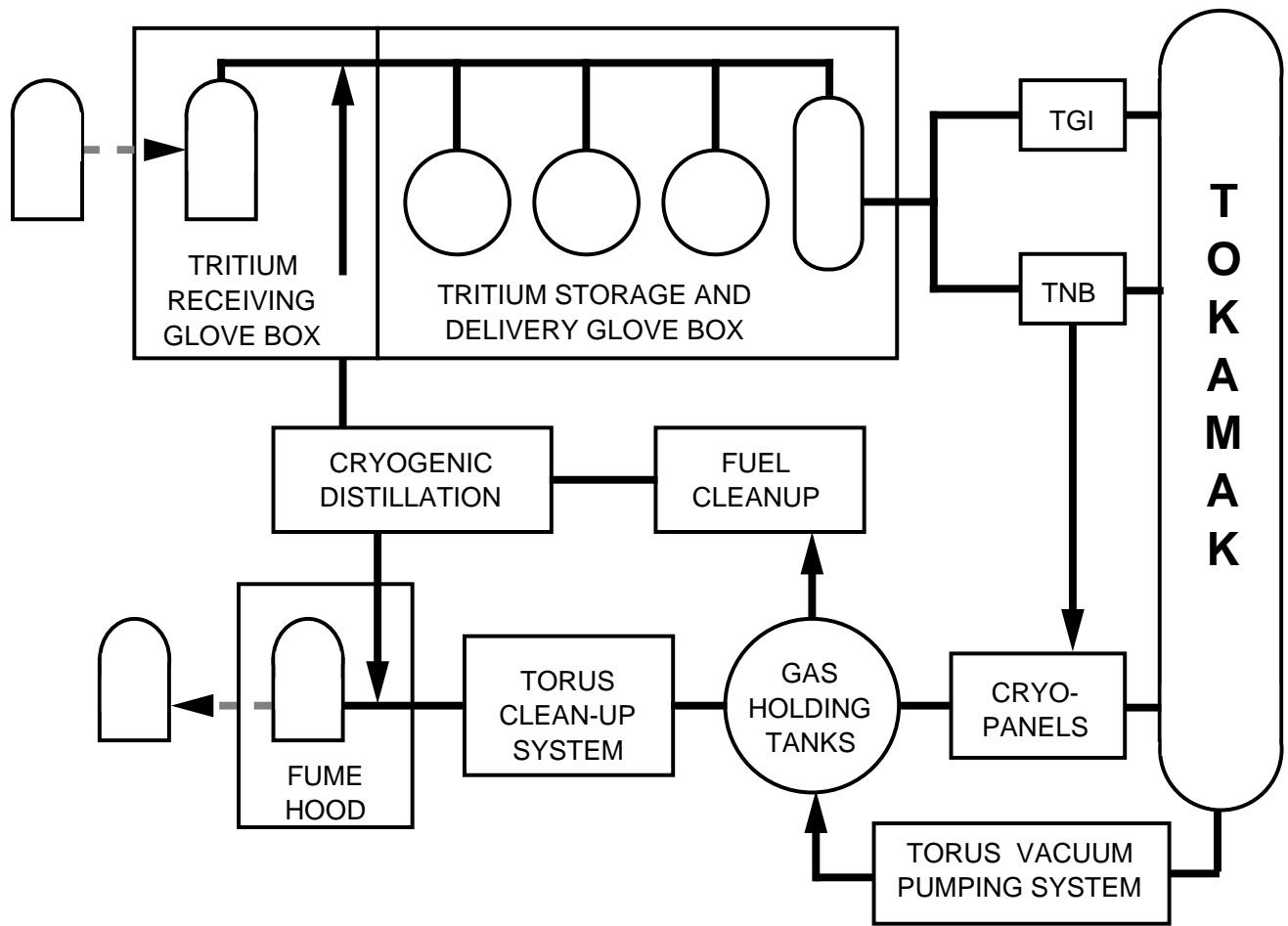


Fig. A2 The TFTR tritium gas fuel cycle (Williams *et al.*, 1996).